Aramco Journal of Technology

SPRING 2023

The *Aramco Journal of Technology* is published quarterly by the Saudi Arabian Oil Company, Dhahran, Saudi Arabia, to provide the company's scientific and engineering communities a forum for the exchange of ideas through the presentation of technical information aimed at advancing knowledge in the hydrocarbon industry.

Editor

William E. Bradshaw
william.bradshaw.1@aramco.com.sa
tel: +966-013-876-0498

Production Coordination

Richard E. Doughty
Corporate Publications, Aramco Americas

Design

Graphic Engine Design Studio
Austin, Texas, U.S.A.

The *Aramco Journal of Technology* gratefully acknowledges the assistance, contribution and cooperation of numerous operating organizations throughout the company.

ISSN 1319-2388

Contents

Novel Retarded Acid System Improves Acid Fracturing in High Temperature Gas Wells

Qasim A. Sahu, Eyad A. Alali, Dr. Amy J. Cairns and Dr. Mohammed A. Sayed

Abstract /

The oil and gas industry continues to rely on chemical methods for well stimulation of carbonate-rich formations; particularly hydrochloric (HCl) acid. The selection is primarily driven by the fact that it is cost-effective and readily reacts with calcium and magnesium-based carbonates to yield soluble products. Subsequently, enhancing the fracture half-length using conventional HCl acid treatments in acid fracturing operations in high temperature reservoirs remain a challenge. This is because the fast reaction rate between HCl acid and the rock matrix causes the acid to be rapidly spent, and therefore, hinders deeper placement into the formation. We tackled these limitations through the development of a novel retarded acid system.

The new acid system is prepared by blending a strong mineral acid with a suitable strong organic acid while minimizing the amount of free water in the formulation as a mechanism to control dissociation of the acid and afford the desired retardation properties. The single-phase low viscosity acid system "LVAS-l" has proven its effectiveness in acid fracturing applications. The technology was introduced in high-pressure, high temperature conditions to fracture multiple conventional gas wells in the Middle East. The motivation for field-testing this system was to significantly increase the etched fracture half-length and maximum attainable pump rates over the current standard emulsified acid system.

This was achieved by controlling the engineering parameters and the acid retardation properties during the treatment. A rigorous post-treatment analysis was conducted to evaluate the performance of this acid system and benchmark it to previously tested acid systems. This includes pressure transient analysis, post-frac flow back, and friction pressure calculations. Pressure measurements relied on installing downhole gauges for friction calculations and pressure build-up (PBU) analysis.

We recently reported on the successful development and deployment of the LVAS-l system. Specifically, the technology exhibits superior retardation properties, the ability to pump at higher rates, and the preparation method reduces operational complexity at the well site. Acid fracturing operations using the new acid system have proven successful, as evidenced by the prolonged gas production rate. Results of the PBU analysis show finite conductive fractures in the reservoir with half-lengths higher than conventional acid systems and negative skin factor. The treatment outcome resulted in a significant increase in the productivity index of the well.

This article describes a success story, i.e., from laboratory to field-scale, in the development and utilization of a new retarded acid system for acid fracturing applications. It highlights essential design parameters specific to the new system and lists the advantages and limitations over conventional emulsified acid systems.

Introduction

Well stimulation treatments for heterogeneous carbonate formations have traditionally relied upon the use of strong mineral acids, e.g., hydrochloric (HCl) acid. Consequently, fast rock/acid reaction rates[1] and corrosion issues pose a significant challenge to the longevity and practical application of such treatments.

One of the earliest means of acid retardation was adding polymer gelling agents[2]; however, such systems are often a significant source of formation damage. Alternatively, a commonly used approach to slow down the acid/rock reaction rate is using acid-in-oil emulsions, i.e., emulsified acids. Subsequently, the viscous nature of these fluids leads to unfavorably high friction pressures during the pumping process[3]. Additionally, the thermal stability is questionable at temperatures exceeding 300 °F.

To address these limitations, we designed and developed a novel engineered acid system that offers improved stimulation efficiency for carbonate reservoirs referred to as the low viscosity acid system (LVAS-l), Fig. 1. LVAS-l is a novel alternative acid system to the existing emulsified acid developed and used to stimulate the carbonate reservoir effectively. The technology was developed to overcome the cumbersome high friction pressure associated with the current emulsified acid system while maintaining comparable retardation properties. This

Fig. 1 *The framework for the development of the single-phase retarded acid system.*

technology offers outstanding stimulation efficiency while reducing the surface horsepower requirements and the operational mixing time.

Development Framework

An extensive lab program was designed to formulate and evaluate the new system's performance, from identifying the optimum acid ratio to developing a corrosion inhibitor package. A series of benchtop carbonate dissolution experiments were performed at room temperature under static conditions to identify the optimal engineered formulation needed to achieve the desired retardation effect.

The success of this approach was supported by coreflood measurements and corrosion loss evaluation. The proposed acid system was evaluated at temperatures and pressures up to 350 °F and 3,000 psi, respectively. A detailed analysis is presented in subsequent testing.

Static Dissolution Tests

This series of dissolution tests were performed at room temperature under ambient pressure and static conditions. Indiana limestone plugs were placed into beakers containing predesigned ratios of acids, i.e., a blend of organic and HCl acid. The best formulation was selected based on the dissolving power of the system and the retardation properties. These tests allowed for initial screening of the optimum acid formulation to use for further evaluation under reservoir conditions.

Figure 2 shows the results of the dissolution tests for LVAS-1.

Reaction Rate Kinetics

One key factor in evaluating the success of an acid system for carbonate stimulation is the reaction rate and diffusion coefficient of the acid system and rock matrix. This is commonly measured using a rotating disk apparatus by controlling the temperature, disk rotational speed, and pressure. Accordingly, a series of experiments were performed and the results benchmarked to available commercial systems in the literature[4-6], Fig. 3.

It is important to note that although the reaction rate literature data is not reported at analogous test conditions, the data still indicates that the LVAS-1 system had the lowest reaction rate compared to other retarded acid systems, particularly at a high temperature.

Coreflooding Analysis

Another evaluation tool is coreflooding experiments, which evaluate the acidizing performance of this new hybrid system. A series of tests were performed, and the results were benchmarked to conventional emulsified acids. Tests were performed using a 12" Indiana limestone core sample at a temperature of 300 °F and a pressure of 3,000 psi. The key parameter extracted from this experiment is the pore volume (PV) of acid required to breakthrough (PV_{BT}).

The industry uses this quantity as an objective function to optimize the acid fracturing treatment. The PV to breakthrough is an indicator that is used to assess the performance of the acid. A minimum volume of acid is desired to form a maximum length of the acid penetration in the reservoir. Figure 4 shows a computed tomography scanned image of the coreflooding experiments at a flow rate of 2 cm^3/min and 5 cm^3/min.

The results presented in Fig. 4 showed that the LVAS-1 system could generate wormholes and only requires 0.28 PVs compared to 0.8 PVs for the emulsified acid under similar experimental conditions[7,8]. This indicates that the LVAS-1 system outperforms the emulsified acid system because fewer volumes of acid are required to achieve the same channel penetration length.

Corrosion Testing

Corrosion management during stimulation treatment is critical. One of the criteria for success for any stimulation job is to maintain the integrity of the wellbore tubular. This is achieved by controlling the corrosion of the LVAS-1 system by developing a suitable corrosion inhibitor package. A suitable corrosion package containing a corrosion inhibitor and intensifier was formulated to control the corrosion.

A corrosion test was conducted using a C1018 metal coupon at 300 °F for 3 hours. No pitting was observed, and the corrosion loss was below the recommended

Fig. 2 *The samples of the results for the static dissolution test. The top image (pre-acidizing) represents the core plug prior to the test. The percentage noted indicates the mass lost from the original mass of the plug. Image (c) is the best formulation from the static test.*

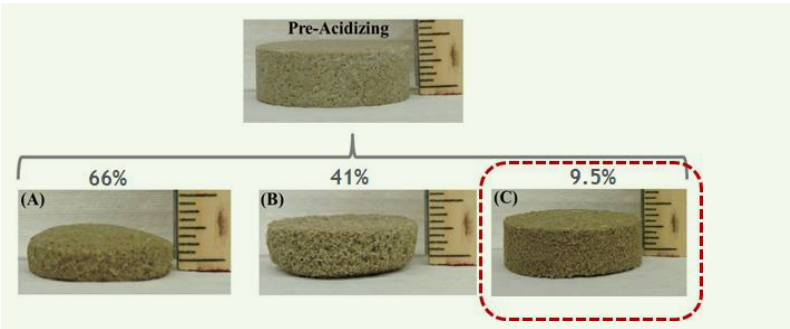

Fig. 3 *The reaction rate comparison of the LVAS-1 system against commercially available systems.*

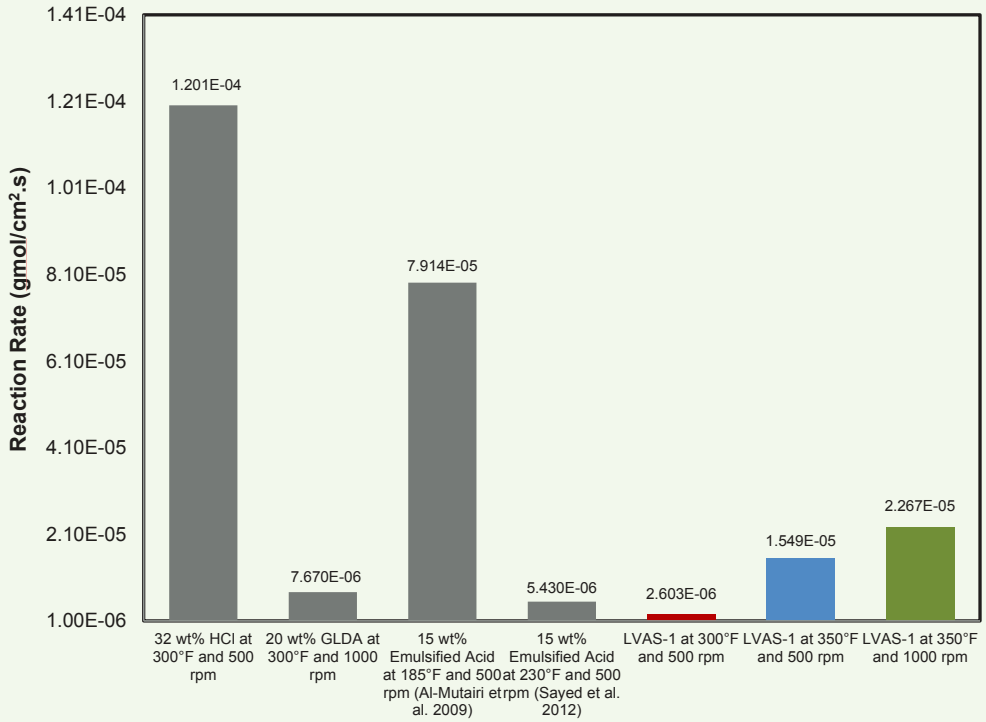

Fig. 4 *The results of the coreflooding experiments at a flow rate of 2 cm³/min and 5 cm³/min.*

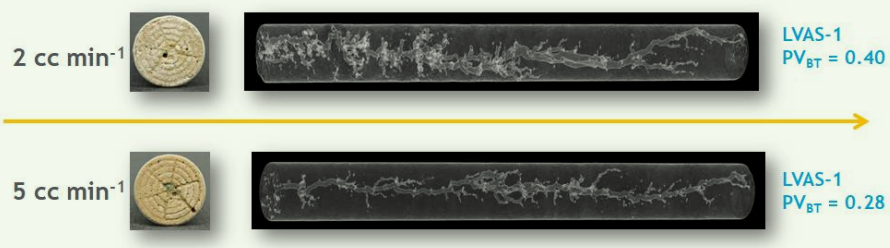

industry standard of 0.05 lb/ft² (0.02 lb/ft²).

Flow Loop Testing

One of the main advantages offered by the LVAS-1 system is the reduction in friction pressure. Friction pressure loss measurement is needed because acid fracturing treatments are performed at a high pumping rate in the range of 40 to 60 barrels per minute (bpm). The set-up consisted of a 10 ft loop, with an inner and outer diameter of 0.5" and 0.37", respectively. Note that the viscosity of LVAS-1 is significantly less as compared to emulsified acids, i.e., 4.28 cP vs. 112 cP, respectively (measured at room temperature).

Using the density and viscosity values, flow rates were selected to mimic laminar and turbulent flow, i.e., estimated to be 1 and 4 gallons per minute (gpm), respectively. As a reference, the average pressure drop was determined to be 11.29 psi for LVAS-1, whereas, under the same conditions, the pressure drop for the emulsified acid was estimated to be 26.32 psi, thereby leading to a 2.3-fold reduction. Note that higher flow rates would be needed in the case of emulsified acids to simulate laminar and turbulent flow due to the fact its viscosity is significantly higher.

Table 1 compares the pressure losses of water (equivalent to LVAS-1) and emulsified acid at two different rates.

Deployment and Execution

The newly formulated acid system (LVAS-1) has been trial tested in one candidate well drilled vertically into a carbonate formation, whereby it was used to perform a single-stage acid fracturing treatment. The mixing procedure and field execution are like the traditional

Table 1 *The pressure drop comparison between emulsified acid and a single-phase system at two different rates.*

Flow Rate (gpm)	Pressure Drop (psi) LVAS-1	Pressure Drop (psi) Emulsified Acid
4.0	11.29	26.3
10.0	38.7	66.9

HCl acid system, and therefore, no extra equipment is needed to prepare nor mix the acids.

Pilot Test 1

The first pilot test was performed on a vertical gas producer drilled to a total depth of 12,095 ft. The well was completed with a 4½" 13.5# cemented liner completion and a production packer across a carbonate reservoir, where it was perforated in a low stress interval with a fracture gradient of 0.7 psi/ft to 0.8 psi/ft.

The formation is a dolomitic limestone comprised of almost 70% calcite and 30% dolomite across the perforated interval.

Treatment Design

Table 2 shows the pumping schedule for the trial test. The fracturing design consisted of three acid cycles, specifically chosen to ensure that all perforated intervals would be stimulated. Each acid cycle contains a pad fluid, LVAS-1 stage, treated water, and a diverter. The purpose of the pad fluid is to initiate and propagate the fracture inside the formation. The pad stage is the main component, along with the injection pressure that will create the fracture geometry.

Then, LVAS-1 is followed to etch the fracture face and ensure there will be a conductive channel after the fracture is closed. A treated water slug is then injected to displace the acid away from the wellbore and accelerate the reaction of LVAS-1 with the formation. Notably, the reservoir temperature exposed to the acid is not the original reservoir temperature due to the cool-down effect resulting from fluid injection. This process will ensure the acid is spent, thereby minimizing the flow back of live acid during the flow back. Table 3 shows the fluid formulation of LVAS-1.

Table 2 *The acid fracturing pumping schedule for the pilot test of the LVAS-1 system.*

Step Name	Rate	Fluid Name	Clean Fluid Volume (gal)
Cool-Down	15	Treated Water	840
		First Acid Cycle	
PAD 1	20	Crosslinked Polymer (35 ppt)	4,500
Acid 1	20	LVAS-1	4,500
Spacer	25	Treated Water	2,000
Diverter 1	25	VES 15%/Fiber	2,200
		Second Acid Cycle	
PAD 2	30	Crosslinked Polymer (35 ppt)	5,000
Acid 2	30	LVAS-1	5,000
Spacer	35	Treated Water	2,000
Diverter 2	35	VES 15%/Fiber	2,800
		Third Acid Cycle	
PAD 3	40	Crosslinked Polymer (35 ppt)	8,000
Acid 3	40	LVAS-1	11,500
Acid 4	45	28% HCl Acid	4,000
Diverter 3	45	VES 15%/Fiber	3,300
Acid 5	50	28% HCl Acid	5,000
Tank Bottom	10	Tank Bottom	3,300
Flush	50	Treated Water	3,000
Over Flush	50	Treated Water	8,000

Table 3 *The fluid formulation for the retarded acid system.*

Additive	Concentration	Units
Corrosion Inhibitor	20	gal/1,000 gal
Inhibitor Intensifier	70	lb/1,000 gal
Organic Acid	487.5	gal/1,000 gal
31% HCl Acid	487.5	gal/1,000 gal
Iron Stabilizer	4	lb/1,000 gal
Chelating Agent	50	lb/1,000 gal
H_2S Scavenger	5	gal/1,000 gal

The last step in the acid cycle is the diverter, which helps to cover the entire treated interval as there is a permeability contrast across the formation. In the last acid cycle, 1.5 wellbore volumes of LVAS-1 was injected to calibrate the friction pressure for the system.

Table 4 summarizes the total fluid pumped in the test. A total acid volume of 530 gal/ft was used in the treatment. The treatment was successfully pumped without any operational issues. The maximum pumping rate achieved is 54.6 bpm, higher than other offset wells in the area.

Table 4 *A summary of the total fluids injected during the acid fracturing treatment.*

Total Fluids Pumped		
Fluid Name	**Quantity (gal)**	**Quantity (bbl)**
Treated Water	15,830	377
Polymer	17,471	416
LVAS-1	21,028	500
Diverter	9,543	227
28% HCl Acid	9,198	219

Performance Evaluation

Following the acid fracturing treatment, the well flowed back at an excellent rate compared to the offset wells' performance. Post-fracturing flow back was initiated without requiring nitrogen lift with coil tubing. Analysis of the flow back samples indicated the acid was fully spent as evidenced by a pH reading of 7 after a shut-in period of 14 hours.

We also relied on downhole gauges installed in the well to perform friction calculation and pressure build-up (PBU) analysis to evaluate the performance of LVAS-1.

Friction Pressure

One advantage of LVAS-1 over emulsified acid is the low viscosity (1 cP to 5 cP). A downhole gauge was installed before the treatment to calibrate the friction numbers for LVAS-1 at different pumping rates. As previously mentioned, the friction pressure was measured at the laboratory scale where the flow rate was low, due to pump restrictions compared to the actual job in the field.

Table 5 compares the calculated pressure from the trial test and the measured frictional losses from the gauge. At a high pump rate, the measured friction pressure was found to be within 8% of laboratory results.

The following equation was used to calculate the friction numbers for LVAS-1:

$$P_f = P_{whp} + P_h - P_{BH} \quad (1)$$

where P_f is the friction pressure, P_{whp} is the surface treating pressure, P_h is the hydrostatic pressure, and P_{BH} is the bottom-hole pressure (gauge).

Figure 5 shows a plot of the friction pressure against the pumping rate of the LVAS-1 system measured from the downhole gauges installed in the well. The laminar flow regimen of the LVAS-1 system appears to be in

Table 5 *The measured and calculated friction pressure for LVAS-1.*

Rate (bpm)	Friction Pressure Measured (Gauge) (psi)	Friction Pressure Calculated (psi)
3.5	93	80
5	175	150
10	642	550
20	2,156	1,840
30	4,443	3,800
40	7,092	6,000

Fig. 5 *The measured friction pressure from the downhole gauges.*

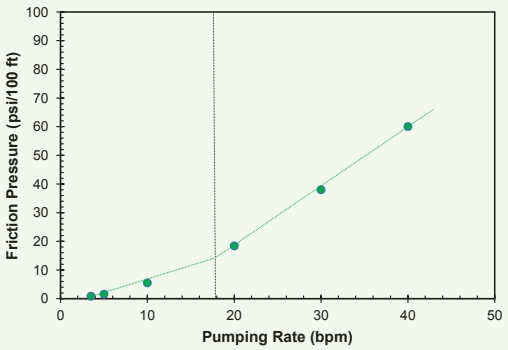

Fig. 6 *A comparison between the frictional losses for the LVAS-1 and emulsified acid.*

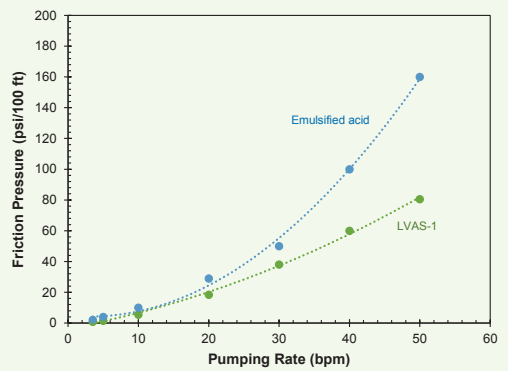

the range of 0 bpm to 18 bpm. Above this rate, the LVAS-1 enters the turbulence flow regime as evidenced in the derivative change at 18 bpm.

Figure 6 compares the frictional pressure generated from the emulsified acid[9] vs. the friction pressure generated from LVAS-1. In the laminar flow regime, i.e., below a 20 bpm injection rate, the friction pressure of LVAS-1 and the emulsified acid is comparable. Subsequently, above this injection rate in the turbulence flow regime, the pressure losses for the emulsified acid are doubled compared to the LVAS-1 system. The 50% pressure reduction explains why we can pump at a higher rate when we utilize the LVAS-1 system.

PBU Analysis

A PBU test was conducted after the flow back. The downhole gauge was retrieved after two weeks of installation to allow the pressure in the well to build up and reach a stable pressure. Figure 7 shows the pressure data analysis in a log-log plot.

The fracturing signature can be easily identified from the shape of the curves. The result shows a finite conductive hydraulic fracture in the reservoir with a half-length up to 208 ft and skin factor of −6.

Conclusions

One pilot treatment with LVAS-1 was successfully field-tested in a carbonate reservoir in the Middle East. The main conclusions from the trial are:

- A comprehensive framework for developing and deploying a new novel retarded acid system referred to as LVAS-1 was successfully executed.
- The treatment was pumped according to the design without any operational issues.
- Utilization of the LVAS-1 system in a single-stage acid fracturing operation led to a reduction in the total mixing time by up to 5 hours, thereby improving operational efficiency.

Fig. 7 *The PBU data in a log-log plot.*

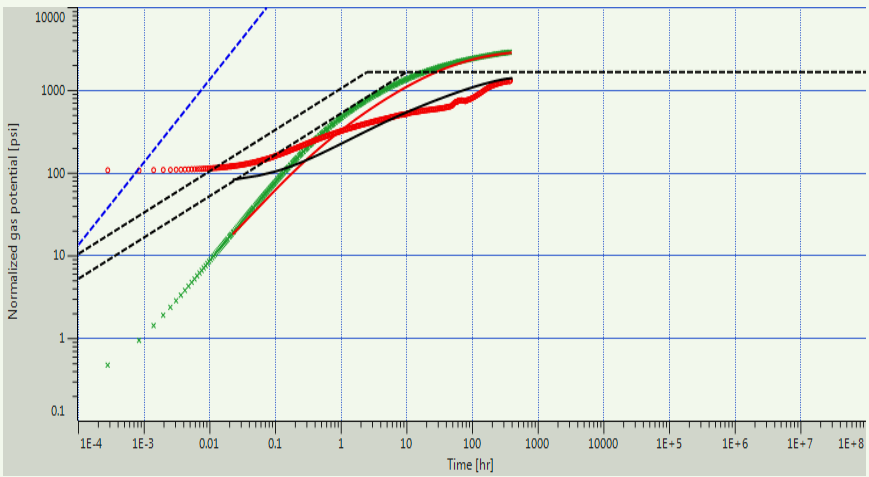

- Downhole gauge measurements confirmed the bottom pressure was maintained above the fracturing pressure during the entire treatment.
- The friction numbers for LVAS-1, calculated at different injection rates, showed a 50% pressure drop reduction compared to emulsified acid.
- The PBU analysis performed in the treated candidate showed a clear fracture signature with a negative skin factor and long fracture half-length.

References

1. Sayed, M., Cairns, A.J. and Sahu, Q.A.: "Low Viscosity Acid Platform: Benchmark Study Reveals Superior Reaction Kinetics at Reservoir Conditions," IPTC paper 20282, presented at the International Petroleum Technology Conference, Dhahran, Kingdom of Saudi Arabia, January 13-15, 2020.
2. Kalgaonkar, R., Bataweel, M., Alkhowaildi, M. and Sahu, Q.A.: "A Non-Damaging Gelled Acid System Based on Surface Modified Nanoparticles," SPE paper 204716, presented at the SPE Middle East Oil and Gas Show and Conference, event canceled, November 28-December 1, 2021.
3. Sahu, Q.A., Arias, R.E. and Alali, E.A.: "Dynamic Diverter Technology Efficiency in Acid Fracturing Applications," SPE paper 197881, presented at the Abu Dhabi International Petroleum Exhibition and Conference, Abu Dhabi, UAE, November 11-14, 2019.
4. Rabie, A.I., Gomaa, A.M. and Nasr-El-Din, H.A.: "HCl-Formic in Situ Gelled Acid for Carbonate Acidizing: Coreflood and Reaction Rate Study," SPE paper 140138, presented at the SPE Production and Operations Symposium, Oklahoma City, Oklahoma, March 27-29, 2011.
5. Sayed, M.A., Nasr-El-Din, H.A., Zhou, J., Zhang, L., et al.: "A New Emulsified Acid to Stimulate Deep Wells in Carbonate Reservoirs: Coreflood and Acid Reaction Studies," SPE paper 151062, presented at the North Africa Technical Conference and Exhibition, Cairo, Egypt, February 20-22, 2012.
6. Al-Mutairi, S.H., Nasr-El-Din, H.A., Hill, A.D. and Al-Aamri, A.D.: "Effect of Droplet Size on the Reaction Kinetics of Emulsified Acid with Calcite," *SPE Journal*, Vol. 14, Issue 4, December 2009, pp. 606-616.
7. Daeffler, C.S., del Valle, J.F., Kariampally, J., Elkhoury, J.E., et al.: "Improving Wormholing Efficiency in Carbonates with a Novel System Based on Hydrochloric Acid," SPE paper 189540, presented at the SPE International Conference and Exhibition on Formation Damage Control, Lafayette, Louisiana, February 7-9, 2018.
8. Abdrazakov, D., Panga, M.K., Daeffler, C. and Tulebayev, D.: "New Single-Phase Retarded Acid System Boosts Production after Acid Fracturing in Kazakhstan," SPE paper 189559, presented at the SPE International Conference and Exhibition on Formation Damage Control, Lafayette, Louisiana, February 7-9, 2018.
9. Crowe, C.W. and Miller, B.D.: "New, Low-Viscosity Acid-in-Oil Emulsions Provide High Degree of Retardation at High Temperature," SPE paper 4937, presented at the SPE Rocky Mountain Regional Meeting, Billings, Montana, May 15-16, 1974.

About the Authors

Qasim A. Sahu

M.S. in Energy Resources and Petroleum Engineering, King Fahd University of Petroleum and Minerals

Qasim A. Sahu is a Petroleum Engineer working with the Production Technology Division of Saudi Aramco's Exploration and Petroleum Engineering Center – Advanced Research Center (EXPEC ARC). Since joining Saudi Aramco in 2013, he has worked in a portfolio of projects leading the development of new technologies in hydraulic fracturing and carbonate stimulation. In less than 8 years, Qasim played a critical role in delivering and implementing sustainable cost-effective solutions to boost the gas production where circular water economy and water sustainability is at heart of those technologies.

He developed and implemented novel engineered acidizing technology that improves operational efficiency, increases stimulation effectiveness, and overcomes pressing field challenges.

Qasim has authored and coauthored more than 15 publications, including peer-reviewed journals, conference papers, granted patent, and invention disclosures. He and his team were shortlisted as a finalist for the Best Oil Field Chemical Award in the 2020 World Oil awards. Also, Qasim received the Saudi Aramco Vice President award in 2015 as a distinguished Society of Petroleum Engineers (SPE) member. He has represented the company in numerous regional and international events promoting knowledge sharing and knowledge transfer across the industry.

Qasim is a member of the SPE and the European Association of Geologists and Engineers (EAGE).

He received his B.S. degree (with first honors) in Petroleum Engineering from King Fahd University of Petroleum and Minerals (KFUPM), Dhahran, Saudi Arabia. Qasim received his M.S. degree in Energy Resources and Petroleum Engineering from King Abdullah University of Science and Technology (KAUST), Thuwal, Saudi Arabia.

Eyad A. Alali

M.S. in Sustainable and Renewable Energy, King Fahd University of Petroleum and Minerals

Eyad A. Alali is a Petroleum Engineer working in the Technology Deployment Group of Saudi Aramco's Exploration and Petroleum Engineering Center – Advanced Research Center (EXPEC ARC). He joined Saudi Aramco in 2015, and has since worked with gas reservoir management, gas production engineering, and the Productivity Enhancement Team in EXPEC ARC's Production Technology Division. Eyad is currently working on technology deployment and commercialization.

His experience includes work in a portfolio of projects focused on developing new technologies in reservoir fracturing, carbonate stimulation, and well intervention. Eyad played a critical role in implementing technologies in the field to enhance production operations with sustainable and cost-effective solutions.

He and his team were shortlisted as a finalist for the 2020 World Oil Best Oil Field Chemical Award. Eyad received the 2021 Exceptional Safety Award from the Loss Prevention Department. He was a highly recommended finalist for 2021 IChemE Global Young Industrialist Award, and was a highly commended finalist for 2022 Middle East Energy Professional of the Year Award. Eyad won the 2022 Society of Petroleum Engineers (SPE) Regional Public Service Award.

He has authored and coauthored more than 10 publications, including peer-reviewed journals and conference papers. Eyad has filed more than 15 invention disclosures and received two granted patents. He is an active member of SPE.

Eyad received his B.S. degree (with distinction) in Petroleum Engineering from the University of Oklahoma, Norman, OK. He received his M.S. degree in Sustainable and Renewable Energy from King Fahd University of Petroleum and Minerals (KFUPM), Dhahran, Saudi Arabia.

Dr. Amy J. Cairns

Ph.D. in Chemistry, University of South Florida

Dr. Amy J. Cairns has held several research and development positions in both academia and industry in the United States and abroad since earning her Ph.D. in Chemistry in 2010. In 2014, she joined the Production Technology Team at Aramco Americas – Houston Research Center. In her role as a Senior Research Scientist, Amy supports the development and characterization of innovative oil field chemical solutions designed to address Upstream field challenges and contributes to sustainability initiatives geared toward advancing technologies to increase the CO_2 storage capacity in geological formations.

Prior to joining Aramco Americas, she worked as a Postdoctoral Researcher at the Pacific Northwest National Laboratory in Richland, Washington. Additionally, Amy worked in Saudi Arabia for 3 years as a Postdoctoral Fellow in the Functional Materials Design, Discovery and Development Group at King Abdullah University of Science and Technology (KAUST), focusing on reticular design and synthesis of a specific class of novel porous solid-state crystalline materials, i.e., metal-organic frameworks.

She has published more than 30 papers in peer-reviewed journals, has presented at numerous regional and international conferences, and has several granted patents. Amy is a member of the American Chemical Society (ACS) and the Society of Petroleum Engineers (SPE).

She received her B.S. degree (with honors) in Chemistry from Saint Mary's University in Halifax, Nova Scotia, Canada, and a Ph.D. degree in Chemistry from the University of South Florida, Tampa, FL.

Dr. Mohammed A. Sayed

Ph.D. in Petroleum Engineering, Texas A&M University

Dr. Mohammed A. Sayed joined the Production Technology Team at the Aramco Research Center – Houston as a Research Scientist in 2013. In this role, he is working to develop new chemical treatments and fluids used in acidizing carbonate reservoirs (matrix acidizing and acid fracturing).

Mohammed is also creating new fluids utilized for hydraulic fracturing in both conventional and unconventional reservoirs, acidizing additives and wettability alteration chemicals, and breakers for polymer systems used in fracturing fluids, as well as developing new solutions for gas hydrate removal and mitigation. He is also responsible for assisting in the preparation and follow-up on programs well acidizing and stimulation treatments, as well as preparing reports on assigned projects or programs in the oil field operations.

Mohammed is a contributor to technical papers and is a member of the Society of Petroleum Engineers (SPE) as well as the American Chemical Society (ACS). He has presented at various industry conferences, including the Offshore Technology Conference (OTC), Middle East Oil and Gas Show (MEOS), and the International Conference on Oil Field Chemistry, as well as publishing peer-reviewed papers in the *Canadian Journal of Petroleum Technology*, SPE *Production and Operation Journal* and *Advances in Water Resources*.

Mohammed received his Ph.D. degree in Petroleum Engineering from Texas A&M University, College Station, TX.

Research and Successful Field Application of Nanosilica System for Gas Shutoff in Horizontal Well

Dr. Ayman M. Almohsin, Hassan W. Al Hashem, Ali A. Sadah, and Mesfer N. AlQahtani

Abstract /

Innovative and cost-effective gas shutoff (GSO) technologies are required to improve the oil recovery and avoid the problems associated with the unwanted gas production. A novel strong and stable material with controlled gelation time was developed to isolate gas production zones over a wide range of parameters, including the temperature, pressure, injectivity duration, and flow rate.

This article details the development of the nanosilica for GSO from laboratory development to successful field treatment. The nanosilica technology is composed of modified nanosilica and an activator, which is used to trigger the viscosity of the system. The gelation time and gel strength of the nanosilica in the presence of different concentrations of the activator have been investigated. In addition, the impact of the temperature on the gelation time was examined. The GSO field treatment was designed to prevent the gas production from a horizontal oil well based on the results obtained in the laboratory at comparable conditions. This article discusses the candidate well selection criteria, job design, field operation, and pre- and post-job production data for evaluating the performance of this technology.

Laboratory results revealed that the two-component system, namely the modified nanosilica, and the activator exhibits low viscosity, i.e., 6 cP prior to the exposure to high temperature. Once the temperature is increased to certain values, the viscosity of the mixture will increase depending on the concentration of the activator such that the start point of colloid gelling ranged from a few minutes to several hours at a given temperature.

Therefore, this fluid system can be placed as a single phase, low viscosity solution into the targeted formation zones, and subsequently gelled inside the formation, resulting in complete plugging. For the job design, production logging tools were run on the E-coil string to detect the gas source and measure the bottom-hole temperature (BHT) required for the formulation of GSO nanosilica, and also to measure the injection pressure to monitor the injectivity. The objective of this job is to isolate the 980 ft of stand-alone screens. Results unveiled the significant potential of nanosilica as a GSO approach to mitigate gas intrusion with a sustainable 65% gas reduction compared to the pretreatment results.

The new trend of using eco-friendly and nanoscale particles in gas control applications is a breakthrough in the oil industry. The use of such technology would improve well productivity, reduce operational costs, and reduce the carbon footprint as well. Laboratory results and field data revealed that the nanosilica for GSO was effective over a wide range of parameters, including the temperature, pressure, and permeability.

Introduction

Nowadays, new technologies are merging to increase the level of oil recovery in an attempt to compensate the increasing demand for energy. These technologies will unlock the potential of the remaining oil in place. The revolution of nanotechnology can promote the possibilities of resolving different challenges beyond the current available technologies due to their apparent potential, especially in the oil and gas industry.

Numerous research projects have been focusing in utilizing nanoparticles in solving different challenges to improve oil/gas production. One such project deals with fine migration in the formation. Magnesium oxide has been stated to yield promising results in this challenging area[1-3]. Another research project focused on controlling water production using nanosilica for water shutoff applications[4-7]. The same research team proposed using nanosilica for gas shutoff (GSO) applications[8].

During the oil production, the presence of gas coning or channeling can lead to a high gas-oil ratio (GOR). Therefore, producing at high GOR is a concern during oil production due to the limitation of gas handling[9]. The actual differential pressure within horizontal wells gradually decrease from heel to toe[10]. The higher the drawdown, the higher the pressure drop, resulting in quicker fluid production rate at the heel of the horizontal section, leading to a faster gas cap breakthrough from the heel.

Herein, this article presents the research and development of a unique nanosilica toward a successful field

application to isolate a gas producing interval in a horizontal well. An advanced approach for GSO intervention relying on real-time downhole data was implemented for the first time in this field.

Nanosilica Development

The project consists of research using nanosilica; the new developed fluid system is an inorganic gel-based system. Figure 1 is a graphic demonstration of the gel development. The fluid system presented in this article comprises two chemical additives: modified nanosilica particles, and an activator. Both chemicals can be mixed at the surface; and can be pumped as a single low viscosity solution.

Upon placing it into the targeted zones, the gelation process is activated via the formation temperature and time. By varying the concentration of the activator, the gelation could be delayed to allow sufficient working time for placement operation.

Some of the main highlights and benefits of the nanosilica fluid system:

- The ability to customize the thermal and rheological properties of the system to fit the purpose.
- A wide temperature application ranging from ambient up to 350 °F.
- Is eco-friendly and 100% reversible.
- Easy mixing because it contains only two chemical additives.
- It is fast, safe, and cost-effective.
- Tested tough solid after cured up to 5,000 psi.

Research Work

Materials

Aqueous dispersion of nanosilica contains approximately 40 wt% active material. The nanosilica dispersion is sterically stabilized and the amorphous silica nanoparticles carry a negative surface charge. Those silica nanoparticles are discrete, and have a smooth, spherical shape.

Figure 2 shows the particle size distribution, using a particle size ~14 nm. The water shutoff system based on the new composition incorporates two main components: nanosilica and a temperature activated activator, both are in liquid form.

Gelation Time Study

Simply stated, gelation time can be defined as the amount of time it takes for the in situ material in the liquid phase to transform into a solid phase. Therefore, gelation time must be known to allow safe pumping operation through the tubular and into the target zone at an anticipated depth of penetration.

In this work, a high-pressure, high temperature (HPHT) viscometer was used to evaluate the gelation

Fig. 2 *The nanoparticle characterization using a nanoparticle distribution analyzer.*

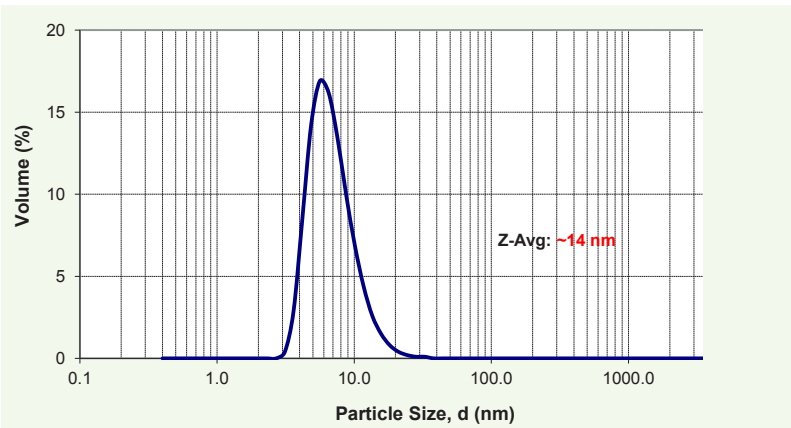

Fig. 1 *A schematic representation of the gelation process for the nanosilica system for GSO.*

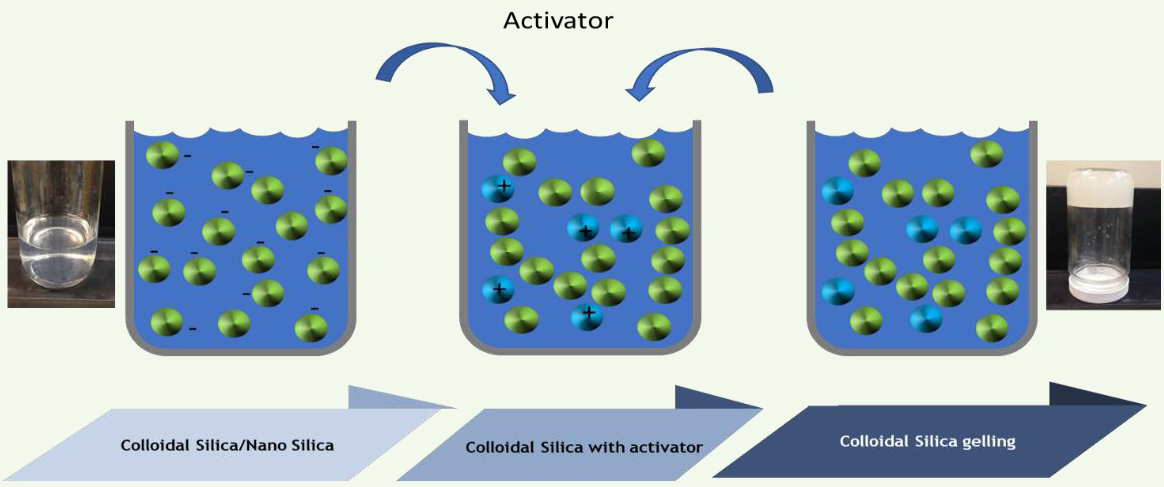

Fig. 3 *The typical gelation time curve for the for nanosilica system using a viscometer (at 180 °F).*

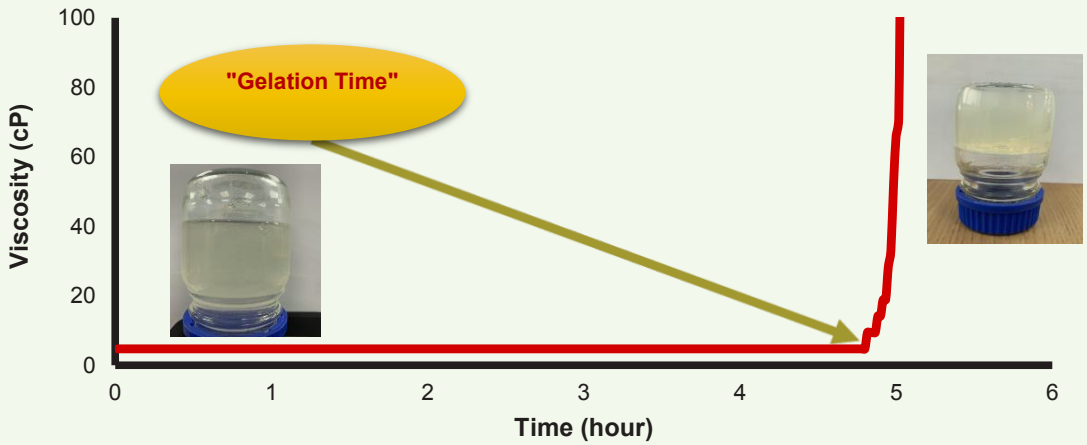

time by observing the drastic transformation in the solution viscosity during measurement. This method is precise and dependable. Figure 3 displays the viscosity against a time curve used in measuring the "gelation time" of the fluid and the picture of a completely gelled nanosilica-based fluid system.

Yard Test

The objective of this test was to evaluate the designed and up-scaled treatment from the batch mixer to the lab-scale formulation. Yard testing was essential to gauge the required time to mix nanosilica to get a quality mixture that matches experimental data. This will assist in designing the pumping schedule.

Breaker Tests

In case the water shutoff gel is solidified in the wellbore, a contingency plan has to be made to break the gel system. Therefore, we deliberate the ability to break the nanosilica gel system at a fixed reservoir temperature equivalent to 200 °F. We prepared and optimized breaker solutions by dissolving non-damaging breaker particles in field water at varied breaker concentrations.

Lab Test Results and Discussions

Gelation Time Test

Viscosity measurement is extremely important in gas/water shutoff applications to ensure desirable properties — an effective indicator of degree of curing. In addition, monitoring the time of curing the nanosilica gel system is essential in designing a proper placement and to avoid any risk during the operation. Throughout the injection into the targeted zone, the reservoir temperature will considerably be reduced and will influence treatment gelation time. The temperature reduction is more pronounced at a higher rate and volume.

Fig. 4 *The effect of temperature on the gelation time with a 40% activator.*

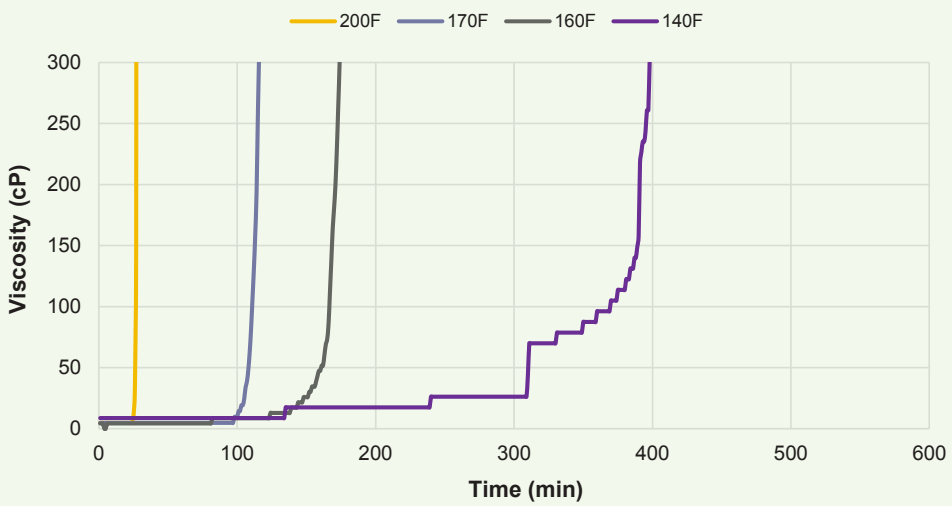

Fig. 5 *The effects of an activator concentration on the viscosity and gelation time.*

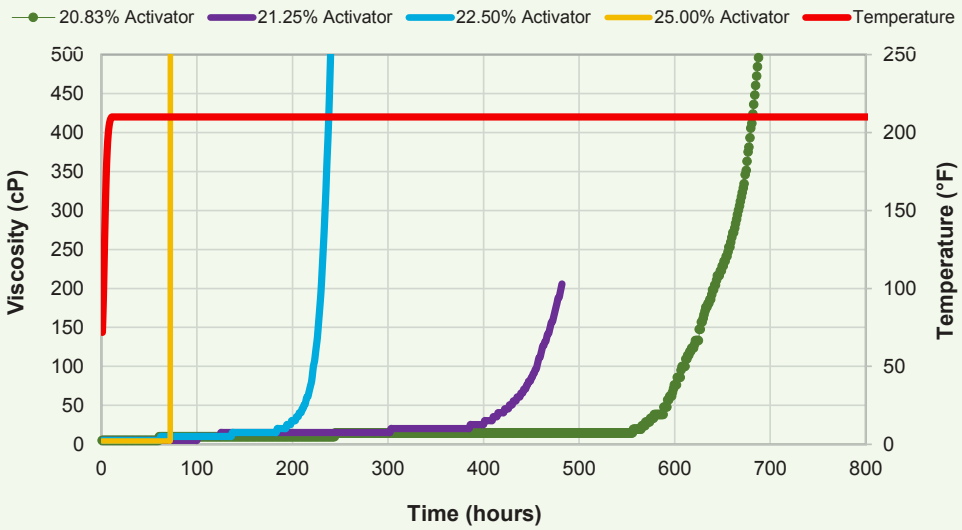

The gelation time of the nanosilica system is mainly based on two main factors: temperature and activator. The gelation time can be modified by the activator concentration and temperature. Figure 4 exhibits the variations in the gelation time of different fluid samples with respect to temperatures: 140 °F, 160 °F, 170 °F, and 200 °F, respectively. According to Fig. 4, the gelation time for a definite system, i.e., a system with a concentration of 40% activator, decreases with increasing temperature. The higher the temperature, the lower the zeta potential of the system. Consequently, the colloidal system becomes less stable and the gelation process is activated.

In addition, Fig. 5 depicts the viscosity vs. time for different formulations at 210 °F. The change in activator concentration greatly affects the gelation time. As seen in Fig. 5, with the same nanosilica, as the activator concentration increased from 20.83% to 21.25%, and 22.5% to 25%, the gelation time decreased from ~550 minutes to 400 minutes, and 190 minutes to 73 minutes, respectively.

Gel Breaker Test

As a contingency plan, we have looked into testing the ability to break the matured nanosilica gel. Out of this experiment, we managed to select the optimum breakage time and breaker concentration at 200 °F to simulate downhole conditions. The experiment was prepared using nanosilica with 20 wt% of activator. Then, we collected 50 ml of nanosilica and poured it into a glass bottle. After that, the glass bottle is placed in a water bath to gel up the nanosilica at 200 °F.

As shown in Fig. 6a, the nanosilica was gelled and fully matured. Following this, we mixed an equivalent volume (50 ml) of breaker sample using field water and 30 wt% of an active breaker. The breaker solution was then poured in the glass bottle on top of the gelled nanosilica at 200 °F. The bottle was positioned again in the water bath. It was observed that after two hours, the cured gel became a liquid solution again, indicating that the nanosilica gel was totally broken-down, Fig. 6b. This reversible process of the nanosilica gel system is a significant advantage of this technology; in case any gel resides in the wellbore that can be broken.

Yard Test Results

Figure 7 represents the batch mixing unit of 50 barrels. The batch mixing started by filling the tank initially

Fig. 6 *A snapshot of two beakers; (a) matured nanoslica gel, and (b) broken gel.*

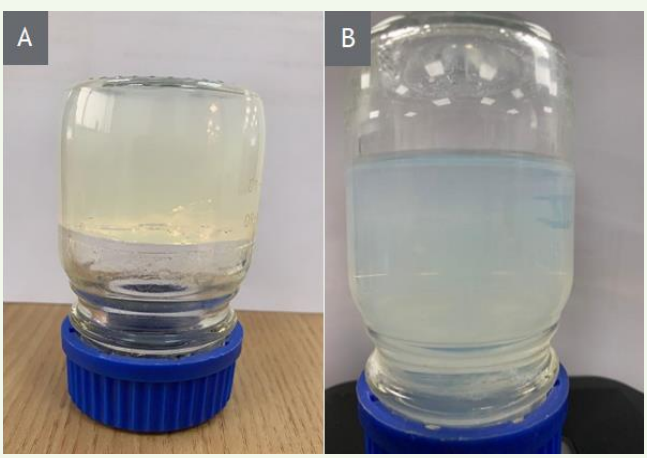

Fig. 7 *The actual batch mixer for oil field applications.*

Table 1 *The benchmark between the yard test and baseline.*

Nanosilica Fluid Properties (25% Act.) at 70 °F	Baseline	Yard Test
pH	11.7 – 12.0	11.78
Density (g/cc)	1.29 – 1.30	1.302
Viscosity (cP)	5 – 6	6

with the required volume of nanosilica fluid followed by the activator volume. After that, we collected a nanosilica solution sample from the batch mixer after 15 minutes of blending. Then, we measured the properties of the sample — and benchmarked it with a baseline, which was prepared earlier in the lab. The measurements incorporates viscosity, density and pH at ambient conditions.

Table 1 lists both samples, which have almost the same fluid properties. Additionally, we compared the gelation time of the baseline and yard test sample by conducting a rheology experiment using a HPHT rheometer at a bottom-hole temperature (BHT) of ~210 °F.

Figure 8 shows that the gelation time of the yard test sample (with 25% activator) is nearly 60 minutes, which is almost matches the gelation time of the baseline sample, which is approximately 70 minutes — with slight delay of 10 minutes. This confirms how accurate the batch mixing was for the yard test.

As for QA/QC in the field-test, we divided it into two parts. The first one is associated with blending

Fig. 8 *The gelation time of the yard test sample.*

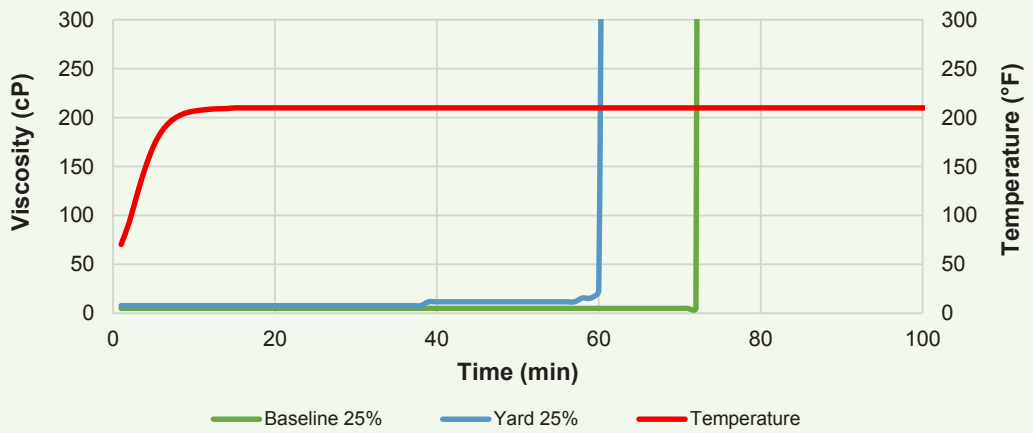

Fig. 9 *The production log clearly shows the gas contribution from the heel.*

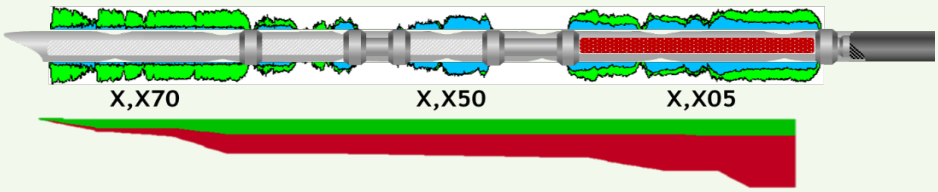

procedures, and the second one is linked to the fluid as explained in the yard test. The QA/QC procedures for blending were as follows:

- Ensure that all mixing equipment and hoses are uncontaminated and free of iron.
- Conduct a water analysis on each frac tank before mixing.
- Ensure that all drums and intermediate bulk containers/totes are not leaking.
- Mix each batch volume separately in a batch tank.
- Collect samples periodically.

Treatment Objective

The main objective of this operation is to sustain reservoir energy by GSO treatment across the gas producing zone as shown from the production log, Fig. 9. The objective of this operation is to isolate the gas production interval by using the newly developed nanosilica fluid system as the complete sealing material.

A coil tubing (CT) using real-time technology was proposed as the most applicable option to convey the nanosilica fluid system and selectively place it into the zone of interest. Through this intervention process, the main steps of the job are as follow:

1. Run in the hole (RIH) with a conventional CT to drift and cleanout the wellbore with a hydraulic jetting tool to ensure that the planned plug setting depths are clear of dirt/debris and provide an adequate seal for pumping/isolation. The cleanout was performed at a high rate while reciprocating across the targeted interval. Thereafter, a bottoms up was performed to ensure clean returns before pulling out of the hole to the surface.
2. RIH with an E-coil to set a permanent millable plug at the blank pipe section below the gas production zone; confirmed from the production log. This is to ensure that the squeezed treatment fluid will not permeate to the lower oil producing zone, inducing damage. The plug setting was confirmed by slacking the CT weight.
3. Using an E-coil, the temperature and pressure profiling has been performed along the gas zone. The temperature has been changed after injecting treated water to cool-down the formation.
4. RIH with a conventional CT to set an inflatable packer above the upper screens and pump a GSO treatment with nanosilica chemical technology. This is to ensure that the tubing and the blank pipe section of the completion is free of nanosilica residuals. The packer setting was confirmed by slacking the CT weight.
5. Mill out the copperhead plug after 30 hours of

Fig. 10 *The recorded temperature profile after pumping 200 barrels of treated water.*

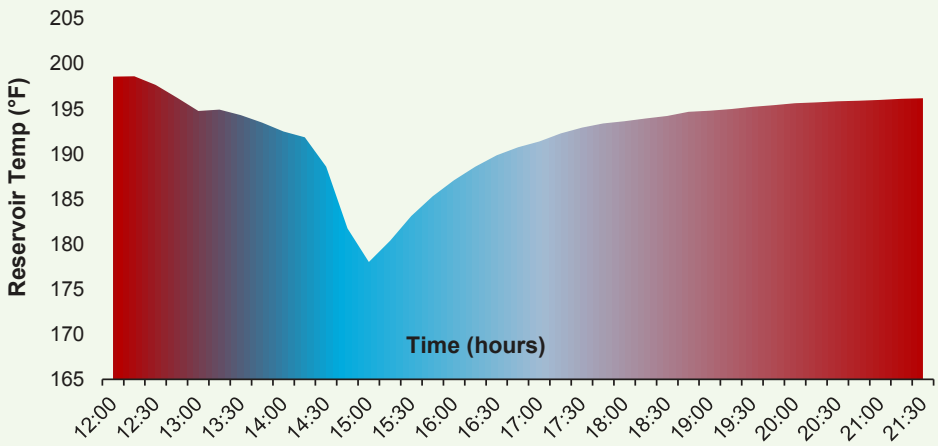

curing time with a conventional CT. This step is intended to reestablish the flow path between the upper part of the completion with the lower oil producing zone after sealing off the gas cusping zone with nanosilica.

6. Clean out and flow back the well to check the well's ability to flow.

The well was further initially evaluated for mechanical GSO means; however, the length of the interval mandated another solution that fits the challenging completion characteristics of the well.

Treatment Selection

The nanosilica fluid system was designed to form a rigged gel when activated by reservoir temperature. It can produce an in situ glass-like material inside the matrix when exposed to gas, where gas will dehydrate nanosilica to form a strong gel system. This system can be an effective method to plug the targeted zone of interest that caused the gas production. The newly developed system was proposed to achieve the target in this challenging gas zone.

This system was tested in a Brea sandstone core having 24% porosity and 370 mD gas permeability at 200 °F. After curing the nanosilica system inside the matrix, there was no gas flow through the core plug, indicating a complete core plugging[8]. The goal of using the nanosilica fluid system was to help isolate the gas interval. The technology is based on nanoscale particle size (~14 nm) at low viscosity (< 10 cP) to enable deeper formation penetration, as well as the ability to plug the target zones with a controlled gelation time. The proposed technology is fully controlled and reversible, making the treatment one of the safest and eco-friendly operations in the industry.

Field Implementation

In considering the volume to be pumped over a long interval, the pumping duration must be estimated based on the injectivity, along with the pumping rate and cooling effect. Figure 10 shows the recorded temperature profile after pumping 200 barrels of treated water, where the temperature dropped from 198.8 °F to 179.5

Fig. 11 *The actual gelation time design for field implementation.*

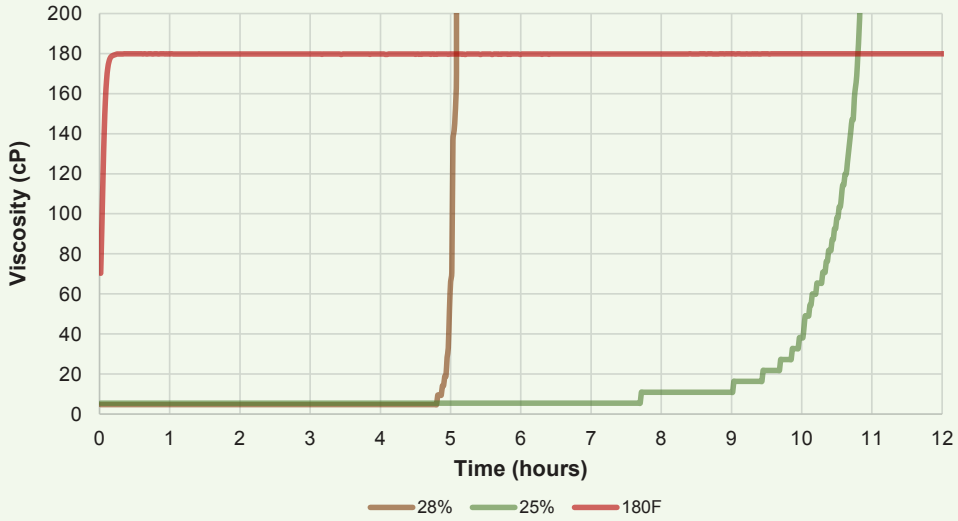

Table 2 *The pumping schedule (574 bbl in total).*

No.	Description	Fluid	Pump Rate (bbl/min)	Vol Pumped (bbl)	Time (min)	Cum. Time (min)
1	Treatment 1	GSO	2	200	100	150
2	Treatment 1	GSO	1.5	150	100	250
3	Treatment 1	GSO	1	150	150	400
4	Treatment 2	GSO	1	80	80	480
5	Displacement	TW	1	80	80	560

Fig. 12 *The depth of penetration for both treatments.*

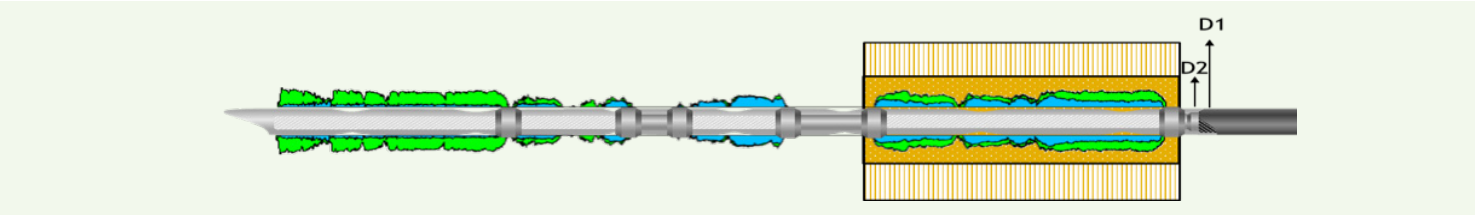

°F. Then, after 5 hours, the BHT almost returned to the original temperature.

Based on the formation temperature, the interval of the zone to be isolated, and the desired depth to penetrate into the subterranean formation around the wellbore, the main treatment volume was determined to be 560 barrels. Two batches were proposed with a longer and shorter gelation time, 10 hours and 5 hours, respectively. The first batch having a longer — 10 hours — gelation time for a deeper depth of penetration. Followed by the second batch, a shorter gelation time — 5 hours, Fig. 11. The purpose of this strategy was to ensure quicker gel development near the wellbore; therefore, improve the plugging efficacy.

A reasonable gelation time should be sufficient to allow pumping of the gellable treatment composition through the CT into the target zone. Table 2 summarizes the pumping of both chemical batches; gelation times of 10 and 5 hours, respectively. As a result, the depth of penetration of the first treatment — 10 hours gelation time — was calculated to be around 3.0 ft (D1), by pumping 500 bbl. After completing the first batch, the second treatment was pumped — a gelation time of 5 hours — with 80 bbl, achieving 1.2 ft of depth invasion (D2)), Fig. 12. Therefore, a total of 580 bbl of nanosilica was prepared and squeezed, helping to ensure 4.2 ft of radial of penetration.

After 30 hours of soaking time, the CT start to drift in the well to mill the copperhead plug and tag the plug at a targeted zone. After several attempts, the CT succeeded in milling the plug and started to drift it to the total depth. After the job, the well was flowing naturally for the last 48 hours to the GOSP and it was tested using a three-phase portable separator under different choke sizes. The rate test showed sustainable well performance with a fourfold reduction of GOR, Fig. 13, at a flowing wellhead pressure of 580 psi and 430 psi downstream pressure, implying the effectiveness of the technology by reducing gas production by more than 65%.

Fig. 13 *The trend post-treatment production.*

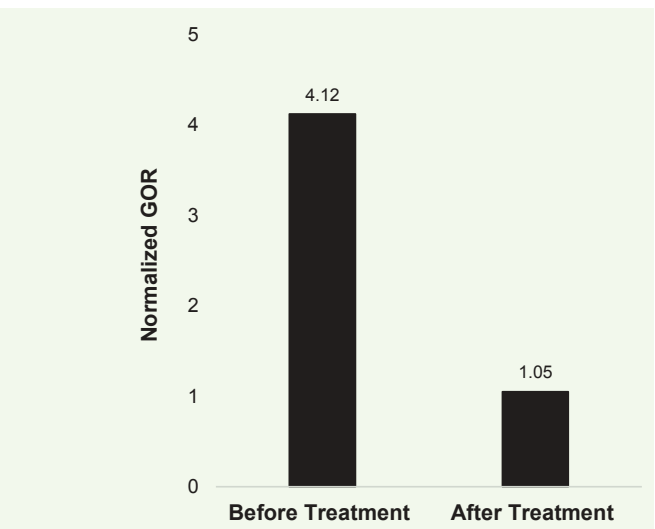

Summary and Conclusions

The nanosilica proved its efficiency to shutoff unwanted gas once the candidate selection, lab testing, job design, and execution are completed properly. For this trial test, adequate reservoir isolation was confirmed based on separate portable tests. The gas interval to be isolated was detected using logging tools. A proper wellbore isolating retrievable plug and an inflatable packer were set using live CT with a real-time downhole casing collar locator, and tension compression and pressure. Intensive lab testing was conducted to cover the required gelation time range. A live CT pipe with real-time downhole temperature measurement was used to monitor the squeeze pumping rate along with the cooling and warm back, which helped to precisely formulate the different nanosilica formulations.

The presented work details the engineered process established to address GSO intervention using a promising nanosilica fluid system for GSO applications. This rigless operation is a cost-effective alternative compared to other solutions. The proposed technology features the following:

- By composition, nanosilica is eco-friendly and environmentally acceptable.
- A water-thin liquid phase that can be injected easily and deeply in a single pumping stage.
- It has easy to mix components; nanosilica and activator.
- It can be formulated with a wide range of gelation time from minute to hours.

- Any excess inside the wellbore can be easily removed either by high-pressure jetting or by a dissolution chemical.
- All these benefits will help increasing the worldwide low success rate of water and GSO treatments.

References

1. Huang, T., Crews, J.B. and Agrawal, G.: "Nanoparticle Pseudo-Cross-Linked Micellar Fluids: Optimal Solution for Fluid Loss Control with Internal Breaking," SPE paper 128067, presented at the SPE International Symposium and Exhibition on Formation Damage Control, Lafayette, Louisiana, February 10-12, 2010.
2. Belcher, C., Seth, K., Hollier, R. and Paternostro, B.: "Maximizing Production Life with the Use of Nanotechnology to Prevent Fines Migration," SPE paper 132152, presented at the International Oil and Gas Conference and Exhibition in China, Beijing, China, June 8-10, 2010.
3. Habibi, A., Ahmadi, M., Pourafshary, P. and Ayatollahi, S.: "Reduction of Fines Migration by Nanofluids Injection, an Experimental Study," SPE paper 144196, presented at the SPE European Formation Damage Conference, Noordwiji, the Netherlands, June 7-10, 2011.
4. Almohsin, A.M., Hung, J., Alabdrabalnabi, M.I. and Sherief, M.: "A Nano Method for a Big Challenge: Nanosilica-Based Sealing System for Water Shut-Off," SPE paper 204840, prepared for presentation at the SPE Middle East Oil and Gas Show and Conference, Manama, Kingdom of Bahrain, November 28-December 1, 2021, event canceled.
5. Lakatos, I., Lakatos-Szabo, G. and Szentes, G.: "Revival of Green Conformance and IOR/EOR Technologies: Nanosilica Aided Silicate Systems — A Review," SPE paper 189534, presented at the SPE International Conference and Exhibition on Formation Damage Control, Lafayette, Louisiana, February 7-9, 2018.
6. Almohsin, A.M., Huang, J., Karadkar, P. and Bataweel, M.: "Nanosilica-Based Fluid System for Water Shut-Off," WPC paper 22-0468, presented at the 22nd World Petroleum Congress, Istanbul, Turkey, July 9-13, 2017.
7. Huang, J., Al-Mohsin, A.M., Bataweel, M., Karadkar, P., et al.: "Systematic Approach to Develop a Colloidal Silica-Based Gel System for Water Shut-Off," SPE paper 183942, presented at the SPE Middle East Oil and Gas Show and Conference, Manama, Kingdom of Bahrain, March 6-9, 2017.
8. Karadkar, P., Almohsin, A.M., Bataweel, M. and Huang, J.: "In Situ Pore Plugging Using Nanosilica-Based Fluid System for Gas Shut-Off," SPE paper 197578, presented at the Abu Dhabi International Petroleum Exhibition and Conference, Abu Dhabi, UAE, November 11-14, 2019.
9. Al-Dhafeeri, A.M., Nasr-El-Din, H.A., Al-Mubarak, H.K. and Al-Ghamdi, J.: "Gas Shut-Off Treatment in Carbonate Reservoir for Oil Wells in Saudi Arabia," SPE paper 114323, presented at the SPE Annual Technical Conference and Exhibition, Denver, Colorado, September 21-24, 2008.
10. Joshi, S.D.: *Horizontal Well Technology*, PennWell Corporation, 1991, 535 p.

About the Authors

Dr. Ayman M. Al-Mohsin

Ph.D. in Petroleum Engineering, Missouri University of Science and Technology

Dr. Ayman M. Al-Mohsin joined Saudi Aramco in 2014 as a Research Engineer. He is currently a Petroleum Engineer working in Smart Fluid Focus Area in the Production Technology Division of Saudi Aramco's Exploration and Petroleum Engineering Center – Advanced Research Center (EXPEC ARC). Ayman's research interests include water and gas shutoff using chemical means.

He received his B.S. degree in Mechanical Engineering from the University of New Haven, West Haven, CT; his M.S. degree in Petroleum Engineering from New Mexico Tech, Socorro, NM; and his Ph.D. degree in Petroleum Engineering from Missouri University of Science and Technology, Rolla, MO.

Hassan W. Al Hashem

M.S. in Petroleum Engineering, Texas A&M University

Hassan W. Al Hashem is an Engineer working in the Upstream Innovation Center of Saudi Aramco's Southern Area Reservoir Management Department. He is responsible for overseeing the company's ambitious program to leverage and develop artificial intelligence solutions to transform the oil and gas industry toward digitization.

Prior to this, Hassan worked as a Reservoir Engineer, mandating and setting strategies to implement sustainable solutions for over 12 fields.

He is the recipient of multiple awards, including the McDougall School of Petroleum Engineering Honor Award, Harold Vance Department of Petroleum Engineering Paper Contest Award and Saudi Aramco Petroleum Engineering and Development Significant Reservoir Management Study Award.

Hassan received his B.S. degree in Petroleum Engineering from the University of Tulsa, Tulsa, OK, and an M.S. degree in Petroleum Engineering from Texas A&M University, College Station, TX.

Ali A. Sadah

B.S. in Petroleum & Natural Gas Engineering, Pennsylvania State University

Ali A. Sadah is a Petroleum Engineer working in Saudi Aramco's Southern Area Production Engineering Department, in the Khurais area. He has 10 years of experience with the company. Ali's experience revolves around the area of electric submersible pumps, gas lift and well intervention.

He also participated in two six-month assignments, one with the Workover Operations Department, and one with the Reservoir Management Department.

In 2012, Ali received his B.S. degree in Petroleum & Natural Gas Engineering from Pennsylvania State University, State College, PA.

Mesfer N. AlQahtani

B.S. in Petroleum Engineering, King Fahd University of Petroleum and Minerals

Mesfer N. AlQahtani is a Production Engineer working in the Khurais Production Engineering Division of Saudi Aramco's Southern Area Production Engineering Department. He has also held several drilling, well completion and unconventional resources positions, covering several onshore and offshore fields.

Mesfer's areas of interest include rigless intervention with coiled tubing (CT), wireline, and compacted workover operations. Throughout his career, Mesfer has worked in multiple projects, including the change out of electric submersible pumps utilizing wireline, and implemented several technologies utilizing in-house chemicals for unlocking well potential and enhancing oil recovery purposes.

In 2010, he received his B.S. degree in Petroleum Engineering from King Fahd University of Petroleum and Minerals (KFUPM), Dhahran, Saudi Arabia.

High Rate Slim ESP Viability Assessment in the Field

Fahad A. Shinaiber, Yhossie S. Windiarto, Mayadah M. Alhashem and Rui F. Pessoa

Abstract /

Producing oil at full potential with an electric submersible pump (ESP) in a slim well remains a challenge in the petroleum industry. A conventional slim ESP system is limited in produced oil delivery rate with an associated risk of damaging the motor lead extension (MLE) of the ESP during the running in hole due to tight clearance. Finding a high rate new slim ESP technology is crucial to enable production of wells at full potential and eliminate slot recovery. This article shares the success stories of testing two high rate slim ESP installations, and provides the advantages and disadvantages for each of the two approaches for a high rate slim ESP design.

The high rate slim ESP design options were assessed through field trials collaborating with different manufacturers. The slim ESP viability evaluation metrics were maximum rates, ESP performances, completion installation simplicity and surface controller compatibility. These metrics ensure eliminating unnecessary costs of ESP replacement in the field.

The first design option is an inverted ESP design with an induction motor installed at the top. Such a design is advantageous in allowing a pump with a bigger outer diameter (OD), eliminating MLE installation on the pump housing due to an increased clearance, and consequently achieving a higher rate.

The second design option uses a permanent magnet motor (PMM) in a standard ESP configuration. The second design with the smaller ESP OD allows high motor speed, thereby providing a higher head capacity and higher flow rate. A modification in the variable speed drive (VSD) design is required to enable controlling the PMM.

The field trial result revealed multiple benefits of the high rate slim ESP systems in the field. The high speed system that utilizes PMM retains the standard ESP configuration, which simplifies well completion and avoids installation complexity. The reduced ESP OD provides more clearance in the well, leading to minimized possible MLE damage during running in hole. Although the VSD modification is possible, the PMM maximum speed will be limited by the maximum capacity of the existing transformer installed in the platform.

Finally, both systems lead to a significant cost avoidance by eliminating the need for slot recovery of the produced well at full potential in a slim well, and avoiding unnecessary replacement of ESP surface equipment. The two systems were already successfully evaluated with a continuous run for more than 365 days without any issues.

Introduction

Artificial lift methods are necessary to meet oil demands worldwide. Currently, an electric submersible pump (ESP) is one of the main methods commonly utilized in the industry for artificial lift. ESPs are essential to achieve a high rate of oil production. They are designed per well installation to ensure maximum efficiency of the ESP system. There are certain well configurations that pose challenges for ESPs. One of which are slim wells. There are complications in the utilization of standard slim ESPs in these wells, such as pump rate limitations, long strings, and tight clearances. The latter two challenges increase the probability of ESP failure.

One of the reasons why slim well casings exist is due to the installation of full-length casing liners to protect the well completion from exposure to corrosive agents, including reservoir fluids and injected chemicals. Liners and other repairs to the casing reduces the internal diameter of the well. This limits the outer diameter (OD) size of the installed ESP system, and subsequently affects the maximum production flow rate[1].

Many fields around the world have well populations completed with slim casing (< 7”). Slot recovery was the only option to enable larger ESP installations and maximize well production. There has been limited research in the field of high rate slim ESPs to address the challenge of suitable ESP designs for slim casing.

One article discussed the qualification and performance of a high speed high rate slim ESP. It has a 3½” OD motor and can operate at a nominal speed of 6,000 rpm and produce up to 5,000 barrels per day (bpd) at the best efficiency point[1]. The ESP uses a permanent magnet motor (PMM) and an inverted configuration ESP design. It went through component testing, a full-size product test, and finally a system integration test that

used a 180-ft deep test well at a manufacturing facility. The final test included a 72-hour uninterrupted function test to assess if the ESP can run for an extended time without interruption. The study concluded with passing the prototyped ESP, but there was no mention of a field deployment.

Another article discussed the results of implementing an ultra-slim cable deployed ESP with an OD of 2.17" and has a PMM[2]. The ESP system was deployed on a carrying cable, eliminating the need of a rig crew. The cable deployed ultra-slim ESP was able to produce between 113 bpd to 1,132 bpd. The ESP system was installed in fields in the U.S., Russia, and Malaysia. The cable deployed ultra-slim ESP was mainly targeting reducing rig crew and workover costs, especially in highly deviated wellbores and sidetracks. It was not designed for high production rates.

In this study, two high rate slim ESP design options were assessed after their successful complete trial test. In evaluating both options, the advantages and disadvantages for each are discussed after field trials with different manufacturers. In addition to assessing the new slim ESP technologies, various ESP string configurations were also requested to maximize the utilization of existing assets installed.

The first slim hole ESP design (A) is an inverted ESP with an induction motor at the top section of the ESP, which eliminates the motor lead extension (MLE) on the pump housing and allows more clearance in the well. The extra clearance space is utilized by increasing the pump's OD, and therefore, increased the production rates. The second slim hole ESP design (B) is a standard ESP configuration with a PMM. The PMM requires a modification in the variable speed drive (VSD) to control the motor. While the second design has a smaller OD, it has a higher motor speed, head capacity, and flow rate.

Design Option (A)

The first design, option (A), is an inverted ESP with an induction motor in the top section of the ESP, Fig. 1. The following discusses the details of the design and performance of this design option.

Key Components

The conventional slim ESP system traditionally has the motor installed at the bottom of the ESP below the pump. This configuration dictates that the MLE is installed on the pump housing section. Therefore, the clearance of the standard slim ESP is minimized as opposed to the proposed inverted configuration by over 90%. The inverted slim ESP — design option (A) — places the motor at the top and the pump at the bottom of the ESP. This design option eliminates having the MLE installed on the pump housing section. Therefore, the clearance between the casing and ESP is increased.

Pump: The modified inverted ESP configuration allows installing a larger OD pump to produce at a higher rate. In a standard ESP configuration, the load generated from the pump will be handled by the protector below the pump. Due to the reversed ESP configuration where the protector and motor sit above the pump, a special design is required to allow the ESP system to handle the load or thrust generated by the pump. A pinned shaft connection is used, which allows the load or thrust to be transmitted to the protector above the pump.

Motor: Three tandem induction motors are required due to the limitation on the maximum horsepower per housing available in a conventional slim induction motor. The modification of the upper tandem motor head is necessary to reduce the clearance of the pothead

Fig. 1 *A schematic of an inverted ESP.*

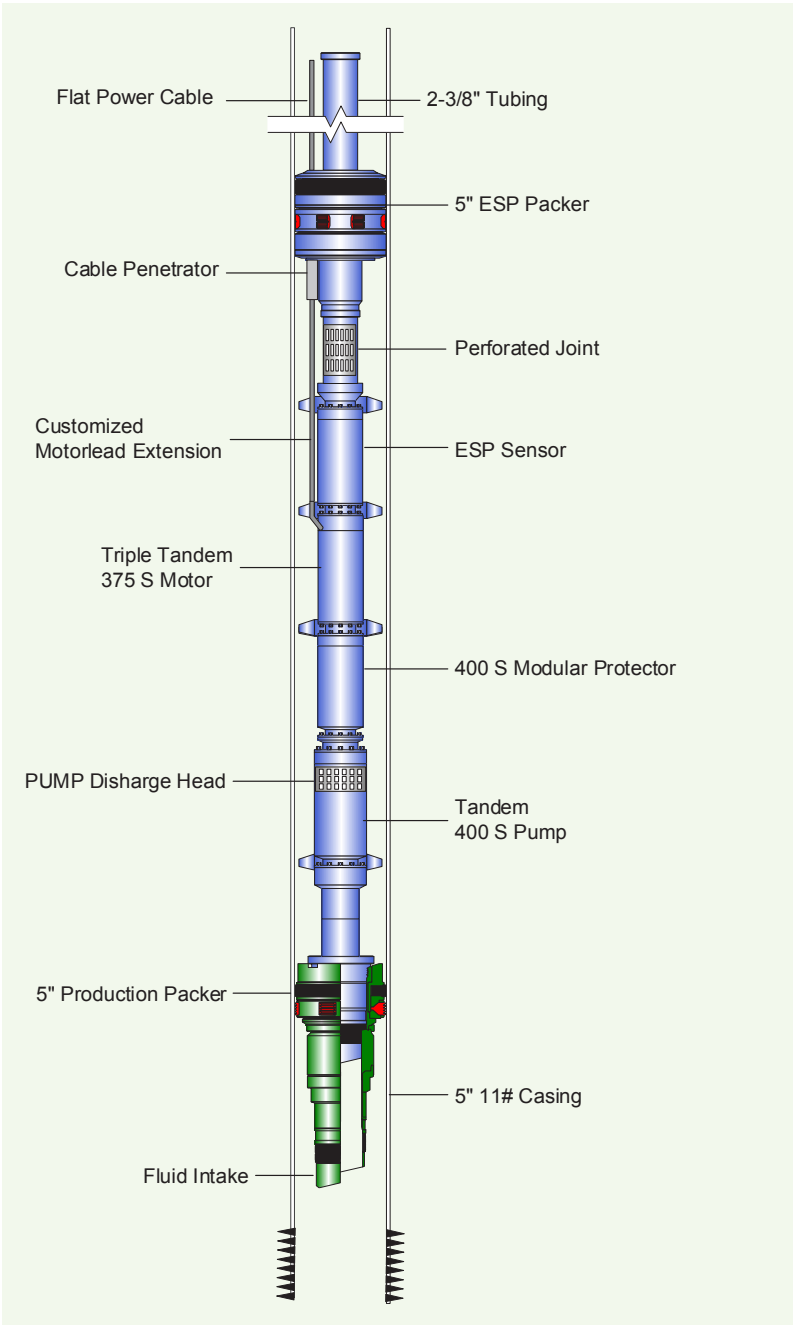

and MLE combined OD.

Metallurgy: Due to the tight clearance, the maximum flow rate was determined by erosion velocity guidelines, which was verified through a computational fluid dynamics simulation. A suitable maximum flow rate selection protects the ESP from the erosion effect to the casing and downhole completion. A proper ESP housing metallurgy was selected in accordance to the recommended maximum erosion velocity.

Slim ESP Packer: The ESP packer design is a retrievable hydraulic set packer, which has an integrated penetrator system to carry three-phase ESP power cables. The inverted ESP is installed between two packers. The lower packer eliminates fluid recirculation from the pump's discharge into the intake. The upper ESP packer protects the casing from well fluid by diverting the produced fluid from the casing and ESP annulus back to the tubing.

Perforated Joint and Discharge Pressure: A special design of the perforated joint and pump discharge pressure vanes is critical to minimize the inertial effects of high pumping fluid velocity through the restrictive opening. The eliminated jetting effects would have led to potential damage on the MLE and cause casing erosion.

Slim ESP Design

Having a proper ESP design and sizing is of great importance for a successful trial of the inverted slim ESP. The model to size the ESP and select equipment used in the design data, include the inflow performance, pressure-volume-temperature (PVT) data, back pressure, well geometry, and target flow rate.

Based on the input data, the flow performance curves and pump curves, the pumping conditions, pump information, protector, motor, MLE, cable, sensor, and conditions at operating frequency were determined.

ESP Performance Analysis

The inverted slim ESP performance was evaluated in a function test as the flow rate was measured across power ranges based on the pump curves. The pump was continuously run within its operating range and met expected flow rates, and proved capable of producing double the rate in comparison to a conventional slim ESP.

There was no major concern during the slim ESP operation. An analysis conducted 1½ years later also revealed no concern during operation despite the increase in downhole rate and water cut.

Design Option (B)

The second high rate, high speed slim hole ESP design, design option (B), is a standard ESP configuration with a PMM, Fig. 2. The following details the design and performance of this design option.

Key Components

Pump: A unique pump design with powder metallurgy-based stages is selected to deliver the target rate. The new metallurgy offers a better stage surface finish, which reduces friction against the flow. The new design delivers higher power efficiency with all the mechanical rotating parts that are designed for high speed (up to 6,000 rpm). The pump was also precisely balanced to decrease vibration and increase reliability.

Following the affinity laws, running with higher pump speed delivers higher discharge flow. The pump has an OD of 3.19", allowing it to have a larger clearance to reduce any potential damage of the MLE installation on the pump housing section.

PMM: Compared to the induction motor, the PMM provides a higher power factor and higher efficiency. The rotor magnets are made of rare earth alloys. The stator is filled with a special high temperature epoxy, which significantly increases insulation resistance. Strong permanent magnets provide higher magnetic flux, leading to a higher power density. The PMM requires a special surface controller and control algorithm to enable tracking the rotor position for the following requirements:

- Control the motor stator and rotor magnetic field flux at a nearly 90° angle.
- Always synchronize the stator magnetic fields with the rotors to maximize torque and eliminate slip.

Overall, the PMM selection delivers more benefits compared to the conventional induction motor, including higher efficiency and power density in a shorter housing. The 3.19" motor OD provides larger clearance

Fig. 2 *A schematic of a high speed ESP.*

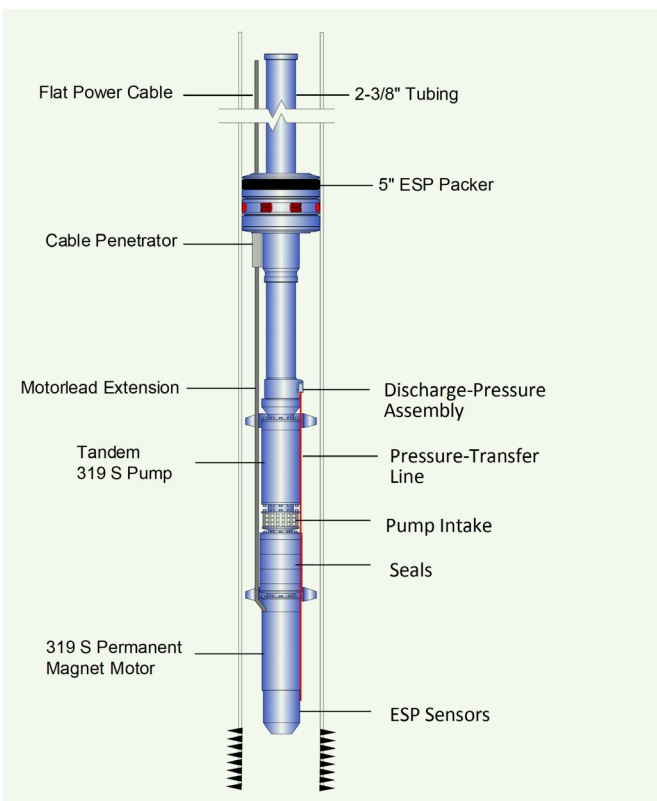

and allows the installation of the sensor line, thereby enabling pump discharge pressure monitoring and optimization.

Modular Slim Protector: The protector provides pressure equalization between the motor and wellbore, and carries the thrust load of the pump. A slim 3.19" OD modular protector was selected to provide additional seals and protection, which consequently extends the ESP run life. It serves to improve performance in wells with highly abrasive laden fluids.

A new design of the head incorporates a special sand diverter system, which forces any sand particles falling from the intake to drop back into the annulus through the drain holes. Using the modular system, the protector was designed to meet specific application requirements according to the well environment.

VSD: A modification in the VSD to control the motor is required to reach the maximum efficiency while operating a PMM. The surface control logic in the VSD is required to track the actual position if the rotor is in the downhole motor and ensure that the stator magnetic field is perpendicular to the rotor magnetic flux generated by the permanent magnets.

To operate the slim ESP with PMMs, a VSD upgrade was completed to modify the existing VSD rather than the costly and challenging replacement of the old VSD using a designed VSD upgrade kit.

Slim ESP Packer: A new slim ESP packer penetrator, the first of its kind in the industry, was developed, qualified, and installed to enable the trial testing and installation of the high rate, high speed slim hole ESP.

Slim ESP Design

Having a proper ESP design and sizing is of great importance for a successful trial of the high rate, high speed slim ESP. The model to size the ESP and select equipment used design data, including inflow performance, PVT data, back pressure, well geometry, and target flow rate.

Based on the input data, the flow performance curves, and pump curves, the pumping conditions, pump information, protector, motor, MLE, cable, sensor, and conditions at operating frequency were determined.

ESP Performance Analysis

The high rate, high speed slim ESP as well as the VSD performances were evaluated in a function test as the flow rate was measured across power ranges based on the pump curves. The high speed slim ESP met the required flow rates and proved capable of producing double the rate in comparison to a conventional slim ESP.

The pump was continuously running within its operating range. There was no major concern during the slim ESP operation. An analysis conducted 2 years later revealed no concern during operation despite the increase in the downhole rate.

Discussion and Conclusions

The results of the field trials revealed the multiple benefits of the two high rate slim ESP systems in the field. The inverted slim ESP design (option A) allowed utilizing a bigger pump and eliminated installing the MLE on the pump housing, which consequently led to minimizing the possible MLE damage during running in hole. Because it used an induction motor, the inverted ESP eliminated the VSD modification requirement and avoided the cost associated with the VSD modification.

The completion architecture of the inverted slim ESP is slightly complicated, which requires minor customization such as to the perforated joint, motorhead of the upper tandem pump to reduce the OD, and pin-shaft at the pump. The pump pin-shaft allows the pump thrust to be transmitted to the protector installed above the pump. The additional packer requirement below the ESP also adds installation cost and rig time.

The high speed system that utilizes PMM (option B), retains the standard ESP configuration, which simplifies well completion and avoids installation complexity. The 3.19" slim ESP compact design affects the total ESP length, making it shorter and less likely to bend the equipment during handling and installation. Although the VSD modification is possible, the PMM maximum speed is limited by the maximum capacity of the existing transformer installed in the field. The high efficiency of the high speed system reduces the required power to produce even higher rates. Expanding installations are necessary to gain more experience in operating a high speed pump and PMM.

Finally, both systems could lead to a significant cost avoidance via eliminating the need for slot recovery of the produced well at full potential in a slim well, and avoid the unnecessary replacement of ESP surface equipment. The two systems were successful in the technology evaluation with a continuous run for more than 720 days without any issues. While extended field performance and multiple installations would confirm the advantages and disadvantages of using either slim ESP design configurations, Table 1 is a brief comparison between the two design options.

Free-Gas Accumulation

While tangible results have so far shown promising performance for both designs, there is a specific concern on the possible free gas accumulation that could affect the reliability of the inverted slim ESP system. Based on the general PVT behavior of oil, oil can appear as mono-phased as liquid with dissolved gas under certain PVT conditions.

With time, some of the dissolved gas in the well fluid will diffuse through the ESP seal into the motor fluid (dielectric oil). The dielectric oil has its own PVT properties and bubble point compared to reservoir fluid. As downhole pressure and temperature change with hydrocarbon depletion or during shutdown and start-up, the dielectric oil can go P_{bubble} or above T_{bubble}, causing the gas to break out of the solution in the motor, ESP seal, or both.

Due to gravity, the free gas will move upwards, accumulating at the top of the ESP components (such as the sensor, motor, and the seal chambers). As the

Table 1 *A brief comparison between the two design options.*

Feature	Design (A)	Design (B)
Description	Inverted slim ESP with an induction motor	Standard slim ESP configuration with a PMM
Rate	140% higher than conventional slim ESPs	60% higher than conventional slim ESPs
Diameter	2.4″ 42% less than conventional slim ESPs	3.2″ 10% less than conventional slim ESPs
Motor Efficiency	78%	95%
VSD Upgrade Required?	No	Yes, to control PMM motor

gas displaces the dielectric oil, it will affect the motor lubrication and increase the motor temperature. The concern is elevated in harsh conditions as gas would contain hydrogen sulfide and corrode the internal copper components of the ESP. The described phenomena is expected, depending on the bubble point and operating pressure at ESP setting depth. If the pressure is above P_{bubble}, free gas accumulation is not expected.

Recommendations

Because of trial testing and evaluating the two slim ESP designs discussed in this study, the following is recommended to capitalize on the benefits of these technologies in slim wells:

- Expand the ESP portfolio to include high rate inverted slim ESPs and PMM high speed slim ESPs for operational experience and future slim ESP technology advancement.

Such practices would enhance the developing ESP technologies and make them more available for slim wells.

Acknowledgments

This article was presented at the SPE Middle East Artificial Life Conference and Exhibition, Manama, Kingdom of Bahrain, October 25-26, 2022.

References

1. Lastra, R., Xiao, J., Lee, W. and Radcliffe, A.: "High Speed High Rate Slim ESP Development and Qualification Testing," SPE paper 194399, presented at the SPE Gulf Coast Section Electric Submersible Pumps Symposium, The Woodlands, Texas, May 13-17, 2019.

2. Gorbunov, D.: "Ultra-Slim Cable Deployed ESP Systems for Oil Field Development and Production," SPE paper 187733, presented at the SPE Russian Petroleum Technology Conference, Moscow, Russia, October 16-18, 2017.

About the Authors

Fahad A. Shinaiber

B.S. in Petroleum Engineering, Montana Tech University

Fahad A. Shinaiber is the Head of the Artificial Lift Division in Saudi Aramco's Production and Facilities Development Department. He oversees all electric submersible pump increment projects in Saudi Aramco's onshore and offshore fields, and the introduction of new artificial lift technologies to Saudi Aramco.

Fahad also has experience working on a number of diversified development projects in Saudi Aramco's offshore and onshore Northern Area fields as a Production and Reservoir Engineer.

He has been an active member of the Society of Petroleum Engineers (SPE) for 26 years, serving as Chairman for multiple SPE Artificial Lift conferences and forums in the Middle East.

In 1999, Fahad received his B.S. degree in Petroleum Engineering from Montana Tech University, Butte, MT.

Yhossie S. Windiarto

B.S in Petroleum Engineering, University of UPN "Veteran"

Yhossie S. Windiarto is a Petroleum Engineer working in the Artificial Lift Unit within Saudi Aramco's Production & Facility Development Department He has over 20 years of artificial lift experience in operations, marketing, and engineering. Prior to joining Saudi Aramco in 2012, Yhossie worked for Schlumberger's Artificial Lift Unit in several locations, including Oman, Indonesia, and Saudi Arabia.

In 1999, Yhossie received his B.S degree in Petroleum Engineering from the University of UPN "Veteran," Yogyakarta, Indonesia.

Mayadah M. Alhashem

M.S. in Mechanical Engineering, King Abdullah University of Science and Technology

Mayadah M. Alhashem is an Artificial Lift Engineer, currently working in the Production Technology Division of Saudi Aramco's Exploration and Petroleum Engineering Center – Advanced Research Center (EXPEC ARC).

Her experience in artificial lift is focused on the latest electric submersible pump (ESP) technologies and ESP failure analysis. Out of her drive to utilize Fourth Industrial Revolution technologies in engineering solutions, she obtained several online certifications, including Python and machine learning.

Mayadah has several issued patents, and is the author of several publications on utilizing machine learning in oil and gas facilities applications.

She received her B.S. degree in Chemical Engineering from University of Southern California, Santa Barbara, CA and her M.S. degree in Mechanical Engineering from King Abdullah University of Science and Technology (KAUST), Thuwal, Saudi Arabia.

Rui F. Pessoa

M.S. in Petroleum Engineering, University of Tulsa

Rui F. Pessoa is a Petroleum Engineer Specialist working as a subject matter expert in the Technical Support Unit of the Artificial Lift Division of Saudi Aramco's Production & Facilities Development Department. He has over 28 years of experience in artificial lift, mostly dedicated to the electric submersible pumping (ESP) method. Rui started his career in 1993 as an ESP Scientist at Intevep, the R&D branch of Venezuela's National Oil Company, PDVSA. He did lab research on pump performance with free gas, high viscosity fluids, gas-liquid separators, ESP with hydro-cyclone for downhole water separation, etc. Rui also provided technical support to PDVSA operational units for all aspects related with ESP, and facilitated several courses.

He switched to the oil and gas services sector with Baker Hughes (BH) in 2005 working for the Artificial Lift Services (ALS) product line where he worked in several positions, such as Lead Application Engineer, Regional Engineer for Latin America, Project Engineer and Engineering Manager. Some of his duties included design, sizing, commissioning, optimization, troubleshooting and reliability of ESPs for a number of customers across several countries. Rui was BH's lead engineer responsible for high-end and renamed ESP subsea projects such as Shell's BC-10 Parque das Conchas and Enauta's Atlanta, and the phase 1 of Equinor's offshore development Peregrino.

Prior to joining Saudi Aramco in 2017, he was working at BH-ALS headquarters and manufacturing facility in the U.S. providing ESP technical support worldwide and end-to-end product engineering improvement.

Rui is the author/coauthor of over 20 papers on ESP.

He received his B.Eng. degree from the Universidad Central of Venezuela, Caracas, Venezuela, and his M.S. degree from the University of Tulsa, Tulsa, Oklahoma, all in Petroleum Engineering.

LWD Laterolog vs. Electromagnetic Propagation Measurements: Which is Telling the True Resistivity?

Ida Bagus Gede Hermawan Manuaba, Mohammad K. Aljishi, Marie Van Steene and James Dolan

Abstract /

The electromagnetic propagation (EMP) measurement frequently acquired with logging while drilling (LWD) tools in high angle wells is sensitive to geometric effects that can mask the true formation resistivity (Rt). Less commonly used, the LWD laterolog measurement is sometimes perceived as providing data too shallow to give the Rt. This article presents modeling and actual examples to demonstrate that the laterolog can provide a superior resistivity measurement for formation evaluation than what the EMP LWD tool does.

We examine the laterolog and EMP resistivities in several high angle wells crossing carbonate formations in 8½" and 6⅛" hole sizes. In the 8½" sections, producers and water injectors (high and low resistivity ranges) were evaluated. In the 6⅛" sections, one reservoir sandwiched between two very high resistivity layers and another borehole in a highly fractured reservoir were examined. The laterolog data were corrected for invasion using a 1D inversion of the memory data. Structure-based forward modeling was used to examine and explain the differences between the resistivity methods.

In the first example, the laterolog data showed a clear conductive invasion profile. While the deepest laterolog real-time resistivity data indicated lower resistivity than the EMP resistivity, the Rt, from the 1D inversion, matched the EMP resistivity. This result validated both measurements and emphasized that those differences were due to invasion.

In the second example, a reservoir zone was initially drilled with resistivity measurements made only by the EMP tool. The LWD laterolog was run several days later, and the resistivity data were much lower in the relogged section compared with the EMP resistivity. The laterolog 1D inversion was unable to resolve the Rt because of the excessively deep invasion that occurred over the course of several days. These two examples demonstrated that when acquired in normal drilling conditions, the laterolog measurements can provide the uninvaded Rt, even in the presence of an invasion.

A reservoir in another example was sandwiched between resistive layers that caused difficult to explain elevated EMP resistivity readings. Structural modeling reproduced the elevated behavior of the EMP data and explained the differences between resistivity measurements. This result showed that the laterolog is better suited to evaluate resistivity in thin reservoirs where there is a high resistivity contrast to the adjacent layer.

Finally, fractured reservoir examples are presented, which show that both the laterolog and EMP can be affected by the presence of fracture swarms.

The examples presented in this article demonstrate that in high angle wells, under normal drilling conditions, invasion corrected laterolog resistivity is nearer to Rt than is the EMP resistivity. Furthermore, the laterolog measurement provides data that are better input to water saturation calculations.

Introduction

This article presents measurements made by two types of logging while drilling (LWD) resistivity tools. The tools are based on different physics principles, i.e., electromagnetic propagation (EMP) resistivity, and laterolog resistivity tools. These tools, measurements, and their use in high angle wells have been thoroughly described[1, 2].

The LWD EMP resistivity tool performs multispaced dual frequency (400 kHz and 2 MHz) measurements, delivering 10 phase shift and 10 attenuation resistivity measurements. The use of multiple transmitter receiver spacings and firings at different frequencies allows for resistivity measurements at various depths of investigation, ranging from ~0.5 ft to as deep as ~4 ft[1, 3]. The slim-hole EMP tool uses a single frequency of 2 MHz, delivering five phase shift and five attenuation resistivity measurements.

In high angle wells, deep resistivity measurements are sensitive to geometric effects, such as bed boundaries, proximity, and eccentering (in oil-based mud systems) effects, Fig. 1. Wu et al. (1996)[2] described the simple two-layer model used for radial resistivity inversion, which does not take shoulder bed effects into account.

Polarization horns occur when the LWD resistivity tool is approaching, crossing, or situated near a layer

Fig. 1 *Relation of axial resolution, bed boundary, and proximity effects[4], where T = transmitter and R = receiver.*

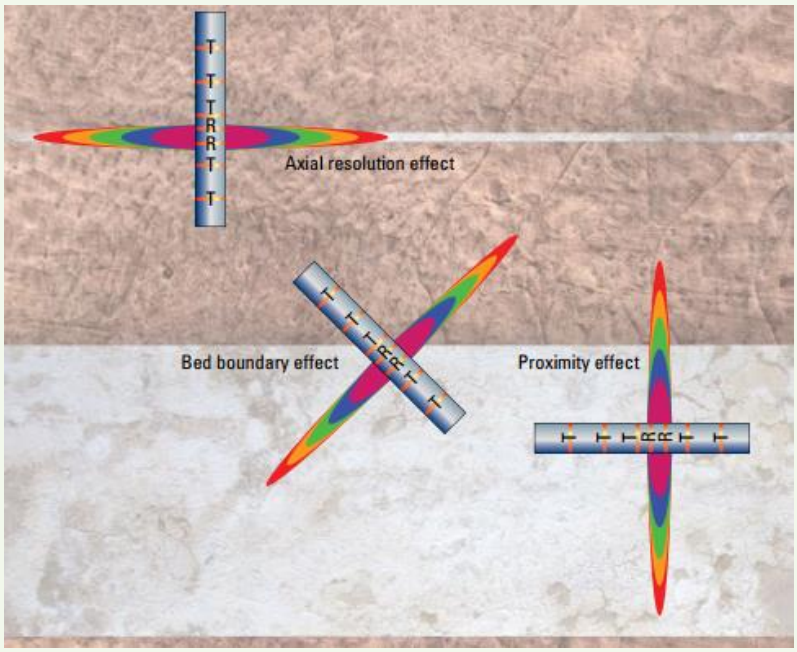

with contrasting formation resistivity (Rt) properties at a relatively low incidence angle, Fig. 2. Polarization horns result from the measurement currents being forced across both layers with contrasting Rt properties. They are caused by a buildup of charge at the layer interface, and the magnitude of the horn will depend on the incidence angle and resistivity contrast across the interface[4].

The LWD laterolog tool operates in water-based mud systems. The tool has two button electrodes and five toroidal antennas for relatively shallow focused laterolog resistivity measurements at multiple depths of investigation and with azimuthal sensitivity. This service also provides ultrahigh resolution resistivity images from a dedicated stabilizer sleeve containing eight buttons. This technology has been well described[5, 6].

Focused laterolog resistivity measurements are relatively shallow (approximately 1.5" to 6.5") compared with the EMP measurements, but they have better axial resolution — approximately 0.4" to 0.6". In high angle wells, the laterolog shallow depth of investigation is a benefit because the resistivities are less affected by nearby layers and bed boundary crossings. These laterolog resistivities are less influenced by bed

Fig. 2 *When EMP currents are forced to cross high angle formation boundaries with a resistivity contrast, polarization horns appear on the resistivity logs at the resistivity interface[4]. The drawing on the right represents phase shift resistivity (ohm.m) vs. depth (ft); the colors represent the different spacings.*

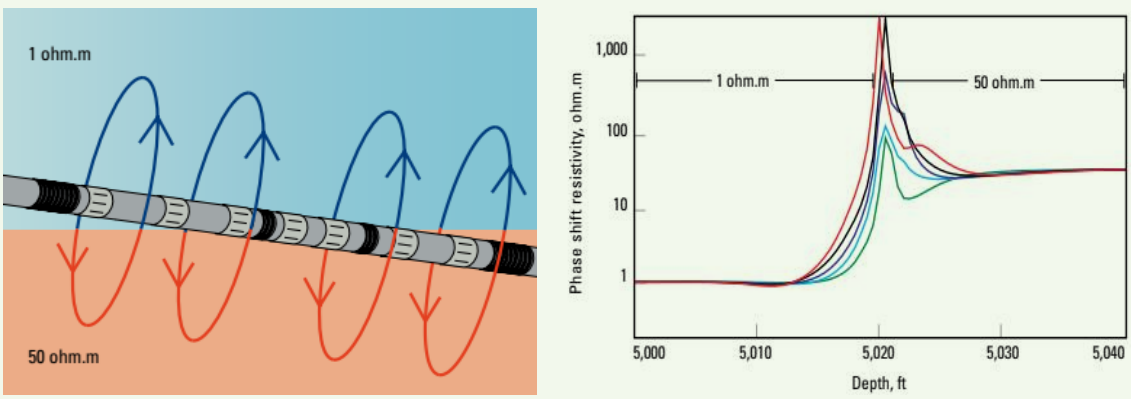

boundary and proximity effects, but are more sensitive to filtrate invasion than is the EMP resistivity due to the laterolog's shallower depth of investigation. This article will further develop the logging conditions in which the deep invasion effect on laterolog resistivity is more likely to occur.

The LWD laterolog resistivity measurements are made by two button sensors located on opposite sides of the tool collar. When the tool rotates, the buttons scan and bend the azimuthal measurements that are averaged into quadrant resistivities (up, down, left, and right). These quadrant measurements allow for detailed azimuthal petrophysical interpretation when the wellbore is nearby, to, or crossing lithological layers.

Laterolog inversion computation used to derive the uninvaded zone resistivity and flushed zone resistivity (Rxo) uses the traditional 1D radial step profile model of the borehole and formation[7]. The inversion provides the Rt (or unflushed zone resistivity), the invaded zone resistivity, and the diameter of invasion, starting from raw resistivity measurements. The process also contains a symmetrization step before the inversion for the 6¾" tools. The symmetrization step allows for eliminating the artifacts due to current distortion when the tool crosses bed boundaries of contrasting resistivities.

True Resistivity Determination Workflow

Figure 3 is the workflow used to determine the Rt. The first step in the workflow is to correct for invasion by applying a 1D invasion correction. This process is performed for both EMP and laterolog measurements. In this process, an automated logic for the EMP measurement[8] provides an estimate of the environmental effects by processing single-effect 1D models for anisotropy, dielectric, eccentering, invasion, and borehole that affect the EMP measurement. The Rt is also derived from the 1D laterolog invasion correction, as detailed earlier.

After estimating the environmental effects, the Rt values from the two inversions (EMP and laterolog) above can then be compared. If the resistivities agree within their measurement uncertainty[9, 10], then the conclusion is the Rt is known, unless both measurements are affected by the same environmental effects in the same way, which is unlikely. If the resistivities are not the same, additional investigation should be performed to comprehend the cause of the difference. 3D petrophysical modeling is a particularly powerful tool to investigate differences.

Thick Homogeneous Reservoir without Invasion

Well-1 was a deviated well, drilled in a water reservoir and to be used for water injection. In the reservoir zones, which were thick and homogeneous, there was no separation between the resistivities of the laterolog radial resistivity profile, Fig. 4 (in Track 3, RES_BS, RES_BM, RES_BD, and RES_BX, which are the laterolog shallow, medium, deep, and ultradeep resistivity curves, respectively). This result indicates that either there is no invasion at the time of LWD data acquisition, or if there is invasion, it is too shallow to affect the laterolog measurements.

The Rt_LAT and Rxo_LAT from the laterolog 1D

Fig. 3 *The workflow to determine the Rt from LWD EMP and laterolog measurements.*

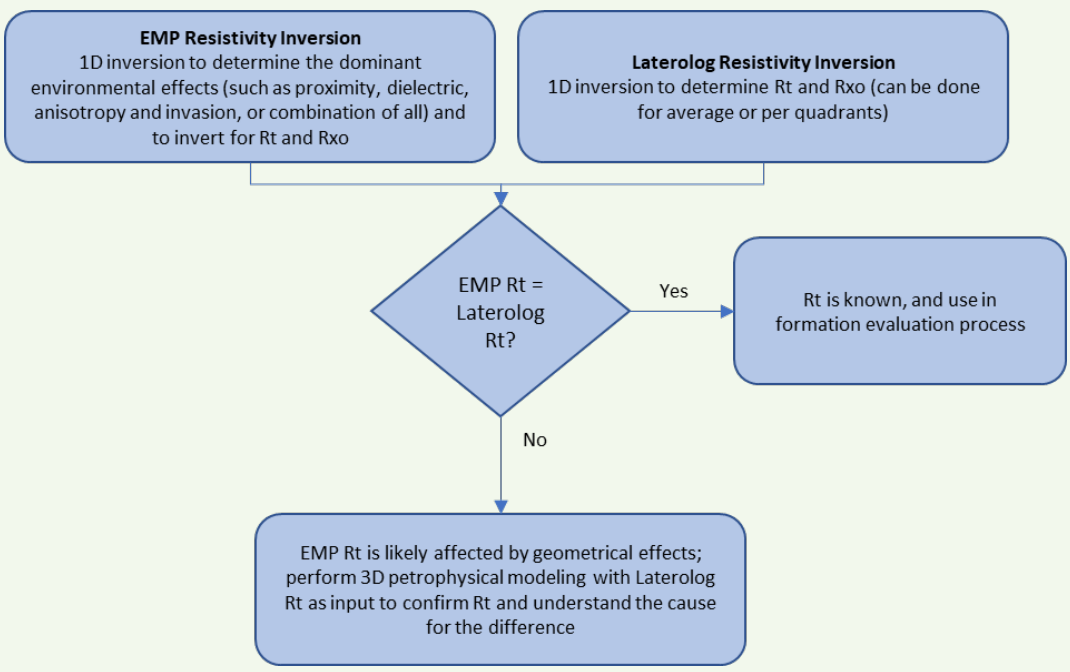

Fig. 4 *Well-1 EMP and laterolog resistivities agree well in the thick and homogeneous reservoir zones. There is either very shallow or no invasion as observed on the laterolog data acquired during drilling.*

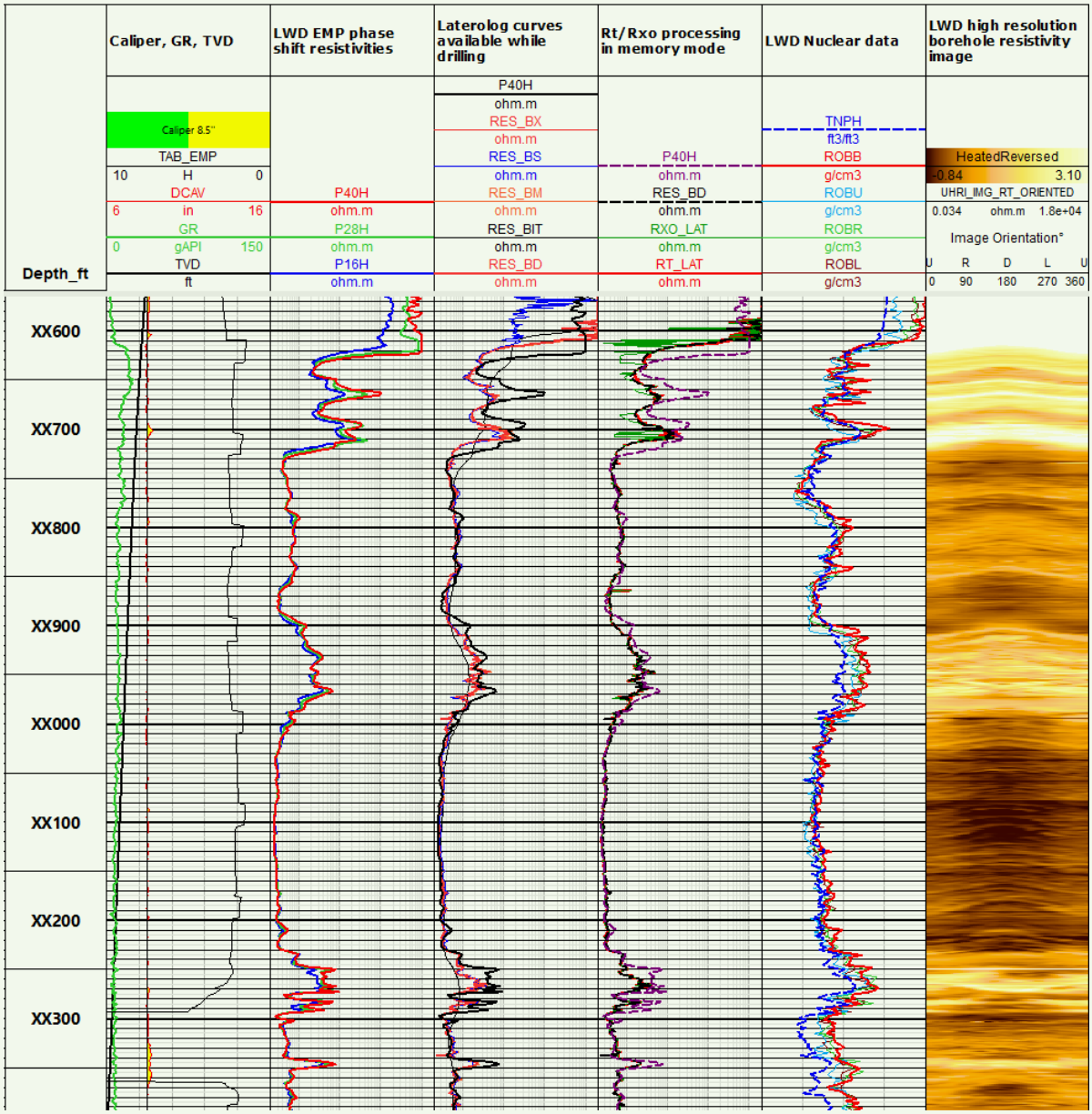

inversion, presented in Track 4 of Fig. 4, are overlapping in the thick reservoirs. The time-after-bit curve indicates the elapsed time from the moment at which the bit entered the formation until a particular sensor reached the depth of interest. In this particular case, the time after bit for the EMP tool (Track 2 in Fig. 4), is about 2 hours.

In some of the thinner layers found, for example between XX600 ft and XX700 ft, discrepancies exist between the EMP and laterolog resistivities. These discrepancies are due to geometric effects in beds with contrasting resistivities. In this case, the laterolog measurement is less affected than is the EMP measurement and provides improved resistivity data. Although 3D petrophysical modeling would be required to confirm this conclusion, there is no geometric effect on the laterolog measurement.

In Fig. 4 and all subsequent log displays, resistivities increase from left to right, bulk density increases from left to right, and the porosity increases from right to left.

Effect of Time After Drilling

The Well-2 example, Fig. 5, illustrates a comparison between laterolog resistivities and EMP resistivities as a function of time.

Fig. 5 *In Well-2, the upper interval was drilled without the laterolog tool, but was logged one week after the hole was drilled. The relog data shows deep invasion. The laterolog Rt cannot be recovered in this interval because the invasion is too deep. The lower interval was logged while drilling. While invasion is also affecting the deep RES_BX, the laterolog 1D inversion can recover the Rt as it matches the deeper EMP tool resistivity.*

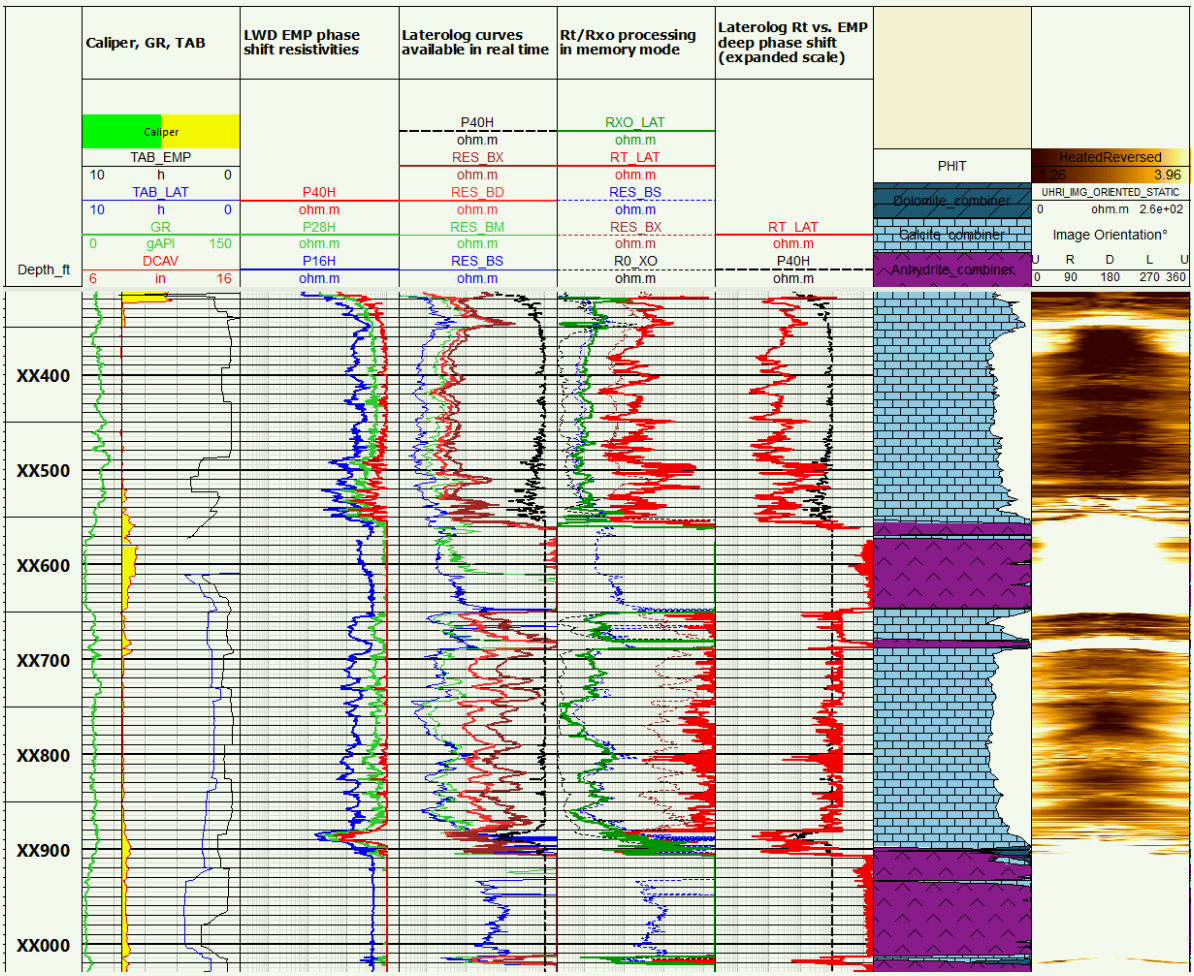

In Well-2, the upper reservoir zone between XX300 ft and XX550 ft was logged with the EMP LWD resistivity tool. The LWD laterolog tool was only used to log Well-2 a week after drilling the section and the top section was relogged before drilling ahead. While the EMP log shows very high resistivity over the upper interval, the laterolog resistivity curves in the relog are much lower due to the deep invasion that took place over the course of a week. The Rt-Rxo laterolog 1D inversion could not resolve the uninvaded Rt because of the very deep invasion.

In the second reservoir interval at XX650 to XX900 ft, both EMP and laterolog tools were used in the same drilling bottom-hole assembly (BHA). The laterolog data indicated a clear conductive invasion profile. While the deepest real-time laterolog curve (RES_BX) showed less resistivity due to invasion than the EMP resistivity measurement, the Rt recovered from the laterolog 1D inversion (RT_LAT in Track 4 of Fig. 5) matches the EMP resistivity. This result demonstrates that in normal drilling conditions where the LWD tools log the formation soon after being drilled, the laterolog data can determine the uninvaded formation resistivity even in the presence of invasion.

In the Well-2 formation section drilled and logged with both EMP and laterolog tools, time after bit is about 20 to 30 minutes for the EMP tool and approximately 1 hour for the laterolog tool due to different tool placement in the BHA.

The Rxo is close to the shallow button resistivity (RES_BS) but still higher than the fully water-filled resistivity calculated during the formation evaluation process (RO_XO shown in the fourth track of Fig. 5), indicating that not all formation fluids have been displaced by the invasion process.

Fractures

Laterolog resistivities are very sensitive to the presence of fractures due to the high-resolution characteristics of the laterolog tool.

Well-3 contained highly fractured and karstified formations, as indicated on the high-resolution borehole resistivity image (image feature interpretation in Track 7 of Fig. 6). A decrease in the laterolog resistivity is shown across most of the conductive fractures and across the karst regions. By contrast, while the EMP tool resistivity also decreases across the same zone, it lacks the vertical resolution to resolve the fine-scaled structural features in this interval. The decrease in the laterolog resistivity can indicate either that the fractures and karsts act as a water corridor, in which case they need to be avoided during completion, or that they are taking in the mud filtrate from the borehole, in which case they could enhance the production as they could indicate good permeability.

In this well, the deep bed boundary mapper was part of the LWD BHA. The deep resistivity inversion image, Fig. 7, reveals that the low resistivity extends well beyond the borehole in this zone. Therefore, it can be concluded that the fractures and karst zones act as a water corridor in this case and that they should be avoided in the completion.

Laterolog Azimuthal Sensitivity

Well-4 is a horizontal well across a carbonate reservoir and positioned beneath an anhydrite cap rock. Figure 8 shows the Well-4 logs, including the borehole resistivity and density images, the EMP resistivity, the laterolog quadrant 1D inverted Rt and Rxo, and the formation evaluation results. Due to the proximity of anhydrite, the resistivity was generally very high (up to 1,000 ohm.m), except for a few zones located near AX500 ft, BX000 ft, CX000 ft, and DX000 ft. In those zones, the high-resolution borehole resistivity image shows that the bottom of the borehole is touching on a more conductive zone — darker colors in the center of the image. This condition corresponds to a resistivity decrease of approximately 10 ohm.m on the laterolog resistivities. This decrease is clearly visible

Fig. 6 *In Well-3, the laterolog resistivities respond to the numerous fractures present in the karstified region interval. The EMP resistivities respond in general but lack the fine resolution of the laterolog resistivities.*

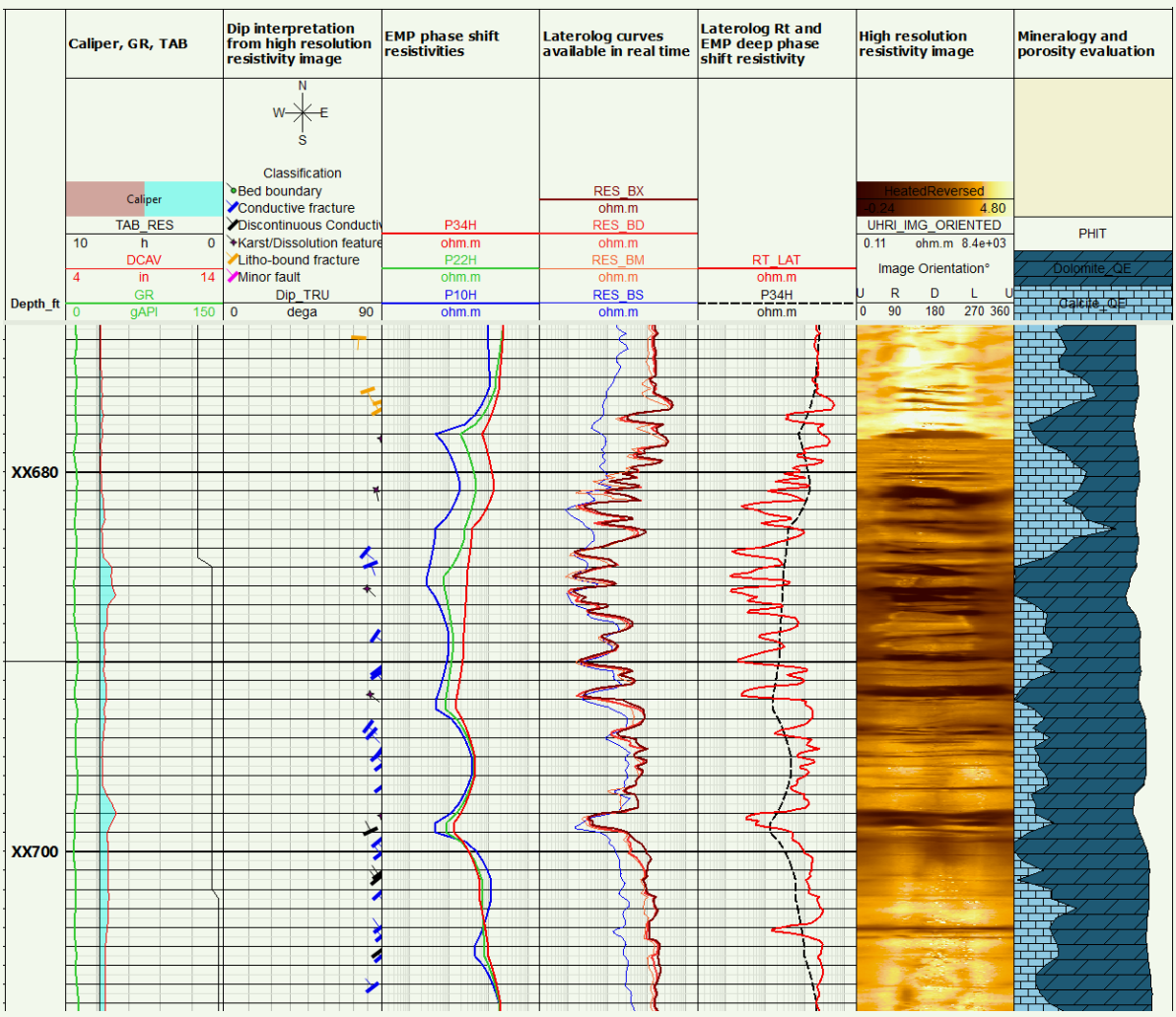

Fig. 7 *Well-3 bed boundary mapper inversion showing the water corridor in the interpreted karst zone.*

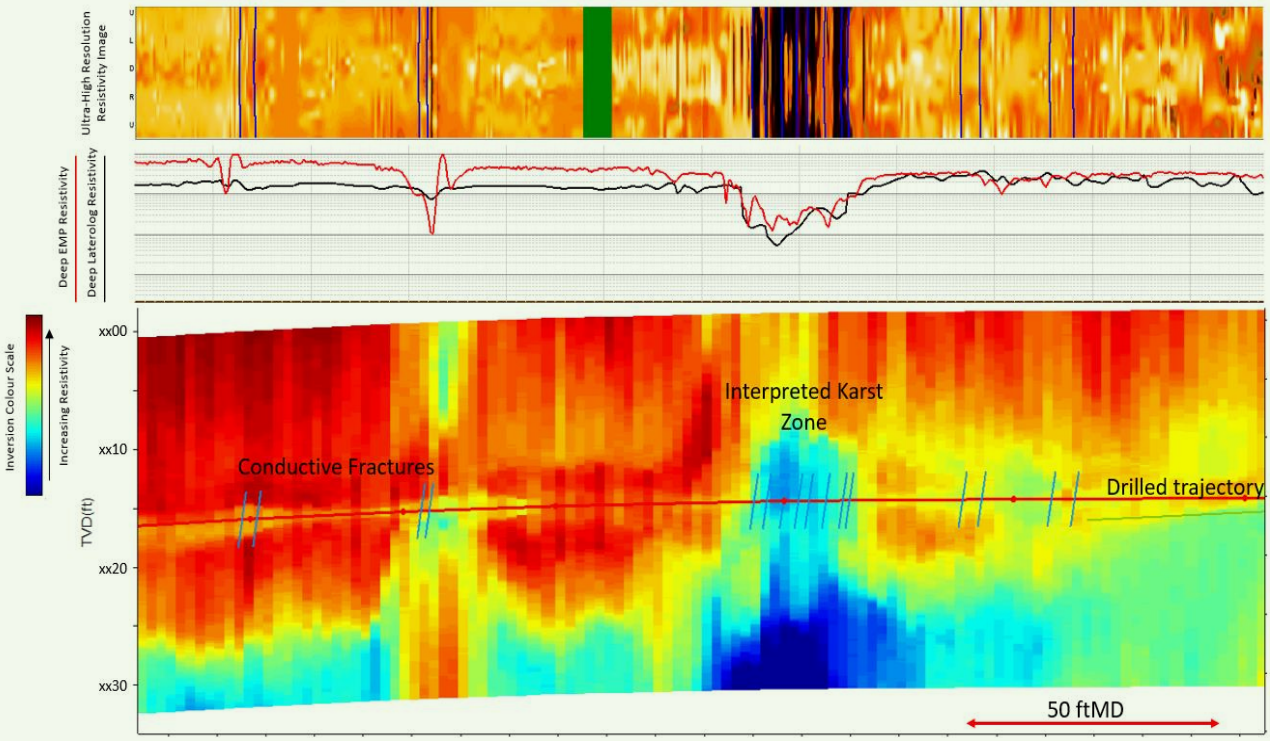

in the bottom quadrant laterolog resistivities, while in comparison, the upper quadrant laterolog resistivities remain relatively high at approximately 100 ohm.m.

The deep EMP phase shift resistivity is always higher than the laterolog resistivity. In the zones near BX000 ft and DX000 ft, the EMP resistivities are clearly saturated due to proximity effects.

Both high resistivity and low resistivity reservoir layers are highly fractured (the high-resolution image fracture interpretation in Track 1 of Fig. 8). The fractures are characterized as resistive in the high resistivity layer and are litho-bound in the low resistivity layer.

The laterolog quadrant data in combination with bulk density and photoelectric factor quadrant data allow for azimuthal formation evaluation. This evaluation process provides valuable information when the reservoir properties vary around the borehole circumference. In this example, the formation evaluation model was simplified to two minerals, dolomite and calcite, although anhydrite could be present in a few zones in the upper quadrant as indicated by the high upper quadrant density in places, e.g., at AX750 ft.

The evaluation of track A in Fig. 8 shows the formation evaluation results considering the average bulk density and photoelectric factor and the deep-phase shift EMP measurement. Evaluations B and C, respectively, in Fig. 8, show the formation evaluation results for the bottom and upper quadrants using the laterolog quadrant Rt and the quadrant measurements for bulk density and the photoelectric factor. This evaluation shows that the low resistivity bottom layer is more calcitic and less dolomitic than the upper resistive reservoir layer. The variations in resistivity also cause water saturation calculation variations between the two layers, although water saturation is not shown here for confidentiality purposes.

Well-5 is a lateral from Well-4, and the Well-5 data is shown in Fig. 9. Similar observations can be made about Well-5 as was performed for Well-4; however, in Well-5, the low resistivity layer in the interval CX500 ft to DX000 ft is sufficiently thick so that the deep EMP resistivity and the laterolog quadrant resistivities match at CX850 ft (red line in Fig. 9). This result confirms that the relatively shallow laterolog resistivity provides a good evaluation of formation resistivity while the EMP can be affected by geometric effects. Geometric effects occur at CX700 ft when the upper part of the borehole brushes a denser and more resistive layer — as observed on the upper density and upper resistivity quadrants.

Petrophysical Modeling Resolves EMP and Laterolog Resistivities

In Well-6, a resistivity difference was observed between the EMP and the laterolog resistivities. The EMP resistivity was constantly higher than the laterolog resistivity, even after making the invasion correction through the 1D inversion process. As a result, resistivity modeling was performed to explain the difference.

Fig. 8 *In Well-4, the borehole was very near to and beneath an anhydrite layer, resulting in the EMP resistivity being saturated in most of the section. The azimuthal sensitivity of the laterolog quadrant resistivities reveal that the reservoir layer, in the lower portion of the borehole, is much more conductive than in the upper portion. The laterolog quadrant resistivities enable formation evaluation per quadrant when combined with the quadrant density and photoelectric factor.*

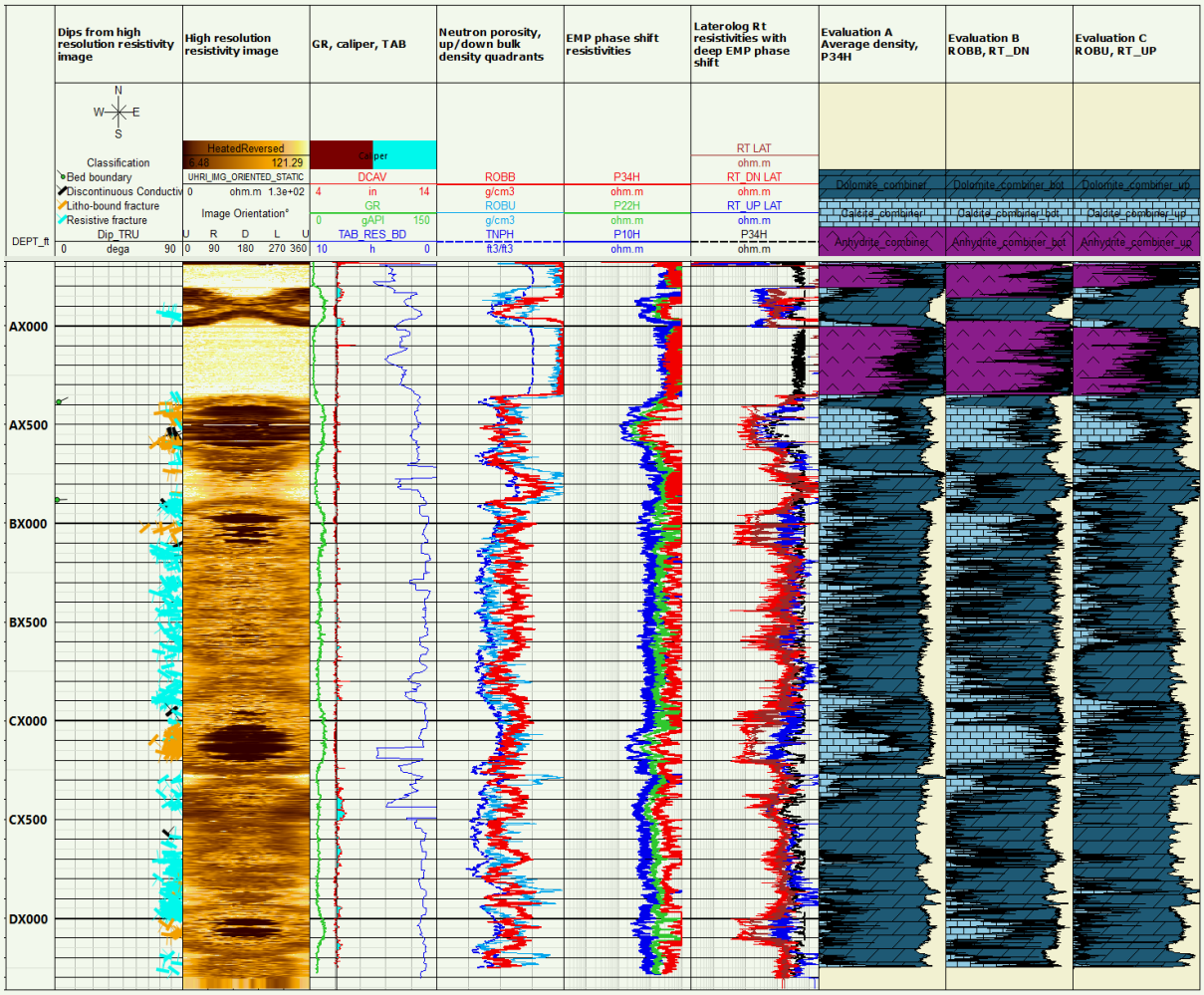

3D petrophysical modeling software was used to model the EMP logs, Fig. 10. A 2D formation model was built. The software presents the possibility of assigning a transverse dip; therefore, the 3D software name, but this option was not considered here. Five reservoir layers were considered in this model, including two very resistive outer layers (Rt = 2,100 ohm.m) and three less resistive reservoir layers sandwiched between the resistive outer layers (inner layer with the lowest Rt = 19 ohm.m and the middle layers at Rt = 35 ohm.m each).

The resistivity of the inner reservoir layer was changed to a Rt of 4 ohm.m at EX500-ft measured depth to reflect the change shown in the logs. The layers' geometry was built such that they reproduce the features observed on the density image. The layers were assigned resistivity, neutron porosity, bulk density, photoelectric factor, and gamma ray responses that represent the actual layer property, free from geometric effects. Once the layer geometry and properties are defined, a forward model was run to simulate the EMP resistivity tool response.

The model was adjusted until a match was obtained between the measured logs and their corresponding simulated response. Preference was given to keeping the model relatively simple to the detriment of perfect reconstruction everywhere. The agreement between measured and modeled density images, displayed in the two bottom tracks of Fig. 10, validates the model geometry (boundary positions and dips).

In the initial crossings of the Zone A reservoir layers, the resistivity reconstruction was not perfect for the EMP phase shift in the lower resistivity intervals; however, reconstruction was good for the EMP attenuation. The laterolog deep resistivity was higher than the estimated Rt, which could indicate it was

Fig. 9 *Well-5 is a lateral from Well-4. In Well-5, the low resistivity layer in the interval CX500 ft to DX000 ft is sufficiently thick that the deep EMP resistivity and laterolog quadrant resistivities match at CX850 ft (indicated by the red line). This result confirms that the relatively shallow laterolog resistivity provides a good evaluation of Rt while the EMP resistivity measurement can be affected by geometrical effects.*

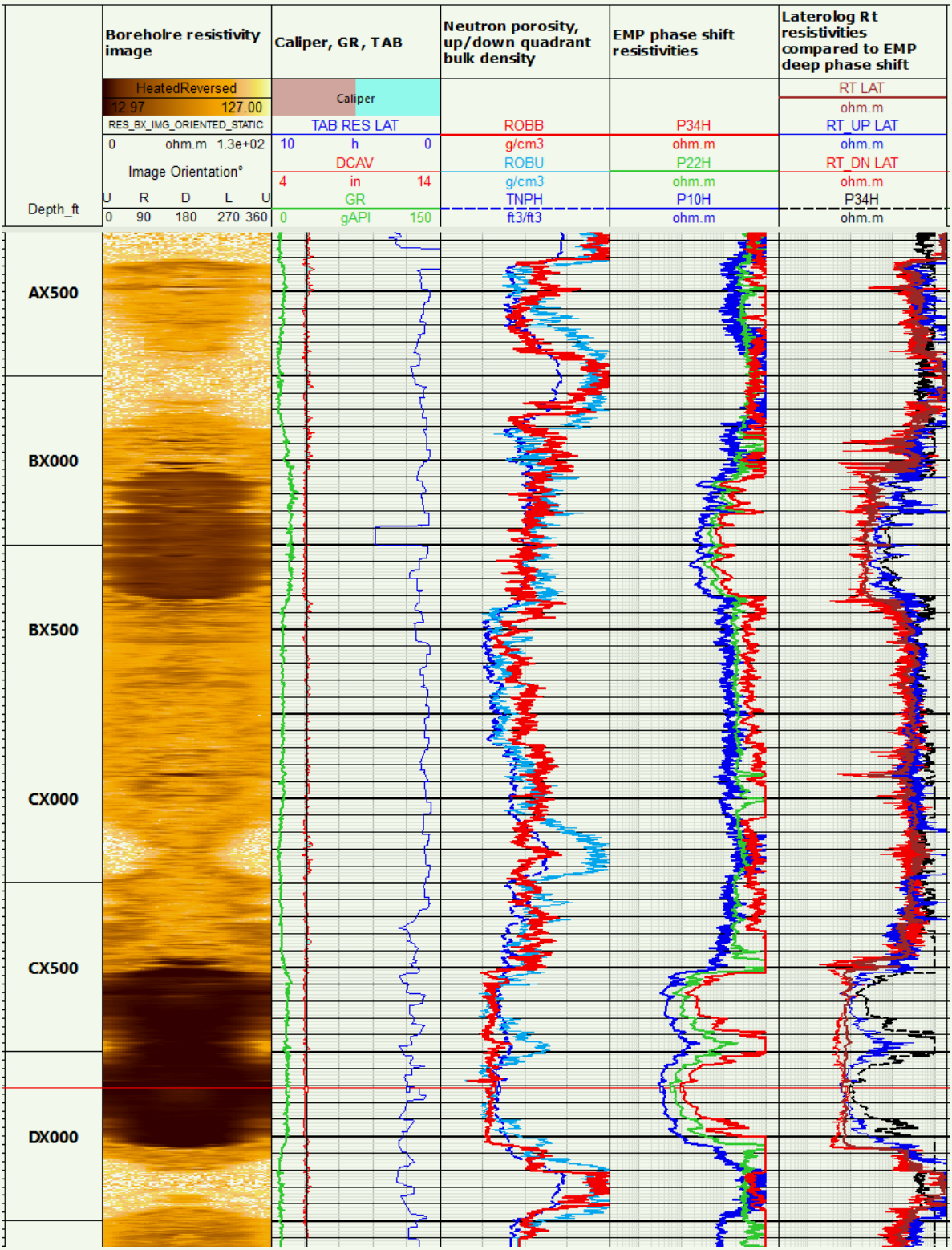

Fig. 10 *The 3D petrophysical modeling of Well-6 was able to reproduce the behavior of the EMP logs. The model explains that the difference between the EMP data and the laterolog data in the reservoir zones is due to geometric proximity effects on the EMP data. The modeling was also able to reproduce the unexpected behavior of all the resistivity logs between Zone D and Zone E. This behavior affects both EMP and laterolog measurements, but at slightly different depths, confirming the dependence on the measurement depth of investigation.*

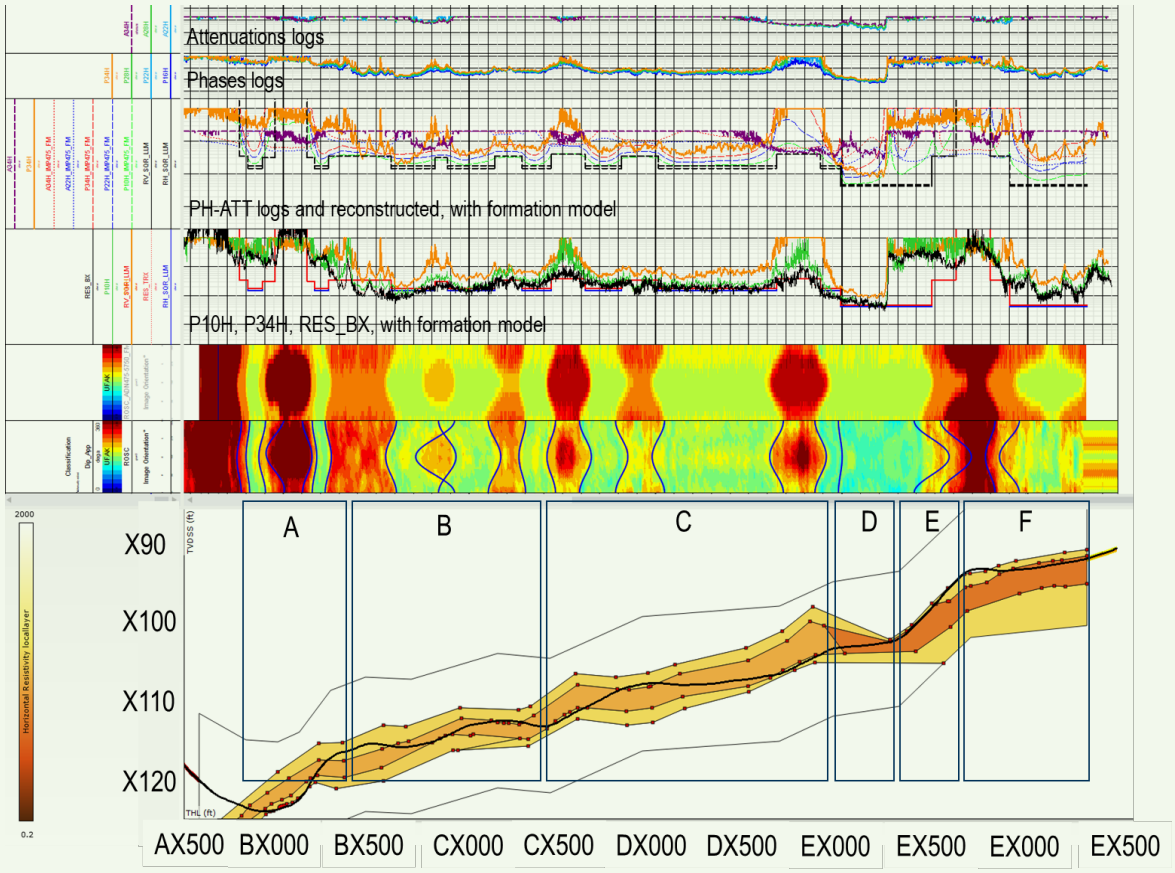

also affected by proximity effects in these intervals, due to the very close proximity of the resistive layer.

In Zone B, the reconstruction of both phase shift and attenuation resistivities was good. Because the laterolog deep resistivity is now overlaying the estimated Rt, this observation confirms that the phase shift and attenuation logs were reading too high because of the proximity of the high resistivity layer.

There was a good match between the measured phase shift and attenuation and the modeled logs in Zone C. The borehole crossed from the inner reservoir layer to the slightly more resistive layer in three intervals. As the borehole moved closer to the very resistive layer, polarization horns were created in those intervals. The reservoir geometry explains why the EMP data is higher than the laterolog data. The good quality reconstruction also indicates that the laterolog is not affected by the same geometric effects as the EMP measurements. In this case, the laterolog reflects the Rt.

In Zone D, there was an excellent reconstruction of the EMP data in both attenuation and phase shift. The laterolog resistivities were less than the EMP resistivity data and matched the Rt model.

Both EMP and laterolog resistivities in Zone E were affected by the proximity of the very resistive outer layer, causing polarization horns that were reproduced by the modeling. The Rt stayed low for a much longer time than the laterolog and EMP resistivity measurements, as the neutron and density indicate that the borehole is still inside the porous reservoir layer.

After a brief exit from the borehole into the resistive top layer in Zone F, the trajectory returned to the reservoir layer.

The 3D petrophysical modeling was able to reproduce the behavior of the EMP logs. The modeling explains that the difference between the EMP data and the laterolog data in the reservoir zones is due to geometric proximity effects affecting the EMP data. The modeling was also able to reproduce the unexpected behavior of the resistivity logs between Zone D and Zone E. This behavior, due to the close proximity of the resistive outer layer while the borehole stayed

within the porous reservoir zone, affected both EMP and laterolog measurements, but at slightly different depths, confirming the dependence on the measurement depth of investigation. The modeling confirmed that the invasion corrected laterolog measurement was generally the nearest to the Rt, except when the borehole became very close to the high resistivity layers, in which case, the laterolog could also be affected by proximity effects.

Conclusions

The experience gained by comparing EMP and laterolog resistivities in several wells helped to verify that laterolog resistivities have better axial resolution and suffer less from polarization and geometric effects than do EMP measurements. Due to their shallower depth of investigation, laterolog measurements are also less sensitive to the resistivity of adjacent layers than is EMP resistivity.

In normal drilling conditions, i.e., when acquiring LWD data while drilling, invasion is sufficiently shallow such that Rt can be well resolved by laterolog resistivities in both hydrocarbon-bearing and water-bearing zones. In those conditions, invasion can usually be corrected for through a 1D inversion. The time after drilling curve in those conditions normally does not exceed 1 or 2 hours.

Relogging a well a long time after a section has been drilled results in a condition in which the Rt cannot be measured with the laterolog tool because excessively deep invasion has occurred.

The laterolog resistivity acquired while drilling provides more accurate resistivity measurements than EMP resistivity in most cases. 3D resistivity modeling can help explain and validate the differences between the laterolog and the EMP measurements.

The laterolog quadrant data are valuable in horizontal wells where the borehole intersects different layers at different azimuths around the borehole. The laterolog quadrant resistivities can be combined with the quadrant density and photoelectric factor to provide formation evaluation results per quadrant.

Acknowledgments

This article was prepared for presentation at the International Petroleum Technology Conference, Bangkok, Thailand, March 1-3, 2023.

References

1. Maggs, D., Horstmann, M., Salehi, M.T. and Barron, M.M.: "Fast and Practical Application of Log Property Modeling to Improve Petrophysical Answers in High Angle Wells: A Case Study," SPWLA paper presented at the SPWLA 61st Annual Logging Symposium, virtual, June 24-July 29, 2020.

2. Wu, P.T., Tabanou, J.R. and Bonner, S.D.: "Petrophysical Interpretation of a Multispacing 2-MHz MWD Resistivity Tool in Vertical and Horizontal Wells," SPE paper 36547, presented at the SPE Annual Technical Conference and Exhibition, Denver, Colorado, October 6-9, 1996.

3. Guan, L., Wang, X., Xiao, D., Shim, Y-H., et al.: "Complex Resistivity Responses Explained Using LWD Laterolog Curves and Images, LWD Propagation Resistivity and Wireline Dielectric Measurements," IPTC paper 19419, presented at the International Petroleum Technology Conference, Beijing, China, March 26-28, 2019.

4. Griffith, R.: *EcoScope User's Guide*, 1st edition, Schlumberger, 2010.

5. Allouche, M., Chow, S., Dubourg, I., Ortenzi, L., et al.: "High-Resolution Images and Formation Evaluation in Slim Holes from a New Logging while Drilling Azimuthal Laterolog Device," SPE paper 131513, presented at the SPE EUROPEC/EAGE Annual Conference and Exhibition, Barcelona, Spain, June 14-17, 2010.

6. Ortenzi, L., Dubourg, I., van Os, R., Shim, Y-H., et al.: "New Azimuthal Resistivity and High-Resolution Imager Facilitates Formation Evaluation and Well Placement of Horizontal Slim Boreholes," *Petrophysics*, Vol. 53, Issue 3, June 2012, pp. 197-207.

7. Cannon, D., Rasmus, J. and Li, Q.: "A Novel Inversion Method for Interpretation of a Focused Multisensor LWD Laterolog Resistivity Tool," SPWLA paper presented at the SPWLA 40th Annual Logging Symposium, Oslo, Norway, May 30-June 3, 1999.

8. Li, Q., Liu, C-B., Maeso, C., Wu, P., et al.: "Automated Interpretation for LWD Propagation Resistivity Tools through Integrated Model Selection," *Petrophysics*, Vol. 45, Issue 1, January 2004, pp. 14-26.

9. Schlumberger: *EMP Log Quality Control Reference Manual*, Schlumberger, Houston, Texas, 2011. *https://www.slb.com/-/media/files/premium-content/drilling/catalogs/arcvision-lqcrm-cat.ashx*.

10. Schlumberger: *MicroScope HD Resistivity and High-Definition Imaging While Drilling*, Schlumberger, Houston, Texas, 2017, 8 p., *https://www.slb.com/-/media/files/drilling/brochure/microscope-hd-br.ashx*.

About the Authors

Ida Bagus Gede Hermawan Manuaba

M.S. in Petroleum Engineering, Heriot Watt University

Ida Bagus Gede Hermawan Manuaba joined Saudi Aramco in June 2014 as a Senior Petroleum Engineer/Petrophysicist working in the Southern Area Petrophysics Unit of the Reservoir Description and Simulation Department. Before joining Saudi Aramco, Ida Bagus worked for several service providers including Western Atlas, Baker Hughes, Precision Energy Services, and Weatherford for almost 17 years as a Wireline Engineer, Logging while Drilling (LWD) Engineer, and Directional Driller.

Since joining Aramco, he has served as a subject matter expert for LWD technologies and interpretation. Recently, Ida Bagus started teaching a Well Log Applications and Operations course at the Aramco Upstream Professional Development Center.

After obtaining his Society of Petroleum Engineers (SPE) certification in 2016, he served as Secretary General in the Indonesian Petroleum Engineers Association-KSA chapter (IATMI-KSA) from 2017 to 2019 and was elected as President, serving from 2019 to 2021.

In 1997, Ida Bagus received his B.S. degree in Petroleum Engineering from Bandung Institute of Technology, Bandung, Indonesia. He received his M.S. degree in Petroleum Engineering from Heriot-Watt University, Edinburgh, Scotland, U.K.

Mohammad K. Aljishi

B.S. in Petroleum Engineering, Louisiana State University

Mohammad K. Aljishi is a Petroleum Engineer working in the Southern Area Petrophysics Unit of Saudi Aramco's Reservoir Description and Simulation Department. Since joining Saudi Aramco in 2018, he has specialized in formation evaluation and petrophysics.

In addition, Mohammad has served in multiple assignments as a Production, Drilling and Formation Evaluation Engineer. Several of the projects include acid stimulation enhancement, well revival optimizations, novel methods of sidetracking operations, and currently, he is specializing in carbonate reservoirs evaluation.

Mohammad was awarded his Society of Petroleum Engineers (SPE) certificate in 2022, and is currently serving as the IT and social media vice president with the Society of Petrophysicists and Well Log Analysts (SPWLA) Saudi Arabia chapter.

In 2018, he received his B.S. degree in Petroleum Engineering from Louisiana State University, Baton Rouge, LA.

Marie Van Steene

M.S. in Mechanical Engineering, Universite Libre de Bruxelles

Marie Van Steene is a Principal Petrophysicist and is presently a Petrophysics Domain Champion for SLB Well Construction Measurements in Saudi Arabia. She started in 2000 with SLB as a Wireline Field Engineer. Marie's work experience includes working in Australia, New Zealand, and India.

She then started working as a Petrophysicist in 2006 in Malaysia. Marie then worked in Egypt and Kuwait, and moved to Saudi Arabia six years ago. Her interests include formation evaluation in open hole and cased hole. She has been a leader of the SLB dielectric and nuclear magnetic resonance special interest groups for several years.

She is currently the vice president of Technology in the Society of Petrophysicists and Well Log Analysts (SPWLA) Saudi Arabia chapter.

In 2000, Marie received her M.S. degree in Mechanical Engineering from both Ecole Centrale Paris and the Universite Libre de Bruxelles, Brussels, Belgium.

James Dolan

M.S. in Geology, Victoria University of Wellington

James Dolan is a Principal Petrophysicist at SLB. His current assignment is as Domain Champion supporting logging while drilling (LWD) petrophysics, geosteering, and reservoir mapping services for offshore projects in Saudi Arabia. Of his 23 years in the industry, 20 have been with SLB.

Since joining SLB, James has had worked as a LWD Field Engineer, Geosteering Engineer, and Petrophysicist. He has extensive experience in both conventional and unconventional reservoirs and has held several assignments in Australasia, Scandinavia, Europe, and Saudi Arabia.

James received his M.S. degree in Geology from Victoria University of Wellington, Wellington, New Zealand.

New Low ECD Organophilic Clay-Free Inverted Emulsion Fluid (OCIEF) Weighted with Manganese Tetroxide Showed Superior Performance in Different Fields: Success Story of Drilling with OCIEF in High Overbalance Environment without Downhole Problems, Stuck Pipe Events and Nonproductive Time

Dr. Vikrant B. Wagle, Dr. Abdullah S. Al-Yami, Dr. Abdullah M. AlMoajil and Michael O. Onoriode

Abstract /

This article describes the success of using a new low equivalent circulation density (ECD) organophilic clay-free inverted emulsion fluid (OCIEF) in different gas reservoirs at elevated temperatures and with differential pressures — up to 4,500 psi. The objective of the article is to highlight the superior performance of OCIEF during the execution, which led to overcoming challenges in such a type of environment without compromising performance.

This article describes several applications where the OCIEF has been deployed achieving optimum drilling performance while minimizing the formation damage of the reservoir. Consequent applications showed how the implementation of work methods, best practices, and optimized drilling parameters successfully allowed to drill the section without downhole problems and pass the production screen test (PST) and finally allow a proper cleanup while producing the well.

Initial deployment of the fluid system shows the required fluid specifications to properly address the slim-hole challenges in a high overbalance environment. Field implementation and continuous fluid performance improvements are reported in this article, showing how the fluid system helped to successfully complete numerous wells in different fields. The versatility of the fluid system in terms of the rheological profile, the thermal stability, and the minimized formation damage characteristics made the OCIEF the sole nonaqueous fluid solution applied in gas reservoirs under extreme overbalance conditions. No more nonproductive time has been experienced over the entire drilling campaign performed with OCIEF.

The new low ECD OCIEF designed a new and enhanced polymer package, without organophilic clay and lignite, and with acid soluble manganese tetroxide (Mn_3O_4) as a weighting agent replaced the usage of water-based fluids without compromising production and with improved performance in extremely challenging gas wells. The proven performance is opening more boundaries for future applications in similar wells.

Introduction

To meet increasing challenges, which were presented by some gas producing fields, it was required to develop an alternate fluid system. Barite-based conventional invert emulsion drilling fluids and formate-based water-based drilling fluids were used to drill wells in these fields.

Conventional barite-based oil-based muds (OBMs) have a significant impact on reservoir producibility. This is due to the use of an acid insoluble barium sulfate weighting agent in addition to the use of organoclay and organolignite used in the formulations. The OBMs, despite these disadvantages, have lower fluid costs and good filtration property as compared to their formate-based counterparts. Wells that are drilled with conventional OBMs are completed with a cased hole completion, whereas the formate-based fluids, due its non-damaging nature, support the option for an open hole completion.

New low equivalent circulating density (ECD) organophilic clay-free inverted emulsion fluid (OCIEF) with manganese tetroxide (Mn_3O_4) as the weighting agent was developed with the motivation to offer improved drilling performance in maturing fields, and the non-damaging nature, due to the presence of the acid soluble

and micronized Mn_3O_4, would help to complete the well with an open hole design.

In a conventional OBM, viscosity is provided by an organophilic clay while a good high-pressure, high temperature (HPHT) fluid loss is achieved through the use of organophilic lignite. In an OCIEF, the organophilic clay and organophilic lignite are replaced by a polymeric viscosifier and polymeric filtration control agent, respectively. A unique gel structure is provided by the use of a polymeric viscosifier in the OBM[1]. Also, it not only increases the cuttings carrying capacity, but also helps to increase barite sag resistance in the fluid[2]. In the absence of low gravity solids in terms of organoclay and organolignite, an OCIEF shows low plastic viscosity (PV) and a higher rate of penetration (ROP) as compared to conventional organoclay-based OBMs[1].

In the new OCIEF described in the article, the solids content has been further reduced by replacing the barite (4.2 SG) with Mn_3O_4 (4.8 SG). The low solids content would result in reduced PV, which in turn would further reduce the surge and swab effects. This would help in better ECD management[3-5]. Another reason for replacing barite is the acid soluble nature of Mn_3O_4. The acid solubility of Mn_3O_4 would make the drilling fluid non-damaging, especially for reservoir zones. Conventional acid-based treatments would also help to break and dissolve the Mn_3O_4 in the event of a stuck pipe[6].

The organoclay-free drilling fluid formulated with a combination of an engineered bridging package and micronized Mn_3O_4 would help for opting for more aggressive well construction designs. The developed OCIEF, owing to the optimized rheology and tight fluid loss, would help in drilling through depleted zones while minimizing the risk of differential sticking as compared to the formate-based fluids. Also, longer lateral sections drilled with a non-damaging OCIEF would help higher reservoir production with an open hole completion design.

This article describes the process for qualification for the OCIEF. The article further describes and summarizes the successful field deployment of the OCIEF to date.

Formulation of Low ECD OCIEF

The OCIEFs were designed based on the following considerations. The fluid was designed to be non-damaging in nature and show acid solubility. The OCIEF was designed for long lateral sections where low ROP can be observed, and with a slim-hole drilling environment with bottom-hole temperature (BHT) of ~300 °F. The OCIEF was tested for drilling in high static overbalance conditions — 3,000 psi to 4,500 psi — and had to be resilient to potential contaminants. The OCIEFs were formulated with the acid soluble Mn_3O_4 with an oil-water ratio (OWR) 70:30, and a water phase salinity of 200,000 ppm to 250,000 ppm.

The OCIEFs were mixed using a Silverson mixer in 2 liter steel cups. The mixing order of the additives is as shown in Table 1. The fluids were then transferred in HPHT aging cells and were subsequently hot rolled at 300 °F for 16 hours. The aging cells after hot rolling (AHR) were then subsequently cooled and depressurized. The hot rolled fluids were then again transferred from the aging cells to 2L mixing cups and mixed using a Silverson mixer at 6,000 rpm.

Two 95 pcf OCIEFs based on differences in the bridging package were formulated. The 95 pcf OCIEF #1 was developed with an engineered bridging package

Table 1 *The mixing order of the two 95 pcf OCIEF formulations.*

Additive	95 pcf OCIEF #1	95 pcf OCIEF #2
Diesel (base fluid) (bbl/bbl)	0.504	0.504
Emulsifier 1 (emulsifier) (ppb)	14.0	14.0
Lime (emulsifier activator) (ppb)	2.5	2.5
Polymeric Rheology Modifier 1 (ppb)	0.5	0.5
Polymeric Filtration Control Additive	6.0	6.0
Freshwater (internal phase) (ppb)	0.234	0.234
Calcium Chloride (shale inhibition) (ppb)	29.0	29.0
Polymeric Rheology Modifier 2	1.5	1.5
Mn_3O_4 (weight material) (ppb)	215.39	215.39
Wetting Agent (ppb)	0.5	0.5
Engineered Bridging Material Package 1 (ppb)	40	—
Engineered Bridging Material Package 2 (ppb)	—	40

of various sized ground marbles. This formulation was specifically for short laterals and lower differential pressures. The acid solubility of the sized ground marbles based package was also an additional benefit of the OCIEF #1 fluid formulation.

An alternate OCIEF #2 fluid was developed for longer intervals with higher overbalance conditions. The OCIEF #2 was formulated with a bridging package that included sized resilient graphite, fibers, and sized ground marble. The bridging package was designed for longer laterals since it was expected that the bridging solids would undergo increased mechanical attrition. Fiber, which was included in the bridging material package, was considered beneficial owing to the higher aspect ratio of fibers as compared to the sized ground marble and sized graphite used in the bridging package. Graphitic bridging agents used in this formulation are not acid soluble; however, the concentration of the sized graphite used is low and was therefore considered to present insignificant damage potential.

A single polymeric filtration control additive was used in both the formulations. It provided the necessary filtration characteristics and had marginal impact on rheology of the fluids. An optimum concentration of a single emulsifier was used in both the 95 pcf formulations. The single emulsifier provided sufficient emulsification of both the external and internal phases and wetting of the solids, which included the low gravity solids, Mn_3O_4, and bridging material package. Both the OCIEFs were formulated with two suspension agents.

Fig. 1 *The BHR and AHR rheology of OCIEF #1.*

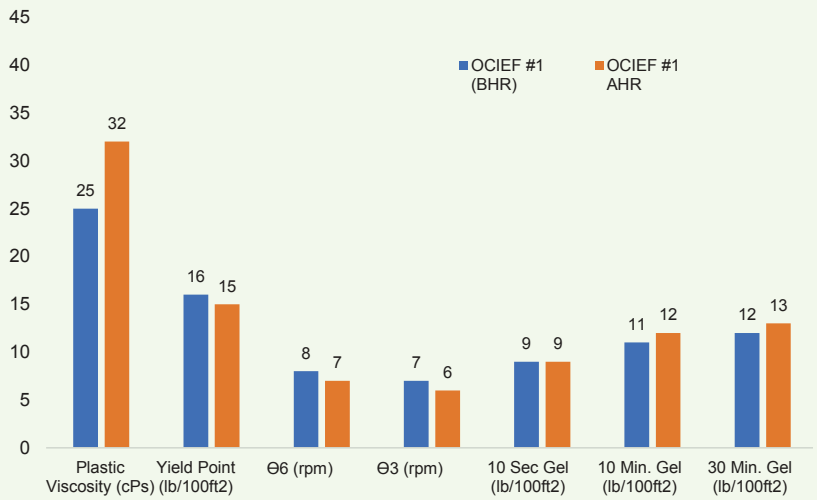

Fig. 2 *The BHR and AHR rheology of OCIEF #2.*

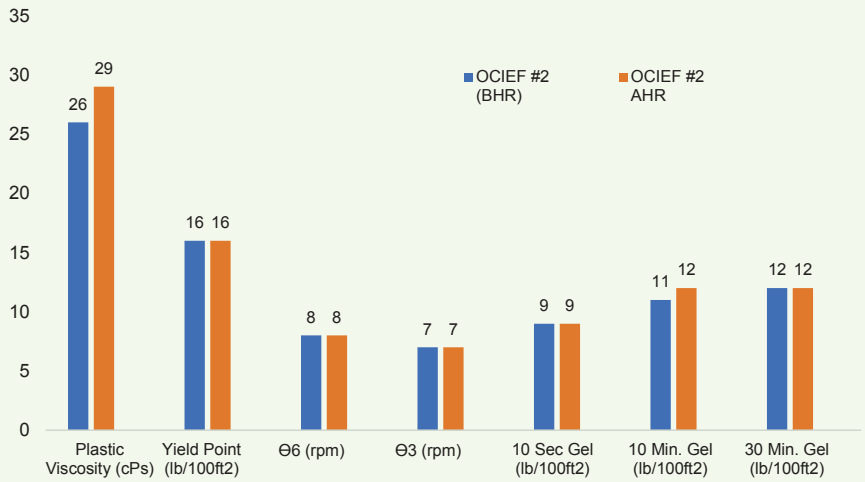

Table 2 The HPHT fluid loss of the two 95 pcf OCIEFs at 300 °F.

Property	OCIEF #1 AHR: 16 hours D	OCIEF #2 AHR: 16 hours D
HPHT Cake (1/32")	2	2
HPHT Fluid Loss (ml)	2	2
HPHT Water Breakout (ml)	—	—

Table 3 PPA testing of the two 95 pcf OCIEFs at 300 °F.

Property	OCIEF #1 AHR: 16 hours D	OCIEF #2 AHR: 16 hours D
PPA Spurt, ml (40 μ, Δ3,000 psi)	0.4	1.6
PPA Total, ml (40 μ, Δ3,000 psi)	3	4.8
PPA Spurt, ml (10 μ, Δ3,000 psi)	1	0
PPA Total, ml (10 μ, Δ3,000 psi)	3.4	0.7

Rheology Modifier 2 was used in the formulations to support a higher initial gel structure.

The OCIEFs were qualified for application-based RP API-13 B2 standards and procedures for OBMs. Fluid properties for the two fluids were tested and reported before hot roll (BHR) and AHR. The rheological properties of the two 95 pcf OCIEFs are provided in Figs. 1 and 2.

Fluid rheology and gel strengths are stable across the BHR and AHR range for both OCIEF #1 and OCIEF #2. Both the fluids showed low PV values. These values can be attributed to the selection and optimum concentration of the polymeric low-end rheology modifiers and emulsifier, as well as the micronized Mn_3O_4. The

Fig. 3 The static aging procedure for the 95 pcf OCIEFs.

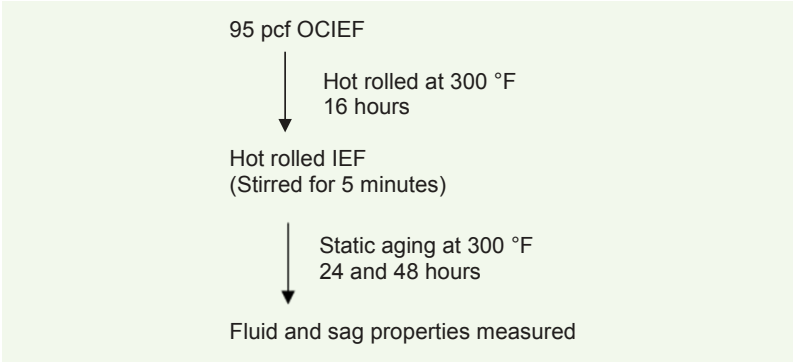

Fig. 4 The rheological properties of the 95 pcf OCIEF #1 after static aging.

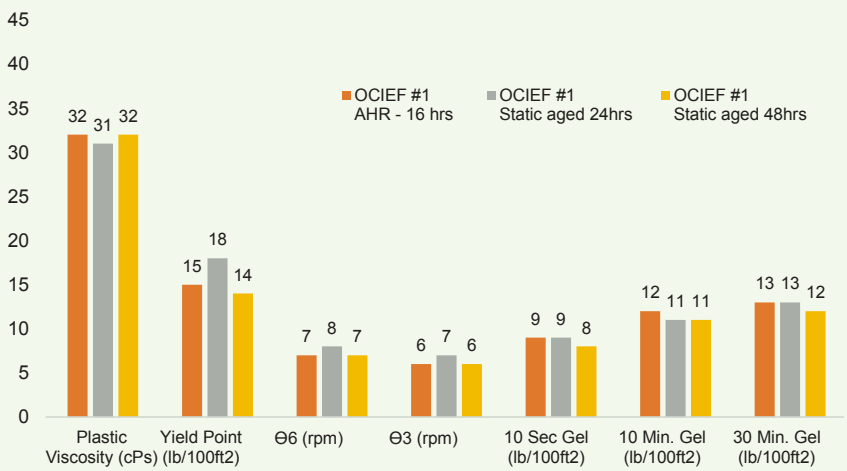

Fig. 5 *The rheological properties of the 95 pcf OCIEF #2 after static aging.*

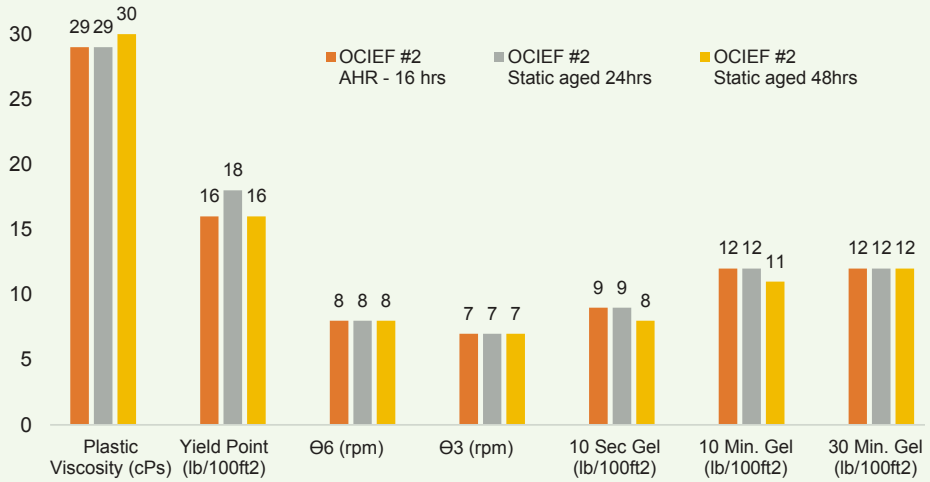

Table 4 *The HPHT filtration properties of the two 95 pcf OCIEFs after static aging.*

Property	UoM	OCIEF #1 AHR: 16 hours D	OCIEF #1 Static Aged: 24 hours S	OCIEF #1 Static Aged: 48 hours S	OCIEF #2 AHR: 16 hours D	OCIEF #2 Static Aged: 24 hours S	OCIEF #2 Static Aged: 48 hours S
HPHT Cake	1/32"	2	2	2	2	2	2
HPHT Fluid Loss	ml	2	2.4	1.2	2	1.6	2.4

Table 5 *The sag properties of the two 95 pcf OCIEFs*

	OCIEF #1 Static Aged: 24 hours	OCIEF #1 Static Aged: 48 hours	OCIEF #2 Static Aged: 24 hours	OCIEF #2 Static Aged: 48 hours
Free Oil (ml)	0	0	0	0
Sag Factor	0.514	0.514	0.507	0.513

low PV obtained for the OCIEFs infers low circulating pressures while drilling in slim-hole applications. The fragile gel structure would also minimize surge and swab pressures during tripping operations.

The emulsion stability of the two OCIEFs is demonstrated by the all oil filtrate observed in the HPHT tests performed at 300 °F. Table 2 lists the HPHT filtration properties and the results of the HPHT fluid loss measurements.

Particle plugging apparatus (PPA) tests were performed for the two OCIEFs. The tests were performed at 300 °F with differential pressures of 3,000 psi. Table 3 lists the results of the tests. Both the fluids gave low spurt loss and total filtrate values.

Successful PPA tests on 10 µ and 40 µ ceramic discs thereby validated the performance of a combination of polymeric filtration control additive and bridging material package. Successful sealing performance against two different (10 µ and 40 µ ceramic discs) permeable media was based on potentially intersecting formations that exhibit heterogeneity in lithology, or potentially wide porosity or permeability ranges. Drilling formations with uncertainties, especially at a high overbalance pressure, presents the risk of differential sticking events.

Static Aging Studies of OCIEFs

Static aging studies were performed on the two 95 pcf OCIEFs to determine the barite suspension ability of the fluids. Figure 3 shows the static aging procedure.

The rheological and filtration properties of the two

static aged OCIEFs are given in Fig. 4, Fig 5, and Table 4, respectively. As can be seen from the figures, the rheological properties viz. PV, yield point, low-end rheology and 10 second, 10 minute and 30 minute gel strengths and HPHT fluid loss of both the static aged fluids are similar to the ones AHR. This shows that static aging did not have any adverse effect on the rheology and HPHT filtration values of OCIEF #1 and OCIEF #2.

Both of the 95 pcf OCIEFs were stable after static aging giving low sag factors and minimal free fluid, Table 5. The 48 hours static aged OCIEFs did not show any thermal gelation tendencies when samples were drawn for the sag tests. Good sag properties observed for the OCIEFs can be due to the low settling tendency of Mn_3O_4 in combination with a rheology modifier and an optimum amount of emulsifier.

Contamination Studies of OCIEFs

Contamination studies were performed on the two OCIEFs, where 10% (vol/vol) water and 35 ppb "Rev Dust" (synthetic drill solids) were used in the study. The following procedure was followed for the contamination studies:

1. Hot roll the 95 pcf OCIEFs at 300 °F for 16 hours.
2. Mix the inverted emulsion fluid with the contaminants for 5 minutes.
3. Hot roll the inverted emulsion fluid at 250 °F for 4 hours.
4. Measure the fluid properties of the contaminated inverted emulsion fluid.

Figure 6 shows the rheology of the contaminated OCIEF #1.

The rheology of the 10% v/v water contaminated OCIEF #1 increased due to the increase in the internal phase of the contaminated fluid. The filtration properties of the contaminated fluid, however, remained tight with a HPHT fluid loss of 2.4 ml at 300 °F. The HPHT filtrate did not show any presence of free water. The 10% v/v water contaminated OCIEF could, however, be treated by adding an emulsifier and diesel-base fluid.

The 35 ppb of Rev Dust was added to OCIEF #1 to simulate contamination by drill solids. Also shown in Fig. 6, the rheology of the Rev Dust contaminated 95 pcf OCIEF increased due to the reactive nature of the synthetic drill solids addition.

Table 6 shows the low HPHT fluid loss of the solids contaminated OCIEF, which can be attributed to the higher rheology and cake building nature of

Fig. 6 *The rheology of the contaminated OCIEF #1.*

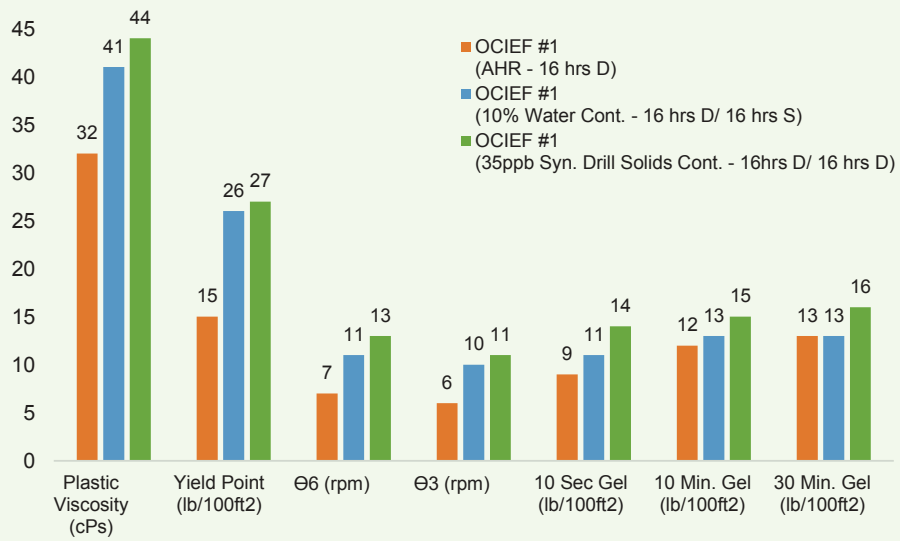

Table 6 *HPHT filtration properties of contaminated 95 pcf OCIEF #1.*

Property	UoM	OCIEF #1 AHR	OCIEF #1 10% H_2O	OCIEF #1 35 ppb Syn. Drill Solids
HPHT Cake	1/32"	2	2	2
HPHT Fluid Loss	ml	2	2.4	1.4

the additional colloidal size clay particles. The high rheology, due to solids contamination, could be easily treated with a higher OWR pre-mix volume that is inclusive of increased concentrations of emulsifier.

HPHT Rheology of 95 pcf OCIEF

A standard HPHT rheometer was used to determine the rheology of both the OCIEF fluids in HPHT conditions. The temperatures and pressures used in the tests for both the fluids were based on a typical well architecture. Figures 7 and 8 provides the HPHT rheology for OCIEF #1 and OCIEF #2, respectively.

The testing showed that the rheology values were consistent for both the fluids across a temperature and pressure range. No significant thickening was observed for both the fluids at higher temperature and pressures. The test data indicates that low ECDs could be expected when these formulations are deployed.

Regain Permeability Testing of OCIEFs

Regain permeability testing was performed utilizing hot rolled 95 pcf OCIEFs on a Clashach synthetic core at a third-party laboratory. The synthetic core material had porosity, permeability, and minerology comparable to the target formation.

The Clashach core samples were saturated in simulated formation brine in a pressure saturator. Detailed methodology to perform the regain permeability testing is given by Wagle et al. (2021)[7].

The test results for the OCIEF application and drawdown are detailed next and summarized in Table 7.

The low filtrate values were recorded at the high

Fig. 7 *95 pcf OCIEF #1 rheology in HPHT conditions.*

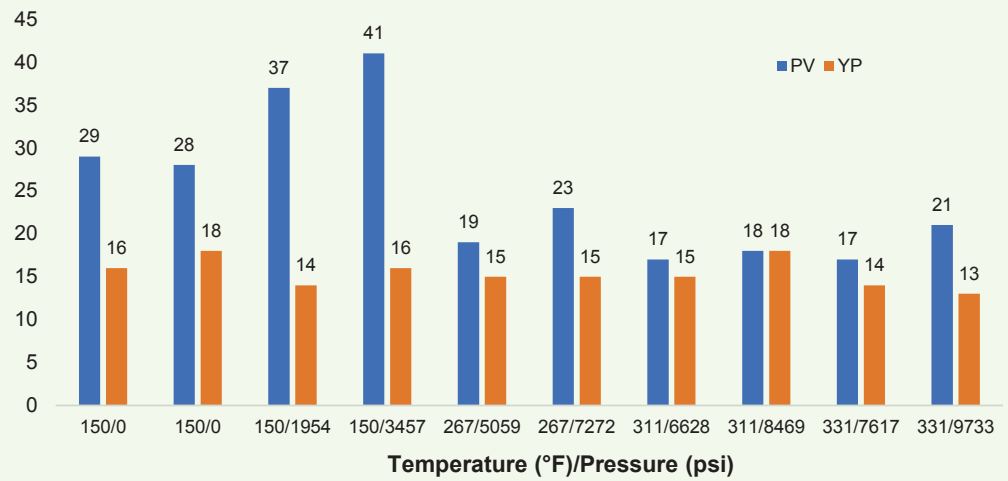

Fig. 8 *95 pcf OCIEF #2 rheology in HPHT conditions.*

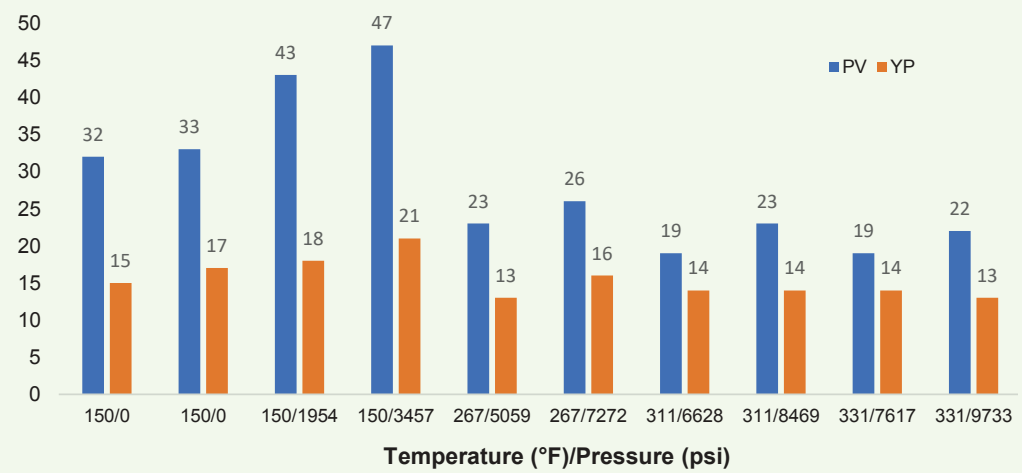

Table 7 The 95 pcf OCIEF application and drawdown.

Core Sample	Pore Volume	Fluid Applied	Total Filtrate Volume Loss (ml) (Pore Vol.)	Base Specific Permeability to Formation Brine Kw (mD)	Base Effective Permeability at CO_2 Kg at Swi (mD)	Effective Permeability to CO_2 after Drawdown Kg at Sr (mD)	Effective Permeability to CO_2 Minus Drilling Mud Cake Kg at Sr (mD)	Effective Permeability to CO_2 After Spindown Kg at Sr (mD) Filtrate Out (ml)
V3	2.873	95 pcf OCIEF #1	1.383 (0.440)	98.6	91.6	36.5 (-60.2%)	37.0 (-59.6%)	88.7 (-3.17%) (0.65)
V14	3.046	95 pcf OCIEF #2	1.648 (0.574)	131	129	70.4 (-45.4%)	83.0 (-35.7%)	126 (-2.33%) (0.40)

overbalance test conditions. This confirms the effectiveness of the filter cake building additives and bridging materials package used in the 95 pcf OCIEFs.

In both tests for the 95 pcf OCIEF #1 and OCIEF #2 fluids, there was an almost complete regain in permeability. The only marginally damaging mechanism that may have caused a decrease in permeability was the residual filtrate and solids that blocked some pore spaces in the wellbore face side of the core samples.

The 95 pcf OCIEF #2 fluid does have slightly better final regain permeability than the 95 pcf OCIEF #1.

Micro-Computed Tomography Scan of Clashach Synthetic Core

A 2D and 3D micro-computed tomography (micro-CT) scan analysis was performed on the Clashach core before and after the coreflood experiment at a third-party laboratory.

The 2D micro-CT scan image, Fig. 9, indicated that within the wellbore end of the core sample exposed to OCIEF #1, the filtrate, as indicated by the white colored areas, invaded just the first few pore spaces to a depth of ~1 mm from the wellbore face after spin down. The low intensity features as indicated by the black colored areas represent pore spaces in the core sample. The (light) high X-ray intensity features represent high density grains or patches of cementation.

The low invasion is also shown by the 3D visualization of the invaded filtrate, Fig. 9. The 3D image indicates the spatial distribution of filtrate invasion (indicated in blue). The micro-CT scan supports the results of the regain permeability study and tight filtration characteristics of the 95 pcf OCIEF.

Acid Solubility of Filter Cake

Acid solubility studies were performed on the 95 pcf OCIEF with the intention to achieve optimal filter cake removal efficiency. A 55 micron ceramic disc was used in the study. The weight of the dry disc was measured

Fig. 9 The 2D and 3D micro-CT scan of the Clashach core sample after spin down.

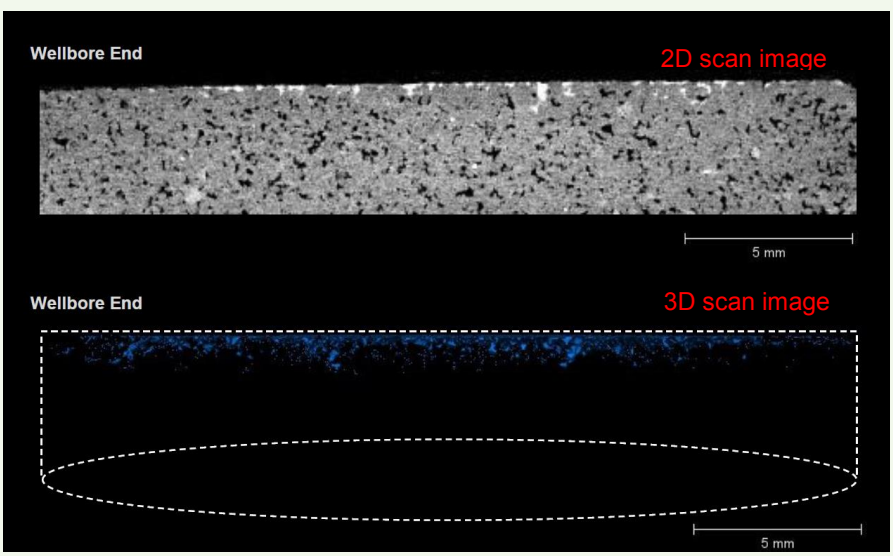

and the disc was then subsequently saturated in diesel for 10 minutes. An HPHT filtration test was then performed on OCIEF #1 for 30 minutes at 300 °F. The 55 micron ceramic disc was then carefully removed after the test and was subsequently weighed. After weighing, the ceramic disc, along with the filter cake, was then subjected to acid treatment. The formulation of the acid treatment is given in Table 8.

The ceramic disc was placed back into the HPHT cell. Then, 100 ml of acid fluid was poured on the filter cake and the HPHT cell was shut-in at 300 °F for 24 hours. After 24 hours, the HPHT cell was cooled down and the ceramic disc was then subsequently weighed. The efficiency of the acid treatment fluid to remove the filter cake was then calculated.

The acid treatment formulated with a combination of 9% formic acid and 2% (w/w) HCl acid gave a high filter cake removal efficiency of 94.5%. Figure 10 shows the filter cakes before and after the treatment with the acid treatment fluid.

Table 8 *The formulation of the acid treatments and removal efficiencies.*

Formulation	Acid Treatment Fluid
Water	141.8 ml
HCl Acid	2 wt%
Formic Acid	9 wt%
Mutual Solvent	10 vol%
Water Wetting Surfactant	0.2 vol%
Corrosion Inhibitor	2.5 vol%
Intensifier 1	4 vol%
Intensifier 2	4 vol%

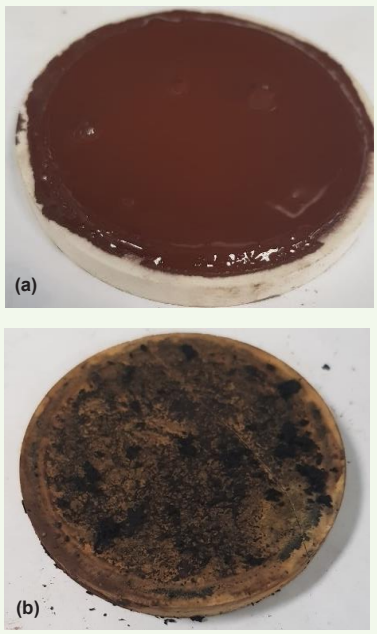

Fig. 10 *The effect of the acid treatment fluid on the 95 pcf OCIEF #1 filter cake; (a) before treatment, and (b) after treatment.*

Formulation of Production Screen Test Fluids

Production screen test (PST) fluids were required for the completion phase. Similar to OCIEF, the PST fluid was also designed for a BHT of ~300 °F and to be non-damaging in nature, and show acid solubility. The PST fluid was expected to show non-impairment characteristics to flow through and flow back, through the pore sizes of the lower completion. Table 9 lists the additives, concentrations and their order of mixing.

The 95 pcf PST fluid formulation included a low concentration of rheology modifiers for the suspension Mn_3O_4 weighting agent. It was desired to have a low rheological profile for the PST fluid to minimize fluid friction losses during the PST and flow back during production.

The fluids were mixed using a Silverson mixer for 60 minutes in a water bath that was used as a heat sink. The PST fluid was mixed for a further 60 minutes in the Silverson mixer to simulate the effect of extended shearing time expected during field application. The PST fluids were tested according to RP API-13 B2 and company PST procedures.

The rheology and density measurements were determined on fresh mixed PST fluid (BHR) as well as a sample of PST fluid contaminated with 50 ppb sized ground marble. Ground marble was added to simulate

Table 9 *The additives, concentrations and their order of mixing.*

Additive	95 pcf PST Fluid
Diesel (bbl/bbl)	0.537
Emulsifier 1 (ppb)	14.0
Lime (ppb)	2.5
Polymeric Rheology Modifier 1 (ppb)	1.0
Polymeric Filtration Control Additive (ppb)	—
Freshwater (bbl/bbl)	0.231
Calcium Chloride (ppb)	32.2
Polymeric Rheology Modifier 2 (ppb)	0.5
Mn_3O_4 (ppb)	251.14

bridging solids contamination arising from inefficient displacement. Ground marble was mixed into the PST fluid in a Silverson mixer for 10 minutes at 6,500 rpm. Figure 11 shows the rheology of the PST fluids.

The 95 pcf PST fluid showed suitable rheology values for the intended application. The 95 pcf PST fluid was contaminated with 50 ppb bridging solids and mixed as detailed above. The rheology and gel strength values of the PST fluid after solids addition increased as expected.

The PST was performed with 5 × 1 liter samples of the PST fluid. The testing was performed with a 10 psi header pressure against 250 µ screen coupons. The PST was also performed on contaminated PST fluid. The PST was performed against a 250 µ screen with a 10 psi header pressure. Figure 12 shows the PST results. The result confirms that the PST fluid does not blind the 250 µ screen coupons.

The full test volume of 5 × 1 liter PST fluid passed through the same screen coupon at a comparable time. The screen coupon was then subsequently recovered from the cell. As shown in Fig. 13, there was no residual buildup on the face of the coupon. In the case of PST with contaminated PST fluid, the test was stopped after 3 × 1 liter samples had passed through the 250 µ screen coupon. This was because the flow through times were comparable to the PST fluid.

Planning and Field Deployment of OCIEF

Well Overview and Fluids Planning

The OCIEF is considered as a good option to drill gas wells for the following reasons:

- It is a less damaging fluid and it has the potential to increase production since there is no damaging additives, such as organophilic clays or barite.
- It has less risk of a differential stuck pipe due to its unique solids' optimization package.
- It has less risk of a mechanical stuck pipe due to its low ECD.
- Its filter cake is acid soluble, which is important for optimum production.
- It has a great potential to increase the ROP compared to conventional OBMs.

Fig. 11 *The rheology of the PST fluids.*

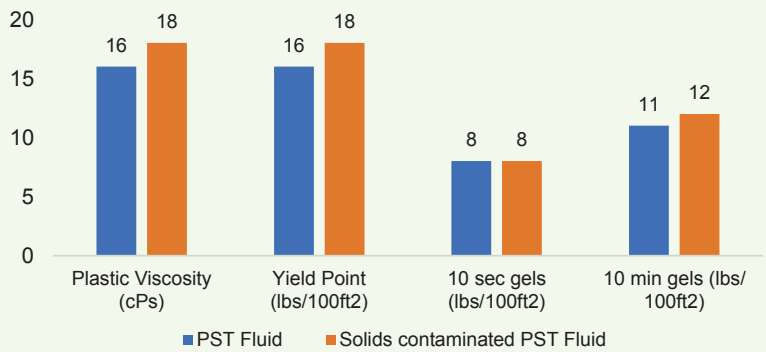

Fig. 12 *The results of the PST testing.*

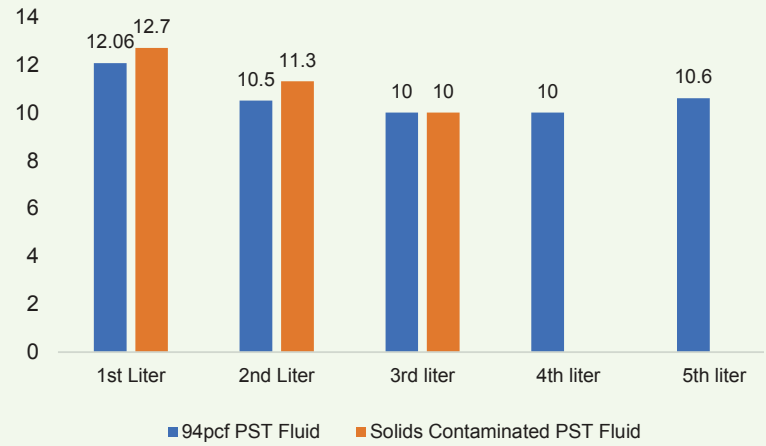

Fig. 13 *The 250 μ screen after the PST.*

The target section was a 5⅞" hole section and the plans were to have a 4½" sand screen completion. Offset wells showed low ROP with conventional OBMs. Using OCIEF for the 5⅞" section was detailed in a prepared mud program based on pre-drill data, offset analysis, hydraulic modeling and agreed KPIs, such as:

- To optimize production compared to offset.
- To have zero stuck pipe incidents while drilling and completions.
- To achieve zero downhole losses while drilling the 5⅞" hole section.
- To run and set 4½" sand screens at target depth.

The OCIEF fluid was initially planned for use on the 5⅞" interval at 85 pcf for wellbore stability. A contingency plan for higher mud weights of up to 95 pcf was also included in the mud program when needed, if the additional wellbore stability was required.

Detection of the types of stuck pipe (mechanical or differential) is critical. For differential stuck pipe reducing fluid density is a good way for mitigation. For mechanical stuck pipe due to geomechanics effect, increasing fluid density is recommended. The 5⅞" interval was planned to be drilled through the target reservoir holding an 89° inclination and a 302° azimuth.

Field Deployment of OCIEF: Drilling Phase

The planned OCIEF density was increased from 85 pcf to 88 pcf to provide additional wellbore stability as observed in offset wells. A total of 1,686 bbl OCIEF fluid was mixed at 70:30 and sheared on surface through a custom-built high-pressure shearing unit connected to the cement unit.

The 5⅞" drilling parameters were 70 rpm to 100 rpm, the weight on bit 14 kftlb to 19 kftlb, flow rates of 240 gpm to 260 gpm, torque 5,000 ftlb to 7,200 ftlb, and the stand pipe pressure ranged from 2,850 psi to 3,585 psi. We started first by running the drilling assembly with a 7" shoe track to drill 10 ft of rat hole with 109 pcf conventional OBM from a previous 8⅜" interval. Then, we pumped 30 bbl of high viscosity 88 pcf OCIEF spacer to displace out the conventional OBM. The 88 pcf OCIEF high viscosity spacer was followed by 88 pcf OCIEF. The 5⅞" hole was drilled at an azimuth of 302° and at an inclination of 88° at controlled ROP — 10 ft/hour to 28 ft/hour.

Mechanical stuck pipe incidents were detected early while drilling when a pressure spike was noted with increased torque and the drill string stalled. We increased the density from 88 pcf to 92 pcf to prevent stuck pipes. Later, LWD had shown indications of formation breakouts, which are also a good indication of geomechanics issues and potential mechanical stuck pipe. The fluid density was increased to 95 pcf to continue drilling successfully. No notable increase in cuttings were observed when circulated out with tandem hole cleaning pills.

A scraper assembly of 9⅝" × 7" was made up and run in the hole with tandem pills for sweeping. Then, a 5⅞" clean out assembly was picked up and run in hole. We had good hole conditions as no tight spots were recorded. A viscous spacer was pumped ahead of the 120 bbl 95 pcf PST fluid that was spotted in the open hole section. The clean out assembly was pulled inside the 7" liner. Then, fluid was circulated over fine 270/325 mesh screens until the OCIEF fluid was deemed PST compliant. The clean out assembly was pulled out of the hole. Then, 4½" sand screens were picked up and run in the hole to the bottom at the required depth successfully.

OCIEF and PST Fluid Observations

Increasing OCIEF density from 92 pcf to 95 pcf at 16,225 ft measured depth with direct additions of water-wet micronized weight material to the circulating system led to an increase in PV and increased demand on free emulsifier dosages.

The subsequent addition of emulsifiers and increased oil content from 70:30 to 79:21 decreased PV from a maximum of 44 cP to 32 cP. We also had to increase fluid loss additive and bridging concentration to mitigate the effect of increased oil and emulsifier treatments. The target PPA properties were of spurt < 2 ml and total PPA < 4 ml (40 μ, 300 °F).

Summary of Field Experience

We have used this innovative OBM for more than 25 applications to date in 10 different fields and in both vertical and horizontal 5⅞" slim-hole well designs at different static overbalance psi, Fig. 14. Drilling performance with the OCIEF has been satisfactory and there have been no stuck pipe events during drilling or completion operations.

The wells drilled with this innovative OBM have resulted in a reduction in invisible lost time when compared to wells drilled with formate fluids in offset wells. This reduction in visible lost time is shown in the elimination of reaming trips — a 12 to 24-hour duration — on wells drilled with formate fluids and other conventional fluids. There have been no instances of stuck pipes due to improper fluid properties, e.g.,

Fig. 14 *Static overbalance psi of the OCIEF wells drilled.*

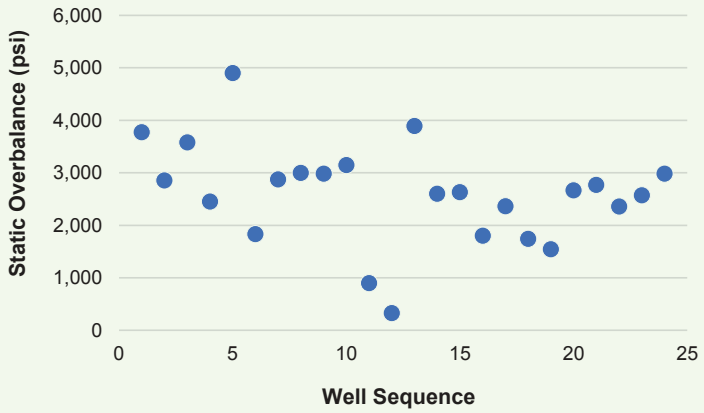

sag, high viscosity fluid.

The innovative fluid was also reused successfully in drilling additional wells with minimum treatments based on density requirements — 75 pcf to 100 pcf. The wells that were drilled with this innovative fluid showed a lower cost by 41% compared to formate fluids. Production from all wells have exceeded expectations validating the fluid's non-damaging design and the successful deployment thereof.

Conclusions

1. The 95 pcf OCIEFs were formulated successfully showing minimal changes to rheological and filtration properties in static aging and contamination studies.
2. Wells were successfully drilled with non-damaging OCIEFs at high overbalance. Risk of differential sticking was successfully eliminated by the use of a combination of polymeric filtration control additives and engineered bridging materials.
3. The OCIEFs can support drilling longer laterals with the potential for higher mud weights if so required.
4. Prudent fluid engineering practices resulted in no instances of notable contamination to the OCIEF.
5. Acid solubility of the Mn_3O_4 based filter cake has been discussed in the article; however, no acid treatment was required to release the pipe during drilling or completion operations.

Acknowledgments

This article was presented at the Abu Dhabi International Petroleum Exhibition and Conference, Abu Dhabi, UAE, October 31 – November 3, 2022.

References

1. Burrows, K., Carbajal, D., Kirsner, J. and Owen, B.: "Benchmark Performance: Zero Barite Sag and Significantly Reduced Downhole Losses with the Industry's First Clay-Free Synthetic-Based Fluid," SPE paper 87138, presented at the IADC/SPE Drilling Conference, Dallas, Texas, March 2-4, 2004.
2. Carbajal, D., Burress, C., Shumway, B. and Zhang, Y.: "Combining Proven Anti-Sag Technologies for HPHT North Sea Applications: Clay-Free Oil-Based Fluid and Synthetic, Sub-Micron Weight Material," SPE paper 119378, presented at the SPE/IADC Drilling Conference and Exhibition, Amsterdam, the Netherlands, March 17-19, 2009.
3. Nicora, L.F., Pirovano, P., Blomberg, N. and Taugbol, K.: "High-Density Invert Emulsion System with Very Low Solids Content to Drill ERD and HPHT Wells," SPE paper 65000, presented at the SPE International Symposium on Oil Field Chemistry, Houston, Texas, February 13-16, 2001.
4. Kulkarni, D., Maghrabi, S. and Wagle, V.: "Synergistic Chemistry Tailors Invert Emulsion Fluids (IEF) with Consistent Rheology to Minimize Equivalent Circulating Density (ECD) Fluctuations," SPE paper 171695, presented at the Abu Dhabi International Petroleum Exhibition and Conference, Abu Dhabi, UAE, November 10-13, 2014.
5. Wagle, V.B., Maghrabi, S., Teke, K. and Gantepla, A.: "Making Good HPHT Invert Emulsion Fluids Great!" SPE paper 153705, presented at the SPE Oil and Gas India Conference and Exhibition, Mumbai, India, March 28-30, 2012.
6. Montgomery, J.K., Keller, S.R., Krahel, N. and Smith, M.V.: "Improved Method for Use of Chelation to Free Stuck Pipe and Enhance Treatment of Lost Returns," SPE paper 105567, presented at the SPE/IADC Drilling Conference, Amsterdam, the Netherlands, February 20-22, 2007.
7. Wagle, V.B., Al-Yami, A.S., Onoriode, M., Butcher, J., et al.: "Low ECD High Performance Invert Emulsion Drilling Fluids: Lab Development and Field Deployment," SPE paper 202115, presented at the SPE/IADC Middle East Drilling Technology Conference and Exhibition, Abu Dhabi, UAE, May 25-27, 2021.

About the Authors

Dr. Vikrant B. Wagle

Ph.D. in Surfactant and Colloidal Science, Mumbai University Institute of Chemical Technology

Dr. Vikrant B. Wagle is a Science Specialist with the Drilling Technology Team of Saudi Aramco's Exploration and Petroleum Engineering Center – Advanced Research Center (EXPEC ARC). His experience revolves around the design of novel, environmentally friendly drilling fluid additives and the development of high-pressure, high temperature tolerant drilling fluid systems.

Vikrant has 50 technical publications and 120 granted U.S. patents, and he has filed several other U.S. patent applications, all in the area of drilling fluids, cementing, and loss circulation.

He received his M.S. degree in Chemistry from the University of Mumbai, Mumbai, India, and his Ph.D. degree in Surfactant and Colloidal Science from the Mumbai University Institute of Chemical Technology, Mumbai, India.

Dr. Abdullah S. Al-Yami

Ph.D. in Petroleum Engineering, Texas A&M University

Dr. Abdullah S. Al-Yami is a Senior Petroleum Engineering Consultant with the Drilling Technology Team of Saudi Aramco's Exploration and Petroleum Engineering Center – Advanced Research Center (EXPEC ARC). He has 24 years of experience with Saudi Aramco and previously worked in different positions, including as a Lab Scientist and Drilling Engineer, conducting research related to drilling engineering.

Abdullah has received several awards during his career, including Saudi Aramco's Research and Development Center (R&DC) Innovation Award and its Successful Field Application Award for his research work. He also received Saudi Aramco's EXPEC ARC Effective Publications Award. A member of the Society of Petroleum of Engineers (SPE), Abdullah was awarded the 2009 SPE Outstanding Technical Editor Award for his work on the SPE *Drilling and Completion Journal*. He also received the 2014 SPE Regional (Middle East, North Africa and South Asia) Drilling Engineering Award, and both the 2015 and 2016 CEO Saudi Aramco Excellence Award. In 2016, Abdullah received Oil & Gas Middle East Award "highly commended" recognition in the category of internal control valve (ICV) Strategy of the Year for his efforts in developing drilling products utilizing a local resources strategy. In 2017, he was awarded the Saudi Arabian Board of Engineering Award.

Abdullah is a coauthor of the textbook *Underbalanced Drilling: Limits and Extremes;* he has 127 granted U.S. patents and 152 filed patents; and has more than 100 publications to his credit, all in the area of drilling and completions.

Abdullah received his B.S. degree in Chemistry from Florida Institute of Technology, Melbourne, FL; his M.S. degree in Petroleum Engineering from King Fahd University of Petroleum and Minerals (KFUPM), Dhahran, Saudi Arabia; and his Ph.D. degree in Petroleum Engineering from Texas A&M University, College Station, TX. Abdullah is currently a Chemistry Ph.D. candidate at KFUPM majoring in Organic Chemistry and Polymer Synthesis.

Dr. Abdullah M. Al Moajil

Ph.D. in Petroleum Engineering, Texas A&M University

Dr. Abdullah M. Al Moajil joined Saudi Aramco in 2005 as a Research Scientist working in the Formation Damage and Stimulation Unit of Saudi Aramco's Exploration and Petroleum Engineering Center – Advanced Research Center (EXPEC ARC). His research interests include formation damage, filter cake characterization and removal, carbonate/sandstone acidizing, fracturing fluids and proppants, dispersants and surfactants in drilling/production operations, sludge characterization and remediation in oil wells, completion fluids, solvents for asphaltene, surface and interfacial properties, fluid rheology, and chemical interactions with swelling elastomers.

Abdullah has contributed to the design of hundreds of successful acidizing and damage removal treatments.

He has authored and or coauthored more than 45 publications, including journals and patents disclosed/granted, and presented over 45 technical papers in Asia, Europe, South/North America, Asia, and Middle East conferences.

Abdullah received his B.S. degree in Chemical Engineering from King Fahd University of Petroleum and Minerals (KFUPM), Dhahran, Saudi Arabia, and both his M.S. and Ph.D. degrees in Petroleum Engineering from Texas A&M University, College Station, TX.

Michael O. Onoriode

B.S. in Chemical Engineering, University of Lagos

Michael O. Onoriode is working as a Petroleum Engineer with the Drilling Fluids Support Team of Saudi Aramco's Exploration and Petroleum Engineering Center – Advanced Research Center (EXPEC ARC).

His experience is centered on the design, deployment, and implementation of novel environmentally friendly drilling and completion fluids for high-pressure, high temperature wells.

Michael received his B.S. degree in Chemical Engineering from the University of Lagos, Lagos, Nigeria.

Comprehensive Design and Diagnostic Approach for Horizontal Completions in Carbonate Environment

Abdulrahman A. Al-Mulhim, Hashem A. Al-Obaid, Abdul Muqtadir Khan, Jon E. Hansen and Dr. Artem Kabannik

Abstract /

The development of tight carbonate reservoirs is moving toward drilling and completing wells with longer laterals. This leads to challenges of longer completion time, a high number of fracturing stages, longer interventions, and eventually, higher costs. Design cycle implementation is required to devise an engineered strategy to mitigate these challenges.

A lateral landing was conducted based on the cross-section grid consisting of two offset horizontal wells completed with up to 13 fracturing stages. A longer lateral greater than 6,000 ft was drilled compared to 4,000 ft in offset wells to view the production potential. With a strategic design involving engineered chemistry and numerical simulation models, a cluster design was devised to reduce the stages. A mathematical algorithm employing tube wave velocity calculations was used as a diagnostic to ensure diversion success after each stage.

The horizontal lateral was landed traversing the prolific layer. Stage reduction sensitivity simulations were conducted using multiphysics numerical models and novel beta factor workflows to evaluate the extent of stage reduction. The design was extended to plan for five stages only, with an increased number of perforation clusters per stage. The reliable diversion chemistry utilized was accompanied by a revised perforation length as dictated by the beta factor workflow. A total of 39 clusters, 2 ft each, were distributed across 6,000 ft with four mechanical isolation plugs.

A novel nonintrusive diagnostic model built on mathematical fundamentals of wave travel-time was used with a Bayesian statistical approach after each diversion pill placement to ensure fracture fluid entry points and enough coverage in each stage. The high fluid viscosity and operating pumps during the water hammer events resulted in a low signal-to-noise ratio (SNR) in the input data. To overcome these limitations, the water hammer events were processed with a combination of two newly developed algorithms: (1) predictive deconvolution, and (2) comb filter, which produced more robust results than the traditional approach. Consequently, the well production was analyzed to show an equivalent or higher productivity index (PI) compared to the offset laterals with up to two times higher stage count.

This article presents a unique example in which an experiment was fully engineered from design to evaluation and monitored with reliable diagnostics. This example gives a blueprint for future completion designs.

Introduction

Horizontal wells in tight gas environments have associated hurdles related to the overall strategy of landing the lateral, completion type optimization along with fracture spacing, production simulations, well engineering workflows (intervention and fracturing), well economics, etc. These challenges get accentuated in carbonates due to acid fracturing. The complex physics involves acid-rock reaction kinetics, geomechanics, and casing/liner deformation mechanisms. A comprehensive drilling to fracturing workflow is essential to optimize the well economics and maximize operational efficiency to realize the production potential of the asset while reducing greenhouse gas emissions.

Well Planning

Background

Commercial success for production performance was achieved in Wells B and C, which were horizontal wells drilled parallel 5 km apart in the same reservoir sublayer. Since the drainage distance was slightly higher than optimum, it was decided to drill another lateral in the same stratigraphic layer; Well-A was drilled between these two wells and was 2 km to 2.5 km away from both its offset wells.

Figure 1 shows a 3D perspective for the wells. The lateral was 6,250 ft and introduced intervention challenges

Fig. 1 *Lateral trajectories in offset area; (a) Wells B and C used to plan for the candidate lateral landing, and (b) Well-A finalized well trajectory in perspective with the offset wells.*

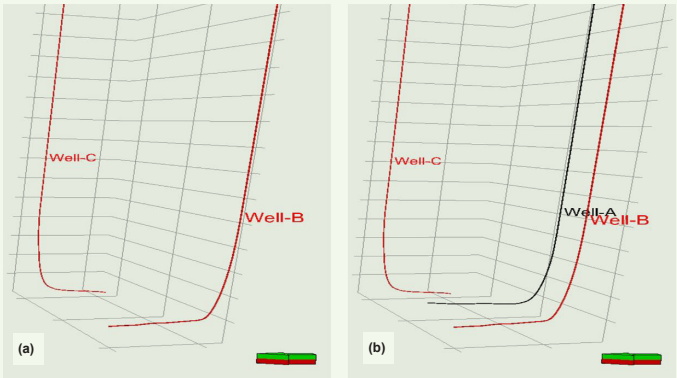

that had to be tackled[1]. Well-B was a similar cemented liner completion as Well-A and Well-C was an open hole lateral completed with packers and fracturing sleeves, increasing the reservoir contact per stage. Considering the challenges in Wells B and C, which were completed with 12 and seven stages, respectively, the stage count increased the wireline interventions, thereby requiring additional time and affecting economics.

The stress cycling in multiple pumping attempts added to the casing/liner deformation risk and required better management. So, broadly, the strategy required a reduced number of stages with managed risk of leaving part of the lateral unstimulated. The risk of bypassing reserves and suboptimal production performance was crucial to manage with engineered strategy implementation.

Lateral Landing

The ideal strategy in the offset area is to drill and log a vertical pilot hole and choose the lateral landing point and trajectory based on that. In this well, the logs and development from Wells B and C were enough to optimize the lateral landing. Figure 2 shows that the lateral trajectory of Well-A traversed the best layers and was placed centrally within the prolific layers. Based on fracture height interpretations from temperature logs conducted after acid fracturing, it is known that fracture heights do not extend much vertically due to the acid spending and mineralogical variations across layers[2].

Therefore, having the wellbore and rock connection in prolific layers of the reservoirs is critical even for completions intended for acid fracturing, which have fractures growing above and below the laterals. Figure 2 also shows the trajectory penetrates across different layers so one critical consideration is to place perforation clusters for the same stage in similar geologic layers. Placing perforations in different layers would introduce an uncertainty of preferential stimulation in one layer or another, lowering overall stimulation efficiency.

Table 1 shows a brief summary of Well-A compared with the offset wells after the lateral landing was completed. It can be seen that the lateral length was much higher in comparison, and it was done to keep a similar net reservoir contact.

Completion Approach

The lateral landed was completed with a cemented liner and planned with plug-and-perforate fracturing stages. The number of fractures created across the lateral and their engineered spacing are critical for optimizing production potential of the asset[3], through numerical modeling of production flow simulation in different scenarios.

Fig. 2 *The lateral trajectory cross section of Well-A across the layer porosity. The green color indicates a higher porosity.*

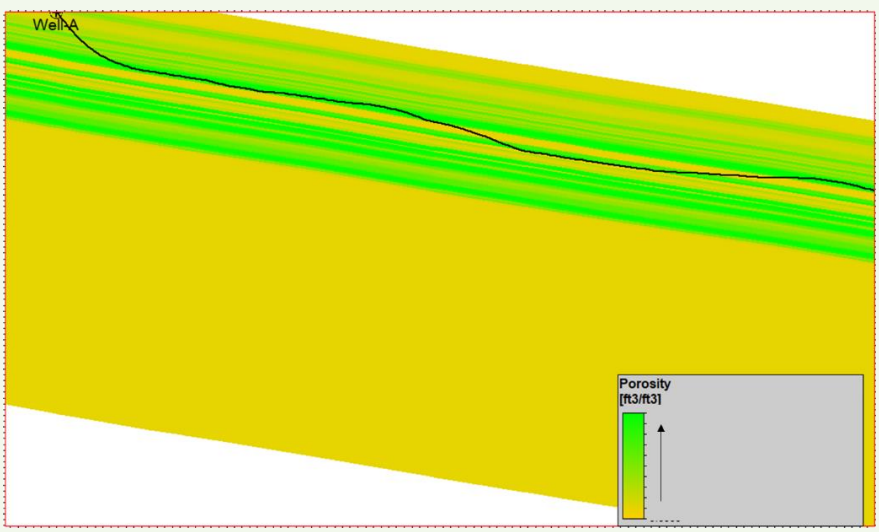

Table 1 *Well completion details for the offset wells. Completion types were a cased hole plug-and-perf style and the open hole multistage fracturing type.*

	Well Type	Completion	Lateral Length (ft)	Net Reservoir Contact (ft)
Well-A	HZ	Cased Hole Plug-and-Perf	6,225	3,905
Well-B	HZ	Cased Hole Plug-and-Perf	4,900	4,935
Well-B	HZ	Open Hole Multistage Fracturing	4,985	3,655

Perforation Strategy

The central strategy was to reduce the total number of fracturing stages while maintaining a consistent number of total clusters and enhancing the stimulation strategy. Reservoir quality/completion quality determination was used to create zones and select perforations[4]. Different rock and reservoir property variations were considered in the zone's generation.

The final plan was with five stages with six to nine clusters per stage, giving 39 clusters along the lateral, Fig. 3. This plan required reliable diversion chemistry and design. The perforation length for each cluster was decreased to 2 ft to ease the plugging of the fracture in the near wellbore region.

Diversion Design and Execution Methodology

A horizontal well drilling, completion, and intervention plan requires considerable cost components, and therefore, an experimental approach such as detailed in this article must use the full extent of available engineering capability. An integrated understanding of the design and execution methodology that was adopted in this well is detailed here to describe the decision making workflow.

Premium chemistry was utilized for acids, and diverters were fully degradable multimodal particulate diverters that have proven success in the region[5]. Design aids utilized were best practices established in the area — optimum acid volumetrics normalized for reservoir net pay — coupled with numerical modeling and other mathematical tools. These tools were validated on multiple cases[6]. An initial treatment schedule was designed with 50,000 to 60,000 gallons of different acid types split in three cycles separated by three diverter pills. The execution analysis relied on fracture pressure understanding and analysis along with a near real-time diagnostic evaluation.

The engineered workflow is described as:

1. Design the appropriate schedule with premium chemistry and volumes.
2. Simulate the design only for cycle 1 with the numerical model for near wellbore diversion[7].

Fig. 3 *A log montage for Well-A at 6,200 ft measured depth. The top track shows the revised five-stage perforation plan. The middle track shows the porosity-permeability variation, and the bottom track shows the mineralogy. Green represents dolomite and blue represents limestone.*

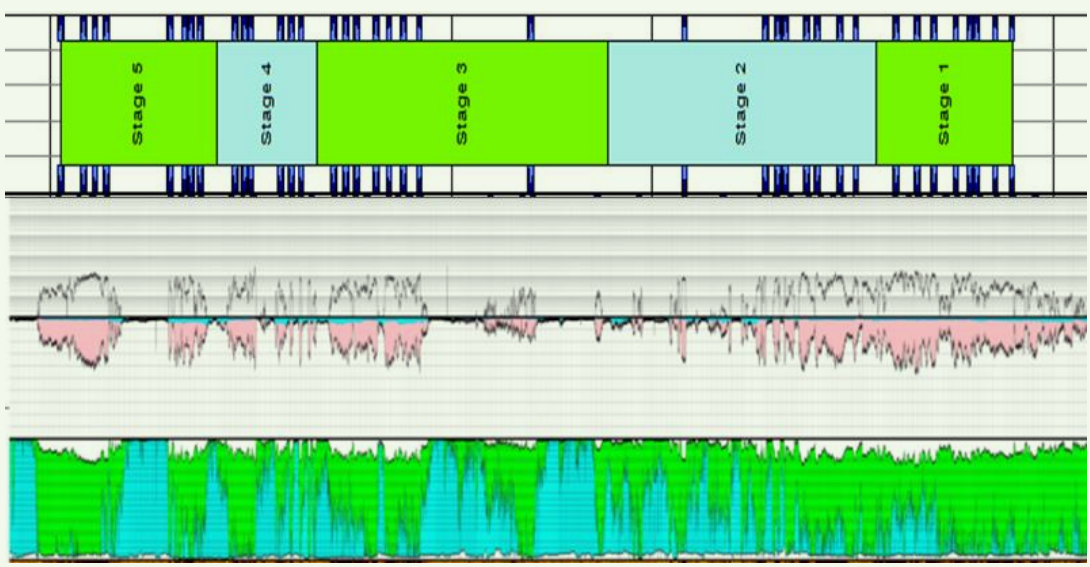

3. Evaluate the etched fracture geometry for different clusters.
4. Utilize the β factor diversion design workflow[8] to calculate the system volume.
5. Design the diverter pill volume and particulate mass to achieve a β value approaching 1. This is based on the validation study[6] in which it was found that diversion success is related to higher values of β approaching a value of 1, which indicates an equality between the system volume available for diversion and the particulate mass.
6. Design the first diverter pill based on the above calculations and input the design into the near wellbore diversion simulator.
7. Study the evolution of flux distribution and etched geometry among different fractured clusters.
8. Extend the same approach for acid cycle 2:
   a. Design and simulate the acid cycle.
   b. Calculate the system volume. The major difference in this cycle is that the calculation for the diverter mass must consider the current areal distribution of particulate per cluster that is still remaining in the near wellbore region from the first diverter cycle and then recalculate the β parameter for the new system volume.

      Therefore, the generalized equation for the system volume calculation will be:

      System volume for i^{th} cycle = Total system volume for i^{th} cycle – Particulate volume still present in the near wellbore region from $(i\text{-}1)^{th}$ cycle.

      In this calculation, the areal particulate distribution from the simulator should be converted to the particulate volume from the physical properties of particulates to effectively calculate the new β.
9. Repeat this process for the rest of the cycles and study the end-of-treatment results.
10. Validate and fine-tune the volumetrics on the fly based on fracture pressures, diversion pressures, and diagnostic findings.

Some of the highlights of the full design execution cycle implementation for one of the stages in this well follows. A similar approach was used for most stages in this candidate well.

Figure 4 shows the geometry at the end of acid cycle 1. The results here are used to evaluate step 3 in the mentioned workflow. It can be seen only three out of eight fractures are receiving major flux. Also shown is the particulate mass distribution across fractures after the first diverter pill is pumped. The result from these plots is used in step 8b in the mentioned workflow. The pressure curve depicts the diversion pressure developed during actual treatment execution. It can be seen that initially the pressure builds up during pill placement and later yields an even steeper pressure rise opening up new clusters. A total of 1,610 psi of diversion pressure was observed and also required the rate to be dropped from 40 bbl/min to 33 bbl/min, clearly indicating successful diversion.

Figure 5 shows a similar summary showing the evolution from cycle 1 to cycle 2. It can be observed that fluid flux has largely been redistributed to two new fractures, and particulate mass concentrations in the near wellbore region has also increased. Some material has moved farther away from the fracture, which

Fig. 4 *Design and execution evaluation for acid cycle 1. Left, etched width evolution showing three fractures being stimulated and three more taking minimal flux. Bottom right, the particulate mass distribution shows diverters effectively plugging some fractures. Top right, the diversion pressure buildup during pill 1 placement of the treatment.*

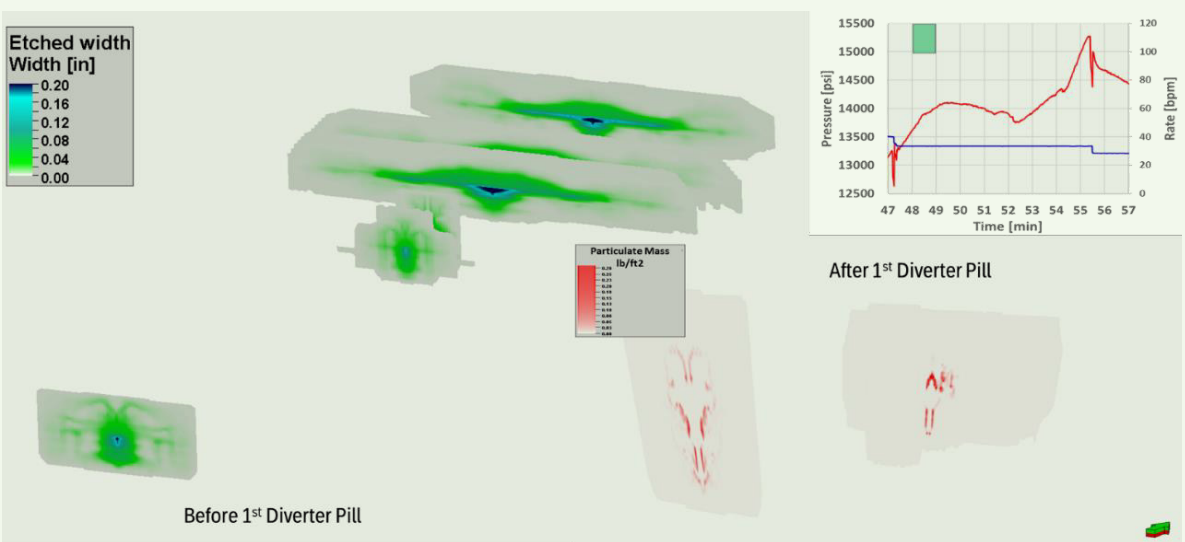

Fig. 5 *The design and execution evaluation for acid cycle 2. Left, the etched width evolution showing two new fractures receiving flux and developing etched geometry. Bottom right, the particulate mass distribution shows diverters in near wellbore region and some movement further away from the fracture increasing particulate skin inside the fracture. Top right, diversion pressure buildup during pill 2 placement of the treatment.*

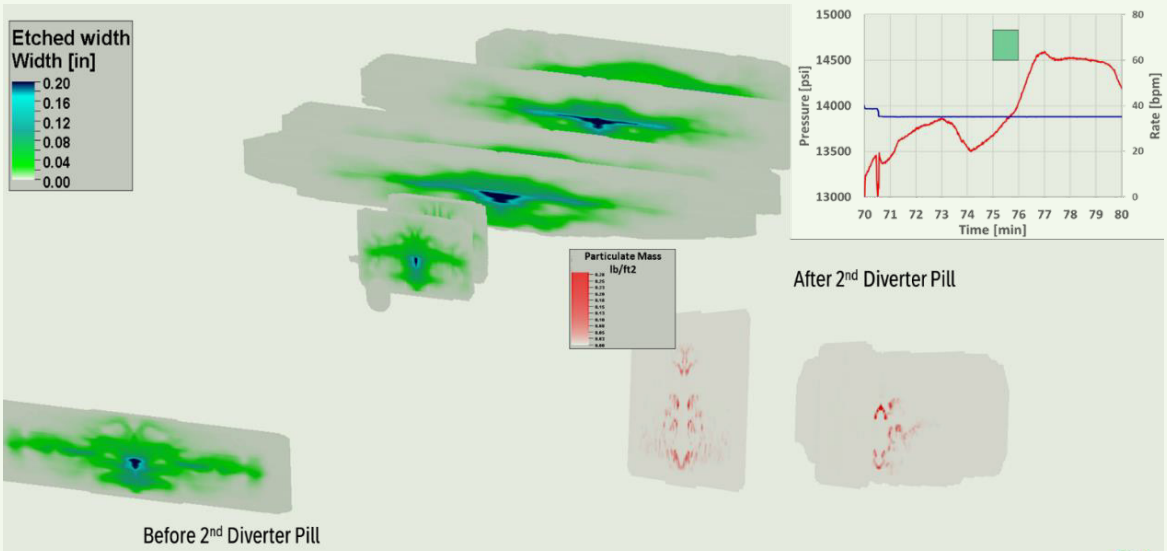

still creates enough skin to effectively reduce high flux distribution, and the treatment benefits from it from the diversion perspective. A diversion pressure of 1,240 psi is also observed during the treatment along with a rate drop from 40 bbl/min to 35 bbl/min.

Figure 6, the cycle 3 summary, shows further stimulation enhancement in the fractures that were not propagated earlier. The increased density of the particulate mass is observed here both in the near wellbore area and deeper into the fractures. A diversion pressure of 710 psi is observed and evaluated after the spurt loss of the diverter is seen. A steady bottom-hole rate of 40 bbl/min was maintained during the pill placement.

Figure 7 shows the final end-of-treatment fracture geometry and the particulate mass distribution. Here, it is important to note the criticality of degradable

Fig. 6 *The design and execution evaluation for acid cycle 3. Left, the etched width evolution showing enhanced stimulation in newly opened fracture clusters. Bottom right, the particulate mass distribution shows increase material density. Top right, diversion pressure buildup during pill 3 placement of the treatment.*

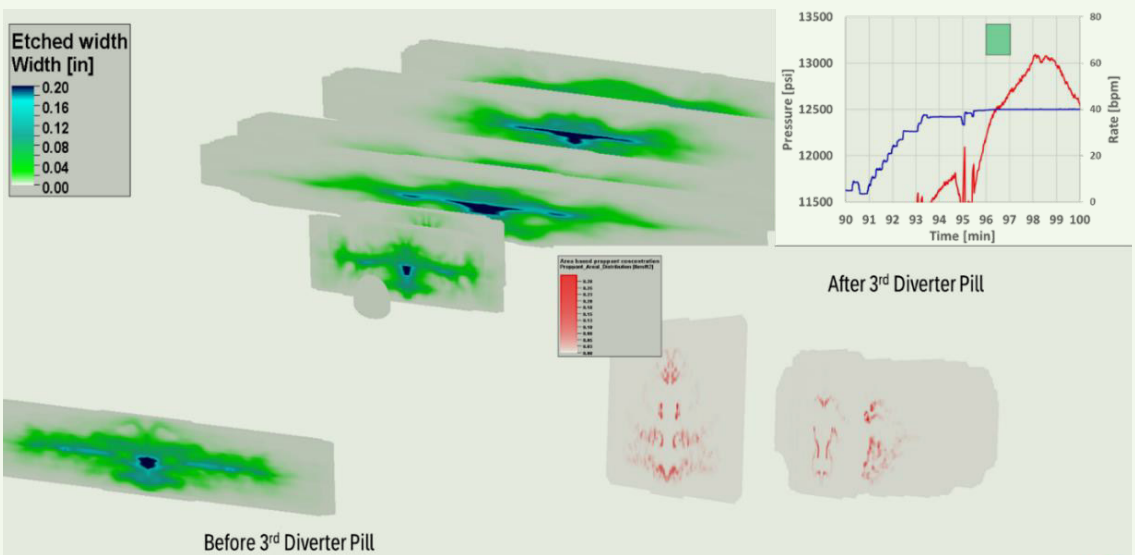

Fig. 7 *The end of treatment fracture properties shown with different perspectives. Left, the etched width evolution showing an increase from three to eight fractures etched with varied degrees of penetration. Right, the particulate mass distribution in all fractures.*

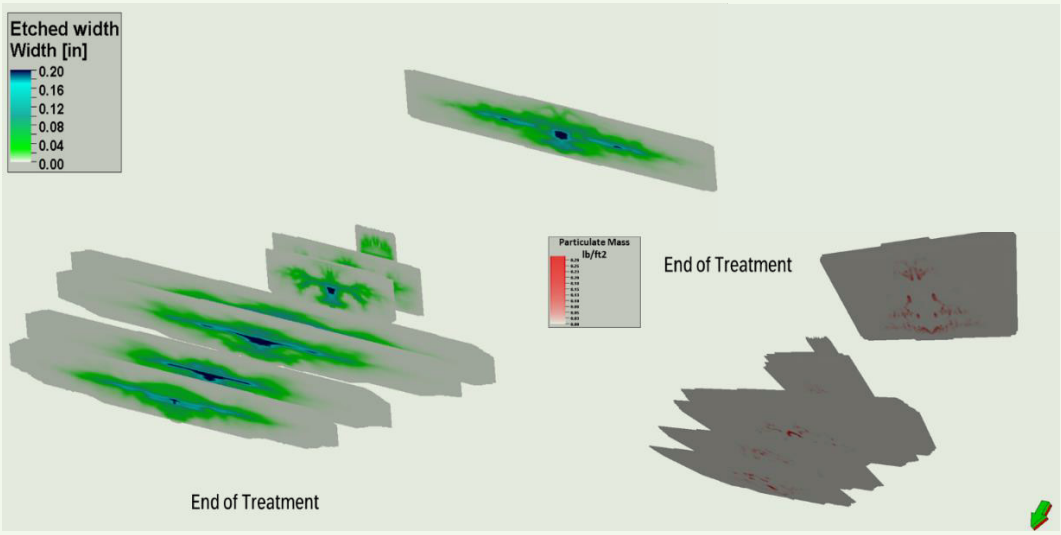

chemistry. If nondegradable material is utilized for similar applications, the skin enhancement created by particulates will restrict the flow capacity of fractures by up to 90%, affecting production performance.

Finally, it can be seen that all eight fractures show successful etching with varied degrees of penetration. The final geometry compared with the cycle 1 geometry shows evolution from three to eight fractures with a stimulation efficiency increase of 167% aided by engineered diversion. Both snapshots here are shown from a different perspective to better demonstrate the evolution of properties in all fractures. Different aspects and further details of the overall design and execution experience on this candidate lateral can be found in Obaid et al. (2022)[9].

Cluster Treatment Efficiency Diagnostics

The workflow relied largely on a successful fracture diversion, and therefore, it was critical to perform a stage-by-stage diversion efficiency diagnosis to adjust the design and perforation strategy or even increase stages if we fail to achieve diversion consistently. A novel nonintrusive technique was used for this purpose.

High Frequency Pressure Monitoring

A recently developed method based on high frequency pressure monitoring (HFPM) was used for the treatment efficiency evaluation in real-time. This new method combines cost-effective hardware consisting of a standard pressure transducer and a high-resolution data acquisition system with modern signal processing algorithms and Bayesian statistics[10]. The borehole pressure oscillation events caused by pump shutdown, called water hammers, are processed to determine the pressure signal reflection times by producing of the signal reflectivity images followed by fluid entry point determination by building the velocity model.

The hydraulic fracturing efficiency is evaluated in terms of detection of the new fluid entry points demonstrating stimulation of the new zones[11]. A recent reported advancement in the HFPM takes advantage of synergy between a nonlinear cepstrum algorithm with the scalar products of the resultant reflection time distributions, which results in high accuracy of the fluid entry point depth determination[12].

Being very sensitive to reflections, even with small amplitudes, the nonlinear data processing algorithms have drawbacks related to the amplification of a periodic pump noise signal that results in multiple strong cepstral peaks that overlap with the wellbore response and can be misinterpreted as multiple downhole reflectors. The weak signal equally contributes to the solution as the strong one due to the cepstrum algorithm nonlinearity, which might lead to unreasonable boosting of weak amplitude reflections or even noise. This is especially critical for the HFPM data with low signal-to-noise ratio (SNR).

In practice, the low SNR in weak water hammers is associated with viscous borehole fluid and the effect of operating pumps during the water hammer events. The acid fracturing is a special treatment type that is associated with these low SNR conditions. These conditions arise due to different physics of rock etching compared to a rock opening in proppant fracturing and leads to a different geometry of well connection with the rock and near wellbore region. Figure 8 is a comparison between water hammer events with high and low SNR witnessed in Well-A. The low SNR water hammer event is characterized by fewer pressure oscillations and weaker signal amplitudes and the appearance of false peaks on the reflectivity image.

To overcome these limitations, the water hammer events were processed with a combination of two newly

Fig. 8 *Examples of water hammer events with high (a), and low (b) SNR. The low SNR water hammer event has fewer pressure oscillations and a weaker reflectivity response.*

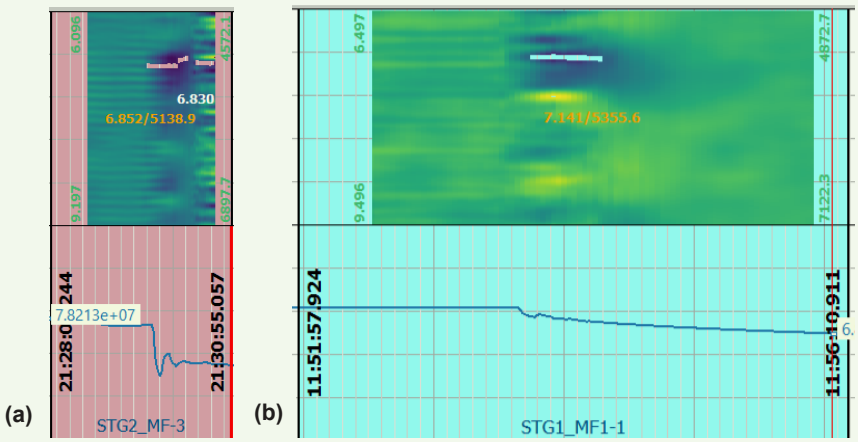

developed algorithms: predictive deconvolution and comb filter.

Predictive Deconvolution and Comb Filter

The predictive deconvolution algorithm[13] is based on the Wiener least squares prediction filter and is inspired by the predictive deconvolution filter introduced by Peacock and Treitel (1969)[14] aimed to remove the multiples caused by seismic wave reverberations in a water layer from marine seismograms. It is a linear algorithm with the intrinsic sensitivity to the surface pressure oscillations that makes it more robust in processing of the low SNR events than the traditional approach.

To suppress the harmonic pump noise, the comb filter is used[15]. The comb filter is sensitive to the periodic structure of the pump noise and that is precisely detected and suppressed from the pressure signal, without affecting the wellbore reflectivity part of the signal.

Figure 9 is the workflow for the processing of a water

Fig. 9 *Processing of a water hammer event with a combination of comb filter and predictive deconvolution.*

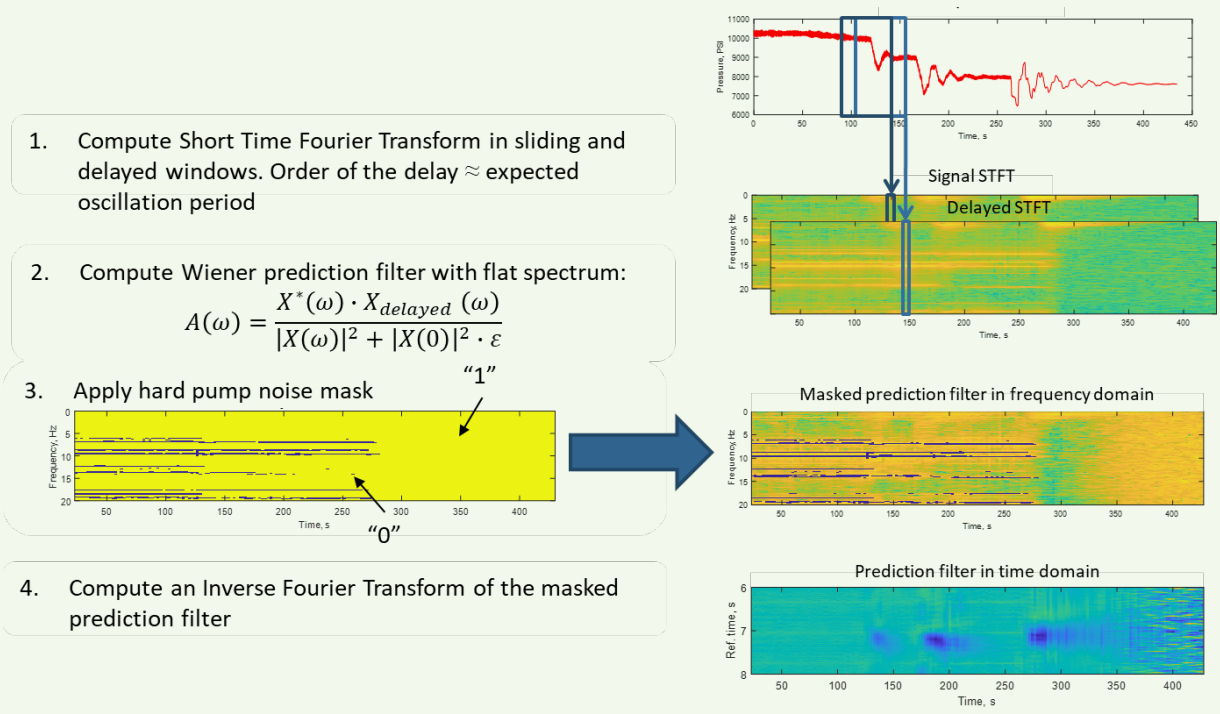

hammer event with a comb filter and predictive deconvolution algorithms. According to the workflow, the short-time Fourier transforms (STFT) for the original and delayed signals are computed. Then the Wiener prediction filter in the STFT domain is computed. The pump noise is approximated with the linear combination of comb shape functions in the STFT domain to produce a pump noise mask equal to 0 in the regions where the pump noise is observed — the intensive horizontal lines in the STFT images — and equal to 1 elsewhere.

Application of the mask to the prediction filter in the STFT domain filters out the pump noise, and the application of the inverse Fourier transform to the masked prediction filter produces the reflectivity image, where the most intensive reflections from the fracture are represented with the blue color.

The obtained reflection times are processed conventionally[10] to produce the fluid entry point plot.

Well-A Treatment Efficiency Analysis

Well-A was the first acid fracturing treatment with a complex treatment schedule — comprising pad fluid,

Fig. 10 *The poor quality of water hammers observed in Well-A necessitate use of novel handling algorithms.*

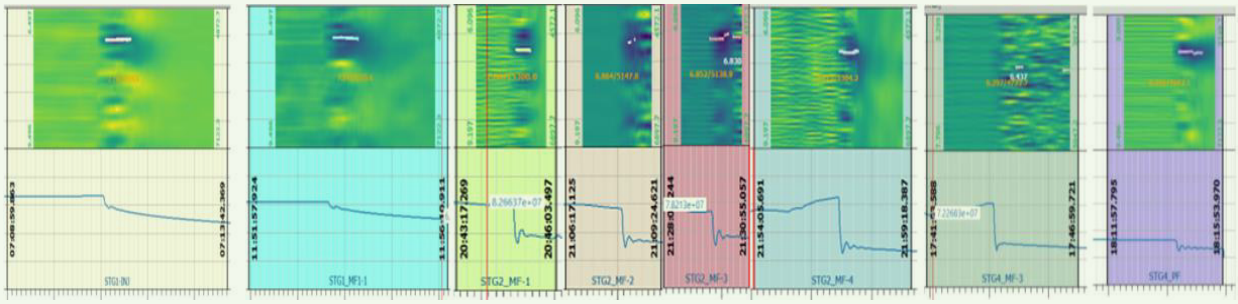

Fig. 11 *HFPM analysis summary with a Gauss plot for Well-A after applying the predictive deconvolution algorithm and comb filter. Cluster 1 implies stage 1, and the stage boundaries (depths) are marked by thick black lines. Events from left to right are from stage 1 through stage 5.*

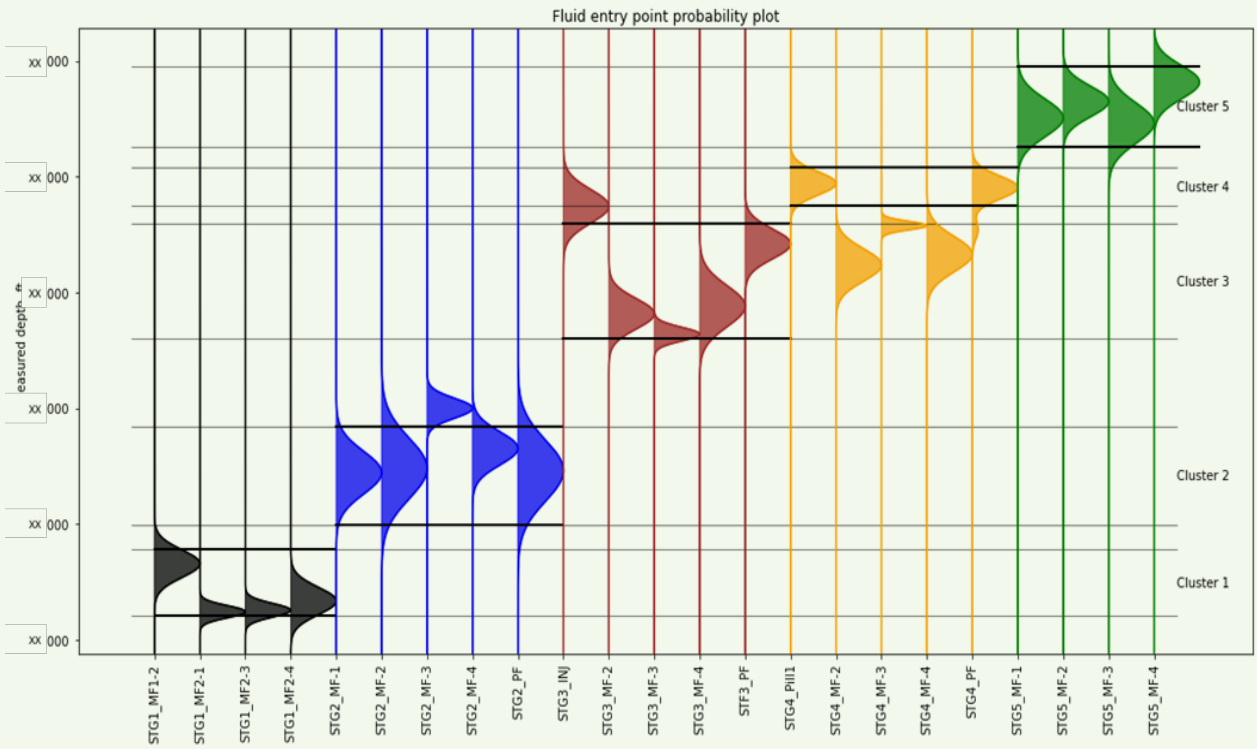

acid, emulsified acid, fiber-laden leakoff control acid, and multimodal particulate pills — to be using HFPM diagnostics. The newly developed noise suppression algorithms were effectively used to analyze the water hammers and fluid entry points. Figure 10 shows the poor quality of the hammer effect for most of the events used for the analysis in this well.

Figure 11 shows the comprehensive analysis for all events — within each stage — with the fluid entry point Gauss plot. The peak of this Gaussian curve of each event represents the expected depth of fluid entry, and the narrowness of the curve shows the prediction resolution. The thick black lines show the stage intervals — stages are depicted as clusters in the figure.

The detailed analysis shows that all the intervals were treated successfully with the diversion sequence. The stage 4 interval showed hydraulic communication with the previous interval based on predictive deconvolution, and this inference was confirmed with the decline pressure transient comparison. The diversion strategy used was especially beneficial for this stage to isolate the communication with stage 3 and effectively stimulate stage 4.

Obaid et al. (2022)[9] shows stage-by-stage details on how the analysis was validated along with the rock mineralogy at each cluster and the stimulation efficiency enhanced through the particulate diverters. The analysis showed that only 12 clusters would have been treated without effective diversion design but with the approach used here, a total of 33 clusters were treated out of 39.

Table 2 is a summary of the resolution of fluid entry points analyzed with each event and the probabilities of treating the target or previous intervals. The resolution values in the table are full widths of the gaussian peaks taken at their half heights. It can be

Table 2 *The summary for the HFPM analysis for Well-A.*

Event Name	Depth Resolution (ft)	Target Cluster Treatment Probability	Previous Cluster Treatment Probability
STG1_MF1-2	285	100%	0%
STG1_MF2-1	121	100%	0%
STG1_MF2-3	134	100%	0%
STG1_MF2-4	275	100%	0%
STG2_MF-1	434	100%	0%
STG2_MF-2	617	100%	0%
STG2_MF-3	201	100%	0%
STG2_MF-4	341	100%	0%
STG2_PF	623	100%	0%
STG3_INJ	340	100%	0%
STG3_MF-2	304	100%	0%
STG3_MF-3	135	100%	0%
STG3_MF-4	412	100%	0%
STF3_PF	306	100%	0%
STG4_Pill1	237	100%	0%
STG4_MF-2	330	0%	100%
STG4_MF-3	94	0%	100%
STG4_MF-4	357	0%	100%
STG4_PF	189	94%	6%
STG5_MF-1	379	100%	0%
STG5_MF-2	310	100%	0%
STG5_MF-3	405	100%	0%
STG5_MF-4	340	100%	0%

Fig. 12 *Evolution of the IPR curve during the choke bean-up and bean-down steps. The highlight and green arrow show the effectiveness of the cleanup. The bean-down IPR curve separation from the initial bean-up curve clearly shows the effect of a fracture cleanup on enhanced productivity.*

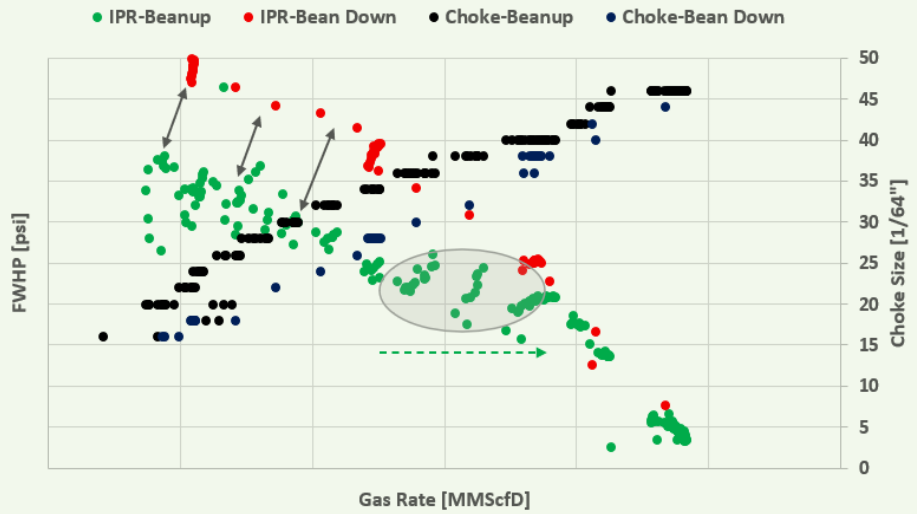

Fig. 13 *The water-gas ratio evolution along with fracturing fluid recovery during the flow back operations.*

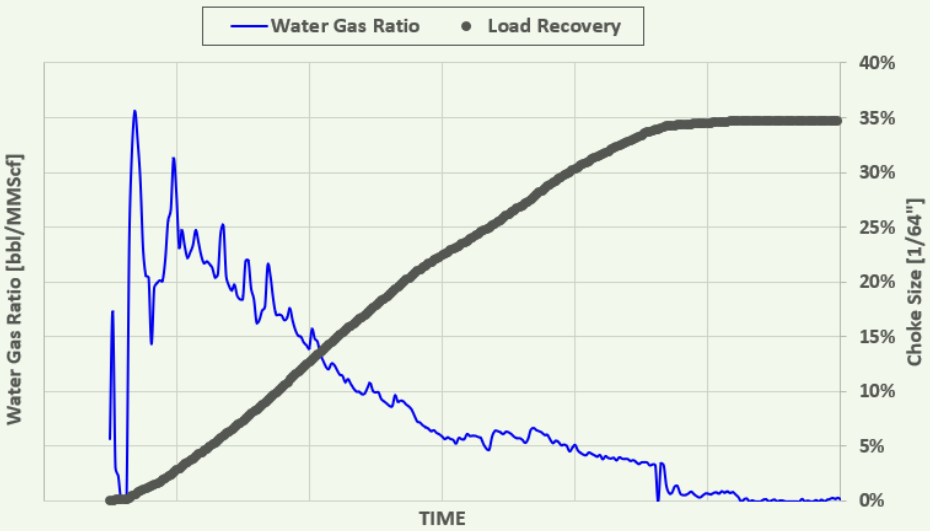

Table 3 *The well completion and reservoir details. Average porosity and permeability are scaled down.*

	Well Type	Completion	Stages	Total Perf. Clusters	Ave. Porosity	Avg. Perm.	Net Reservoir Contact (ft)	Total Acid (gal)
Well-A	HZ	Cased Hole Plug-and-Perf	5	39	1.00	0.13	3,905	291,200
Well-B	HZ	Cased Hole Plug-and-Perf	12	36	0.90	1.00	4,935	574,200
Well-C	HZ	Open Hole Multistage Fracturing	7	N/A	0.70	0.11	3,655	402,800

seen that even with large-stage intervals the resolution was acceptable. For statistical understanding, the resolution, R, is correlated with the standard deviation, σ, through the equation $R = 2\sigma\sqrt{2og2} \approx 2.4\sigma$. The peak of the Gaussian represents the expected depth and a narrower Gaussian implies higher confidence in the prediction.

The table also shows the probability of the fluid entry point existing in the current interval and previous interval. The square of probability function is calculated for the part of the curve in the current or previous interval and gives the probability of fluid entry point existing in that particular interval. For this candidate well, it can be seen that the probability of treating stage 4 started from 0% and increased to 94% based on HFPM interpretation, which can be accredited to diversion techniques utilized as detailed earlier.

Well Potential Evaluation

It is important to understand the yield of the experimental approach related to the well planning and completion. To ensure the evaluation phase was robust, a multiphase flow meter was used to enhance and optimize the plug milling, fracture cleanup, and deliverability phases.

Multiphase Flow Meter Utilization

The flow meter was utilized to enhance the engineering workflow on multiple fronts[1]. Figure 12 shows the inflow performance relationship (IPR) evolution through the fracture cleanup and well deliverability phases. It shows the steady IPR curve expansion — green dots moving from left to right — as the choke opening increases at and beyond 34/64". The horizontal part of the curve shows stabilization of the flow and the IPR steadily expanding with an increasing gas rate, but no increase in the drawdown, implying increasing productivity index (PI).

After that, at the slope change, a linear trend can be observed with an increased choke opening beyond 40/64", which is indicative of the end of flow back as far as the realization of the maximum well potential is concerned. Following that, in the bean-down period, the IPR — red dots moving from right to left — shows a clear separation from the initial/bean-up IPR, also marked with black arrows in the figure, which shows the effect of the fracture cleanup on well productivity. At the end of flow back, a three-rate stepdown was performed, which enabled establishing the final IPR (deliverability) without the need of a full separator setup.

An important parameter in post-fracturing flow back is the fracturing fluid recovery factor. It enables engineered decision making at the conclusion of flow back. Figure 13 shows different phases of water recovery where a slope change is evident in the water-gas ratio curve at different stages. A similar slope change can be correlated in the load recovery. When the recovery and water rate slow considerably, estimated time can be calculated, and flow back operations can be concluded. The candidate well showed a recovery factor of 25% to 34%.

Production Analysis

All the analyses in the design phase with numerical models and confirmations from fracture pressure and other diagnostic methods was validated when we compared the post-fracturing flow back potential. Parameters of the gas rate and flowing pressures were captured after fracture cleanup was achieved. Looking at production parameters only can give a skewed perspective without understanding the variations in reservoir development, stages, and acid pumped.

Table 3 details these variations for the three offset wells. Even though Well-C has only seven stages, it was an open hole lateral with packers and sleeves. In these completions, as demonstrated by Asif et al. (2021)[16], with the aid of sonic noise log diagnostics, each stage can have from three to nine fractures, depending on the open hole interval. Therefore, seven stages could have up to 40 total fractures contributing to production,

Fig. 14 *The offset wells' production comparison with post-fracturing flow back and normalized PI over multiple reservoir treatment parameters.*

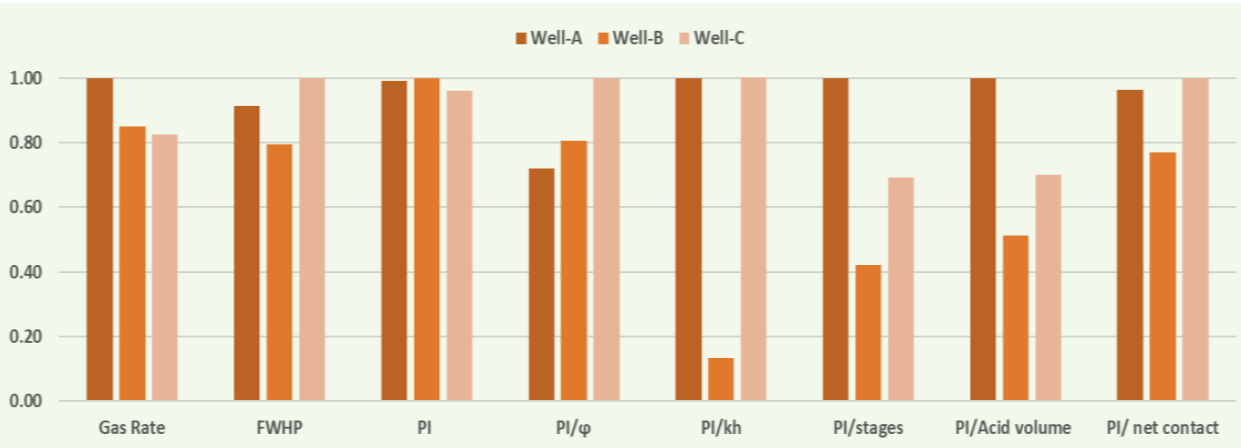

which is comparable to Well-B.

Figure 14 shows the calculated PI, which was comparable for all three wells. It is indicative of the fact that even with a diametrically different approach used in Well-A, the stimulation efficiency was enhanced to a level similar to that in the other wells. When the PI was normalized over different properties such as porosity, permeability, net reservoir contact, stage count, and acid volumes to capture the discrepancies from the reservoir and fracturing perspectives, it can be observed that Well-A performed comparably or better than other wells.

Way Forward

A production log on the candidate well will be completed to confirm the analysis of increased stimulation effectiveness. Production flow logs have traditionally been utilized as a diagnostic for the evaluation of diversion and stimulation efficiency. The analysis is very reliable, but because it is done after the fact, it can be used as an evaluation tool rather than a real-time tool. The results of such an integrated completion workflow can be improved by broadly using the HFPM diagnostic tool to improve stimulation efficiency. Khan et al. (2022)[17], and Khan et al. (2022)[18] have recently innovated a number of machine learning algorithms in fracturing applications for the treatment design, fracture geometry diagnosis, and rheology prediction.

A similar predictive workflow has been developed in which multiple wells conducted with this diagnosis are integrated to further enhance the completion design with the aid of data analytics. As shown by Khan et al. (2022)[19] and Pooniwala et al. (2022)[20], more chemistry and morphologies of products can be used for fluid loss or for effective plugging of rock at smaller sizes. Digital processes can also be used to precisely predict the chemistries using the method described by Yudin et al. (2021)[21].

Conclusions and Summary

1. Without sacrificing production potential, the fracturing design for a horizontal well in a carbonate tight gas environment was able to reduce the number of fracturing stages by 62%, from 13 stages down to five stages.
2. An experimental well engineering approach was used to evaluate the fluid entry points and cluster efficiency; a novel diagnostic tool created for viscous fluids and noisy situations was used in conjunction with perforation optimization, diversion chemical selection, and diversion design tools.
3. The overall assessment and analyses incorporates aspects from the diversion pressure reaction, fracturing treatment pressure trends and decline transients, HFPM diagnosis, and offset area production comparison. With the right diversion design and chemistry aids, the integrated analysis reveals a 275% increase in stimulation efficiency, resulting in an increase in stimulated clusters from 12 to 33.
4. Before the production flow log, we can infer that the efficiency of the stimulation is the same as in the offset wells, which had up to 58% more stages. After the flow analysis is conducted, the validity of all productive clusters can be determined.
5. The proposed approach can help to considerably reduce greenhouse gas emissions broadly through seven areas:
    a. Lower the pumping time through the reduction of stages.
    b. Less trucking for fracturing water and chemicals by reducing the amount of treating fluids.
    c. Fewer wireline plug-and-perf interventions.
    d. Less mixing and handling of chemicals.
    e. Lower milling time by reducing the number of isolation plugs.
    f. A reduced flow back time by reducing the amount of fluid recovery to achieve fracture cleanup.
    g. Fewer site days for well engineering workflow.

Acknowledgments

This article was presented at the Abu Dhabi International Petroleum Exhibition and Conference, Abu Dhabi, UAE, October 31 – November 3, 2022.

References

1. Alharbi, A., Khan, A.M., AlObaid, H., Ashby, S., et al.: "Effective Well Engineering Approach for Completion Intervention, Stimulation and Flow Measurements to Enhance Efficiency and Production Performance," SPE paper 210685, presented at the SPE Asia Pacific Oil and Gas Conference and Exhibition, Adelaide, Australia, October 17-19, 2022.
2. Rahim, Z., Al-Kanaan, A.A., Kayumov, R. and Al-Jalal, Z.: "Sequenced Fracture Degradable Diverters Improve Efficiency of Acid Fracturing in Multiple Perforated Intervals Completion Assembly," SPE paper 188187, presented at the Abu Dhabi International Petroleum Exhibition and Conference, Abu Dhabi, UAE, November 13-16, 2017.
3. Khan, A.M. and Olson, J.: "Impact of Hydraulic Fracture Fairway Development in Multistage Horizontal Laterals — A Production Flow Simulation Study," SPE paper 205859, presented at the SPE Annual Technical Conference and Exhibition, Dubai, UAE, September 21-23, 2021.
4. Almulhim, A., Hamid, S., Khan, A.M. and Hoong, C.C.: "A Novel Stimulation Design Approach Revives a Challenging Gas Field," SPE paper 202427, presented at the SPE Asia Pacific Oil and Gas Conference and Exhibition, virtual, November 17-19, 2020.
5. Alabdulmuhsin, A., Alkulaib, H., Hansen, J. and Khan, A.M.: "Self-Degradable Particles Mitigate Communication between Stages in Multistage Acid Fracturing Completion," SPE paper 202612, presented at the Abu Dhabi International Petroleum Exhibition and Conference, Abu Dhabi, UAE, November 9-12, 2020.
6. Almulhim, A., Khan, A.M., Hansen, J., AlObaid, H., et al.: "Validation of a Novel Beta Design Factor for Enhancing Stimulation Efficiency through Field Cases

and Near Wellbore Diversion Model," SPE paper 210439, presented at the SPE Annual Technical Conference and Exhibition, Houston, Texas, October 3-5, 2022.

7. Khan, A.M., Emelyanov, D., Romanovskii, R. and Nevvonen, O.: "Advanced Modeling Capability to Enhance Near Wellbore and Far-Field Bridging in Acid Fracturing Field Treatments," SPE paper 206255, presented at the SPE Annual Technical Conference and Exhibition, Dubai, UAE, September 21-23, 2021.

8. Khan, A.M., Usova, Z. and Yudin, A.: "Integrated Workflow with Experimentation, Modeling, and Field Implementation Framework Enhances Fracture Diversion Understanding in Carbonate Reservoirs," SPE paper 205665, presented at the SPE/IATMI Asia Pacific Oil and Gas Conference and Exhibition, virtual, October 12-14, 2021.

9. AlObaid, H., Khan, A.M., Hansen, J., Khudorozhkova, A.: "Stimulation Efficiency with Significantly Fewer Stages: Perforation Strategy Combined with Multimodal Diverters and Novel Nonintrusive Monitoring Algorithm," SPE paper 210472, presented at the SPE Annual Technical Conference and Exhibition, Houston, Texas, October 3-5, 2022.

10. Parkhonyuk, S., Fedorov, A., Kabannik, A., Korkin, R., et al.: "Measurements while Fracturing: Nonintrusive Method of Hydraulic Fracturing Monitoring," SPE paper 189886, presented at the SPE Hydraulic Fracturing Technology Conference and Exhibition, The Woodlands, Texas, January 23-25, 2018.

11. Kabannik, A.V., Parkhonyuk, S., Korkin, R., Litvinets, F., et al.: "Can We Trust the Diversion Pressure as a Decision Making Tool: Novel Technique Reveals the Truth," SPE paper 193180, presented at the Abu Dhabi International Petroleum Exhibition and Conference, Abu Dhabi, UAE, November 12-15, 2018.

12. Korkin, R., Parkhonyuk, S., Fedorov, A., Badazhkov, D., et al.: "High Frequency Pressure Monitoring and Data Analytics for Stimulation Efficiency Determination: New Perspectives or Potential Limits," SPE paper 199762, presented at the SPE Hydraulic Fracturing Technology Conference and Exhibition, The Woodlands, Texas, February 4-6, 2020.

13. Kabannik, A.V.: "Method of Determining Depths of Wellbore Reflectors," U.S. patent application US20210032978A1, 2021.

14. Peacock, K.L. and Treitel, S.: "Predictive Deconvolution: Theory and Practice," *Geophysics*, Vol. 34, Issue 2, April 1969, pp. 155-169.

15. Kabannik, A.V.: "Method and System for Monitoring a Wellbore Object Using a Reflected Pressure Signal," U.S. patent application US20210032984A1, 2021.

16. Asif, A., Hansen, J., Khan, A.M. and Sheshtawy, M.: "Integration of Post-Fracturing Spectral Noise Log, Temperature Modeling, and Production Log Diagnoses Water Production and Resolves Uncertainties in Open Hole Multistage Fracturing," SPE paper 204668, prepared for presentation at the SPE Middle East Oil and Gas Show and Conference, event canceled, November 28-December 1, 2021.

17. Khan, A.M., BinZiad, A., Al Subaii, A., Alqarni, T., et al.: "Supervised Learning Predictive Models for Automated Fracturing Treatment Design: A Workflow Based on Algorithm Comparison and Multiphysics Model Validation," SPE paper 205310, presented at the SPE International Hydraulic Fracturing Technology Conference and Exhibition, Muscat, Oman, January 11-13, 2022.

18. Khan, A.M., Sharan, S., Venugopal, K., Venkataramanam, L., et al.: "Data Engineering and Supervised ML Enabled Predictive Model for HPHT Fracturing Fluid Rheology — Digital Laboratory Approach," IPTC paper 22085, presented at the International Petroleum Technology Conference, Riyadh, Kingdom of Saudi Arabia, February 21-23, 2022.

19. Khan, A.M., Isaev, V. and Plyashkevich, V.: "Expanding the Degradable Fluid Loss Additive Application Spectrum through Advanced Slurry Transport Modeling, Theoretical and Experimental Integration," IPTC paper 22144, presented at the International Petroleum Technology Conference, Riyadh, Kingdom of Saudi Arabia, February 21-23, 2022.

20. Pooniwala, S., Malik, A., Khan, A.M., Plyashkevich, V., et al.: "Novel Morphology Self-Degradable Fiber Enables Enhanced Stimulation Fluid Diversion in High Temperature Carbonate Formations," IPTC paper 22205, presented at the International Petroleum Technology Conference, Riyadh, Kingdom of Saudi Arabia, February 21-23, 2022.

21. Yudin, A., Khan, A.M., Romanovskii, R., Alekseev, A., et al.: "Control Over the Fracture in Carbonate Reservoirs as a Result of an Integrated Digital Stimulation Approach to Core Testing and Modeling," SPE paper 206636, presented at the SPE Russian Petroleum Technology Conference, virtual, October 12-15, 2021.

About the Authors

Abdulrahman A. Al-Mulhim

B.S. in Petroleum Engineering, University of Leeds

Abdulrahman A. Al-Mulhim is a Gas Production Engineer working in Saudi Aramco's Southern Area Production Engineering Department. He is responsible for designing intervention programs, supervising operations, monitoring wells' performance, and acting as a point of communication between different organizations.

Abdulrahman is the author of several Society of Petroleum (SPE) papers. He also was selected to present a paper at the Abu Dhabi International Expedition and Conference (ADIPEC) in November 2018.

In 2013, Abdulrahman received his B.S. degree in Petroleum Engineering from the University of Leeds, Leeds, U.K.

Hashem A. Al-Obaid

B.S. in Petroleum Engineering, King Fahd University of Petroleum and Minerals

Hashem A. Al-Obaid is a Gas Reservoir Engineer working in the South Ghawar Gas Reservoir Management Division of Saudi Aramco's Gas Reservoir Management Department.

He joined Saudi Aramco as a Gas Production Engineer in 2013. Since then, Hashem has been involved in completing gas wells in both carbonate and sandstone reservoirs, with experience in coiled tubing, wireline, well integrity and pumping.

He is an active member in the Society of Petroleum Engineers (SPE). Hashem is a certified SPE Petroleum Engineer.

He is the author and coauthor of several papers and presentations.

Hashem received his B.S. degree in Petroleum Engineering from King Fahd University of Petroleum and Minerals (KFUPM), Dhahran, Saudi Arabia.

Abdul Muqtadir Khan

M.S. in Petroleum Engineering, University of Texas-Austin

Abdul Muqtadir Khan is currently working as a Lead Technical Engineer for fracturing and stimulation, where he is involved in fracturing projects. Abdul joined Schlumberger in 2013 as Fracturing Field Engineer in South Texas. After two years in that position, he was given the role of a Lead Technical Engineer in Saudi Arabia.

Since 2015, Abdul has been in charge of fracturing and production technical support, providing support for optimization and special projects to Saudi Aramco's Production Engineering Division.

He has 7 years of experience in fracturing treatments in both conventional and unconventional wells.

In 2010, Abdul received his B.S. degree in Petroleum Engineering from Maharashtra Institute of Technology, Pune, India. In 2013, he received his M.S. degree in Petroleum Engineering from the University of Texas at Austin, Austin, TX.

Jon E. Hansen

B.S. in Petroleum Engineering, Texas A&M University

Jon E. Hansen has approximately 30 years of experience in oil industry. He worked in PJ as a Stimulation Specialist. Following this, he joined Saudi Aramco and then retired in 2022.

Jon received his B.S. degree in Petroleum Engineering from Texas A&M University, College Station, TX.

Dr. Artem Kabannik

Ph.D. in Seismic Tomography, Trofimuk United Institute of Geology, Geophysics and Mineralogy

Dr. Artem Kabannik started his career with Schlumberger as a Wireline Engineer spending two years in field locations of Canada and Chad. Currently, he is working in the Novosibirsk Technology Center based in Russia as a Senior Scientific Computing Engineer.

Artem is focusing on the development and implementation of methods for real-time monitoring of hydraulic fracturing stimulation treatments and cementing operations.

In 2005, he received his Ph.D. in Seismic Tomography in Application to Earthquake Data Processing, from the Trofimuk United Institute of Geology, Geophysics and Mineralogy, of the Siberian Branch of the Russian Academy of Sciences, Novosibirsk, Russia.

Synthesis of Epoxy Resin-Based Geopolymer Utilizing Saudi Arabian Volcanic Ash for Primary Well Cementing Applications

Khawlah A. Alanqari, Dr. Abdullah S. Al-Yami and Dr. Vikrant B. Wagle

Abstract /

Conventional cement production possess huge environmental concerns, which is considered globally the third largest source of carbon dioxide (CO_2) emissions into the environment. This is due to the decomposition of carbonates that produce approximately 900 kg of CO_2 for every 1,000 kg of cement produced. As a substitute, geopolymer cement can reduce the CO_2 emissions by 80% because there is zero CO_2 emissions through the geopolymer cement production. Moreover, geopolymer cement can be prepared utilizing waste materials such as fly ash. In Saudi Arabia, we have enough volcanic ash to sustain the development of this eco-friendly cement. Furthermore, geopolymer binders show exceptional mechanical, chemical, and environmental benefits in comparison to conventional cement. In addition to the geopolymer properties, liquid epoxy resins are known to increase bonding with the casing; thereby, increasing the wellbore integrity.

In this study, we successfully developed a novel epoxy resin-based geopolymer cement utilizing Saudi Arabian volcanic ash for primary cementing applications for the oil and gas industry. This was done by adding an epoxy resin formulation to the geopolymer slurry. This novel cement shows an excellent strength and good rheological properties with a controlled setting time. The objective of this article is to detail and explain the synthesis of this cement, geopolymer slurry preparation and epoxy resin formulation. Also, to investigate the effect of adding the epoxy resin formulation to the geopolymer slurry in terms of the final cement strength, thickening time and rheological properties, as well as to detail lab testing.

To prepare the epoxy resin-based geopolymer, the volcanic ash particles were activated first by a mixture of sodium hydroxide (NaOH), sodium silicate $(Na_2O)_x \cdot SiO_2$, and water. Then, an epoxy resin formulation was added to the geopolymer slurry that contains an epoxy resin along with a curing agent. The amount of the epoxy resin formulation was varied to study the effect of adding the epoxy resin into the geopolymer slurry in terms of the final cement's setting time and compressive strength.

This was done to develop a cement with excellent strength and a controlled setting to ensure the right cement placement. In addition, the chemical conditions were evaluated to simulate a variety of downhole conditions to prove the effectiveness of this novel geopolymer composition as a cement for primary cementing applications. The lab testing includes gelling time and compressive strength measurements, as well as a chemical analysis of the Saudi Arabian volcanic ash.

Introduction

Geopolymers are inorganic polymers that act as binders and rigid materials. The synthesis of these binders includes a polycondensation reaction between silicate (SiO_2) and aluminate (Al_2O_3) species under alkaline conditions to form a network of Si and Al atoms all linked through oxygen atoms[1, 2]. The final gel product is a sodium aluminosilicate hydrate (N-A-S-H) gel, and it comes in a 3D chain with a tetrahedral structure[3, 4]:

Aluminosilicates source (SiO_2, Al_2O_3)	+	Alkaline activator (M-OH, Na_2SiO_3 solution: M: K+, Na+, etc.)	Poly-condensation reaction ⟶	Geopolymer Sodium aluminosilicate hydrate gel (N-A-S-H gel)

Geopolymer cement displays various mechanical, chemical, and environmental benefits in comparison to conventional Portland cement. It shows exceptional mechanical properties such as higher compressive strength, low permeability values and better durability[5]. It has a higher resistance to various acids and temperatures[6, 7]. Moreover, geopolymer binders can reduce carbon dioxide (CO_2) emissions significantly into the environment.

This is due to zero production of CO_2 emissions while preparing the geopolymer cement. Whereas, ordinary Portland cement produces extensive amounts of CO_2 emissions. According to Eqn. 1, there is one ton of CO_2 emissions for every one ton of cement production[8, 9].

$$5\ CaCO_3 + 2\ SiO_2 \rightarrow (3\ CaO, SiO_2)\ (2\ CaO, SiO_2) + 5\ CO_2 \quad (1)$$

Besides the mechanical, chemical, and environmental benefits of geopolymer binders, they can be prepared from industrial waste byproducts that are rich in Si_2O and Al_2O_3 species, such as fly ash and ground granulated blast furnace slag, and others as well as from clays such as metakaolin[10, 11]. These waste materials are considered as aluminosilicate source materials.

A geopolymer binder was successfully developed utilizing Saudi Arabian volcanic ash for primary cementing application[12]. The prepared binder has a good strength and setting time. This was done by activating the local volcanic ash particles under a high pH medium — sodium hydroxide (NaOH) and sodium silicate $(Na_2O)_x \cdot SiO_2$ solution.

Both the compressive strength and setting time are strongly affected by the concentration of the activation solution. Therefore, the highest compressive strength within 24 hours; 2,565 psi, was found with the activation solution of $(Na_2O)_x \cdot SiO_2$ and NaOH that contains the following addition ratio and molarity, Na_2O, $NaOH/Al_2O_3$ ratio of 0.65 and a 6 Molar (M) of NaOH solution, respectively. The gelling time and mixability decrease by increasing the addition amounts of the alkaline solution. The gelling time decreased from 13:09 hr:min to 5:20 hr:min by increasing the molar ratio of Na_2O, $NaOH/Al_2O_3$ from 0.45 to 0.65 with a final geopolymer strength of 340 psi and 2,565 psi, respectively.

In other words, we must sacrifice the final geopolymer binder strength to prepare a geopolymer slurry with a convenient setting time. To minimize the substantial decrease in compressive strength while maintaining a good workability, we plan to introduce an epoxy resin into the geopolymer slurry.

Epoxy resin has been widely used in the oil field for many applications such as drilling, completion, and production. It was used as a primary cement for zonal isolation[13], a resin-based cement to improve well integrity[14], a cement additive in primary cementing, a loss circulation material to cure severe losses while drilling[15], and in strengthening unconsolidated sands[16].

The objective of this article is to develop a novel epoxy resin-based geopolymer cement utilizing Saudi Arabian volcanic ash for primary cementing applications for the oil and gas industry with good compressive strength and controlled setting time. In this study we will explain and detail the synthesis of this cement, geopolymer slurry preparation, and epoxy resin formulation. Also, we will investigate the effect of adding the epoxy resin formulation to the geopolymer slurry in terms of the final cement strength, thickening time as well as to detail lab testing.

Materials and Methods

This study utilizes a local fine volcanic ash where 80% of the particle sizes of the utilized sample is less than 45 µm. For the activation solution, we developed an alkaline mixture of a 6 M NaOH and $(Na_2O)_x \cdot SiO_2$ solution, all mixed with distilled water[12]. The NaOH comes in a shape of pellets (solid) with 98% purity. These pellets are dissolved in distilled water and kept overnight for the NaOH solution preparation. The $(Na_2O)_x \cdot SiO_2$ solution has a ratio of SiO_2:Na_2O between 2.0 and 3.02, and it was obtained commercially.

The epoxy resin formulation contains two epoxy resins along with a curing agent and an emulsifier. The two epoxy resins are C12-C14 alkyl glycidyl ether and bisphenol-A-epichlorohydrin epoxy resin with the reactive diluent oxirane mono [(C12-C14)-alkyloxy) methyl] derivatives. These resins are indicated in this study as resin 1 and 2; respectively. The curing agent is DETA, which is an amine curing agent. Also, we utilized polyaminated fatty acid as an emulsifier. The epoxy resins, curing agent, and the emulsifier are all obtained commercially.

The lab testing includes characterization of the volcanic ash sample, gelling time, and compressive strength measurement.

Epoxy Resin-Based Geopolymer Preparation

The epoxy resin-based geopolymer preparation involved the preparation of a geopolymer slurry by activating the volcanic ash particles with a mixture of NaOH, $(Na_2O)_x \cdot SiO_2$ and water[12]. Then, an epoxy resin formulation was added to the geopolymer slurry that contains an epoxy resin along with an amine curing agent and an emulsifier.

In this study, we prepared four different testing formulations. The first formulation is a reference that contains a previously developed geopolymer cement with no addition of resins[12]. In the other three formulations, we varied the additional amount of the resin formulation to study the effect of adding the epoxy resin into the geopolymer slurry in terms of the final cement's setting time and compressive strength, Table 1. In addition, testing conditions are set to simulate downhole conditions. Our goal is to increase the final cement strength while having a controlled and convenient setting time. This is highly important to develop a resin-based geopolymer that is appropriate for primary well cementing applications.

Epoxy Resin-Based Geopolymer Cement Slurry Preparation Procedure

The geopolymer cement slurry formulations are prepared in the lab using the standard American Petroleum Institute (API) blender[17]. The maximum speed used during slurry preparation was 12,000 rotations per minute (rpm). The geopolymer cement slurry was mixed in the blender for 1 minute at 4,000 rpm and 1 to 2 minutes at 12,000 rpm.

X-ray Powder Diffraction

The analytical X-ray powder diffractometer with a cobalt X-ray tube is used to measure the high-resolution

Table 1 *The geopolymer testing formulations*

Geopolymer Slurry			Resin Formulation	
Volcanic Ash Sample	Fine Volcanic Ash Average Particle Size Distribution: 45 μm		Epoxy Resin 1	80 g
SiO_2/Al_2O_3 (in Volcanic Ash Sample)	6.14		Epoxy Resin 2	20 g
Na_2O, $NaOH/Al_2O_3$	0.43		Emulsifier	7.7 g
NaOH Molarity	6 M		Curing Agent	3 g
Testing Formulations	FR	F1	F2	F3
Volcanic Ash: Resin Formulation by Volume	100:00	80:20	70:30	50:50

X-ray powder diffraction (XRD) data of the volcanic ash sample. This technique is used to determine the crystallographic structure, chemical composition, and physical properties of a material[18].

Ultrasonic Cement Analyzer

The ultrasonic cement analyzer (UCA) is used to measure the relative strength development of the epoxy resin-based geopolymer slurries under high-pressure, high temperature (HPHT) to simulate downhole conditions[17].

We ran UCA tests on all four of the prepared formulations. The test temperature and pressure were 150 °F and 2,400 psi, respectively.

Consistometer

Standard API HPHT consistometer is used to measure the thickening time of all the prepared epoxy resin-based geopolymer slurries under HPHT conditions to simulate downhole conditions. The thickening time is the time taken by the geopolymer slurries to reach a consistency of 70 to 100 Bearden units of consistency[17].

We performed thickening time tests on all four of the prepared formulations. Where in each test, the resin-based geopolymer slurry is poured from the blender into an API slurry cup. The resin-based geopolymer slurry is then placed in the consistometer and is then subsequently subjected to the required temperature and pressure.

Results and Discussion

XRD

The local volcanic ash sample was tested by XRD for characterization. This test shows the exact chemical composition, and the results are listed in Table 2. The XRD result shows that the volcanic ash sample is 70% amorphous material, and mainly contains 44.44%, 15.97%, and 8.53% of SiO_2, Al_2O_3, and CaO species, respectively. The SiO_2 and Al_2O_3 species can be activated with an alkaline solution to undergo the geopolymerization reaction.

UCA

Based on UCA results, we found that by adding 20% of the resin formulation into a geopolymer slurry, the final cement strength increased from 340 psi into 830 psi, Table 3. In addition, the results show that the final cement strength of the resin-based geopolymer is linearly affected by the resin formulation addition amounts.

In other words, by increasing the resin formulation amount from 20% to 50% by volcanic ash volume, the compressive strength increased from 830 psi to 2,340 psi, respectively, Fig. 1.

Table 2 *The details of the XRD composition of the volcanic ash sample.*

Compound	Wt%
Amorphous Material	70
Labradorite: $Ca_{0.65}Na_{0.32}(Al_{1.62}Si_{2.38}O_8)$	19
Augite: $Ca(Fe, Mg)Si_2O_6$	6
Forsterite: Mg_2SiO_4	5
CaO (%)	8.53
SiO_2 (%)	44.44
Al_2O_3 (%)	15.97
Fe_2O_3 (%)	13.2
MgO (%)	7.89
K_2O (%)	1.37

Table 3 *The compressive strength results of the geopolymer testing formulations*.*

	FR	F1	F2	F3
Compressive Strength (psi)	340	830	1,570	2,340
*Test Length: 24 hours				

Fig. 1 *The epoxy resin-based geopolymer of formulation 3 with a strength of 2,340 psi.*

Consistometer

Similar to the UCA results, the thickening time results are strongly affected by the resin formulation addition amounts, Table 4. For example, the thickening time increased from 13:09 hr:min to 17:20 hr:min by adding 20% of the prepared resin formulation into the geopolymer slurry. This is due to the interference of water molecules in the geopolymer slurry. Water molecules can form hydrogen bonds with the resin's epoxy groups, which can delay the amine curing agent nucleophilic attack on the resin's epoxy groups.

As a result, there is dilation in the resin polymerization and gelling time. On the other hand, the setting time decreased from 17:20 hr:min to 8:10 hr:min, by increasing the additional amount of resin formulation from 20% to 50%, respectively; because the water amount becomes less effective in delaying gelation by increasing the resin formulation addition. This means that by adding more than 30% of an epoxy resin formulation into a geopolymer slurry, it can accelerate the reaction rate and decrease the setting time.

From test results, we found that the compressive strength of the resin-based geopolymer cement was increased when increasing the additional amount of the resin formulation. Moreover, the gelling time was strongly affected as well by varying the resin formulation amounts; where, the setting time decreased when more than 30% of resin formulation was used.

Table 4 *The thickening time results of the geopolymer testing formulations.*

	F_R	F1	F2	F3
Thickening Time (hr:min)	13:09	17:20	11:45	8:10

Conclusions

We successfully developed a novel epoxy resin-based geopolymer cement utilizing Saudi Arabian volcanic ash for primary cementing applications for the oil and gas industry. This was done by adding an epoxy resin formulation to the geopolymer slurry. The geopolymer slurry was first activated by an alkaline solution that includes a NaOH 6 M and a Na_2SiO_3 solution. We investigated the effects of varying the resin formulation addition amounts on both the synthesis and mechanical properties of the resin-based geopolymer cement.

Test results indicated that the resulting compressive strength is linearly affected by the additional amounts of the resin formulation. The compressive strength increased from 830 psi to 2,340 psi by increasing the resin formulation amount from 20% to 50% by volcanic ash volume; respectively. Moreover, the setting time was strongly affected by the additional amount of resin formulation into the geopolymer slurry. Where, the thickening time decreased when 30% and more of resin formulation was used.

Acknowledgments

This article was presented at the Abu Dhabi International Petroleum Exhibition and Conference, Abu Dhabi, UAE, October 31 – November 3, 2022.

References

1. Davidovits, J.: "Geopolymers — Inorganic Polymeric New Materials," *Journal of Thermal Analysis*, Vol. 37, 1991, pp. 1633-1656.
2. Xu, H. and Van Deventer, J.S.J.: "The Geopolymerization of Alumino-Silicate Minerals," *International Journal of Mineral Processing*, Vol. 59, Issue 3, June 2000, pp. 247-266.
3. Srinivasan, K. and Sivakumar, A.: "Geopolymer Binders: A Need for Future Concrete Construction," *International Scholarly Research Notices*, Vol. 2013, 2013.
4. Amritphale, S.S., Bhardwaj, P. and Gupta, R.: "Advanced Geopolymerization Technology," Chapter in *Geopolymers and Other Geosynthetics*, (eds.) Alshaaer, M. and Jeon, H-Y., Intech Open, 2019.
5. Salehi, S., Ali, N., Khattak, M.J. and Rizvi, H.: "Geopolymer Composites as Efficient and Economical Plugging Materials in Peanuts Price Oil Market," SPE paper 181426, presented at the SPE Annual Technical Conference and Exhibition, Dubai, UAE, September 26-28, 2016.
6. Bu, Y., Du, J., Guo, S., Liu, H., et al.: "Properties of Oil Well Cement with High Dosage of Metakaolin," *Construction and Building Materials*, Vol. 112, June 2016, pp. 39-48.
7. Khalifeh, M., Todorovic, J., Vrålstad, T., Saasen, A., et al.: "Long-Term Durability of Rock-Based Geopolymers Aged at Downhole Conditions for Oil Well Cementing Operations," *Journal of Sustainable Cement-Based Materials*, Vol. 6, Issue 4, 2017, pp. 217-230.
8. Davidovits, J.: "Geopolymer Cement for Mitigation of Global Warming," Geopolymer Institute, 2010.

9. Worrell, E., Price, L., Martin, N., Hendriks, C., et al.: "Carbon Dioxide Emissions from the Global Cement Industry," *Annual Review of Energy and the Environment*, Vol. 26, November 2001, pp. 303-329.

10. Luukkonen, T., Abdollahnejad, Z., Yliniemi, J., Kinnunen, P., et al.: "One-Part Alkali-Activated Materials: A Review," *Cement and Concrete Research*, Vol. 103, January 2018, pp. 21-34.

11. Palomo, A., Blanco-Varela, M.T., Granizo, M.L., Puertas, F., et al.: "Chemical Stability of Cementitious Materials Based on Metakaolin," *Cement and Concrete Research*, Vol. 29, Issue 7, July 1999, pp. 997-1004.

12. Alanqari, K.A., Al-Yami, A.S. and Wagle, V.B.: "Preparation of a Synthetic Geopolymer Cement Utilizing Saudi Arabian Volcanic Ash for a Sustainable Development: Method, Preparation and Applications," IPTC paper 22617, presented at the International Petroleum Technology Conference, Riyadh, Kingdom of Saudi Arabia, February 21-23, 2022.

13. Alanqari, K.A., Wagle, V.B., Al-Johar, A.S., Al-Yami, A.S., et al.: "Primary Cementing Utilizing Epoxy Resins as Additive: Experimental and Application," SPE paper 202648, presented at the Abu Dhabi International Petroleum Exhibition and Conference, Abu Dhabi, UAE, November 9-12, 2020.

14. Wagle, V.B., Al-Yami, A.S., AlKhalaf, S., Alanqari, K.A., et al.: "Novel Resin-Cement Blend to Improve Well Integrity," SPE paper 204279, presented at the SPE International Conference on Oil Field Chemistry, The Woodlands, Texas, December 6-7, 2021.

15. Alanqari, K.A., Wagle, V.B., Al-Yami, A.S. and Mohammed, A.: "A Novel Epoxy Resin Composition as a Lost Circulation Material: Formulation, Lab Testing and Field Execution," SPE paper 204301, presented at the SPE International Conference on Oil Field Chemistry, The Woodlands, Texas, December 6-7, 2021.

16. Wasnik, A., Mete, S. and Ghosh, B.: "Application of Resin System for Sand Consolidation, Mud Loss Control and Channel Repairing," SPE paper 97771, presented at the SPE International Thermal Operations and Heavy Oil Symposium, Calgary, Alberta, Canada, November 1-3, 2005.

17. Nelson, E.B.: *Well Cementing*, Schlumberger Educational Services, Elsevier, 1990, 1,515 p.

18. Kasap, S.O.: *Principles of Electronic Materials and Devices*, 3rd edition, McGraw-Hill, 2006, 874 p.

About the Authors

Khawlah A. Alanqari

M.S. in Chemistry,
San Diego State University

Khawlah A. Alanqari is a Petroleum Scientist with the Drilling Technology Team of Saudi Aramco's Exploration and Petroleum Engineering Center – Advanced Research Center (EXPEC ARC). She received the Outstanding Young Professional Award at the EXPEC ARC 2021 Annual Awards. In addition, Khawlah was shortlisted for a number of global awards and received "highly commended" in the category of the Young Energy Professional at the Energy Institute 2020 Awards.

She has 11 granted patents, and 21 filed patent applications in the area of drilling fluids, cementing and loss circulation, as well as a number of published technical publications and journal papers. received her B.S. degree in Chemistry from the University of Dammam, Dammam, Saudi Arabia. She received her M.S. degree in Chemistry with a specialization in organic and organometallic chemistry from San Diego State University, San Diego, CA in 2017. She has a three years of research experience from a synthetic organic chemistry lab at San Diego State, focusing on the development of new reactions and methodologies in organic synthesis.

Khawlah also gained academic experience from working as a Chemistry Lecturer at Jubail University College before joining Saudi Aramco in 2018.

Dr. Abdullah S. Al-Yami

Ph.D. in Petroleum Engineering,
Texas A&M University

Dr. Abdullah S. Al-Yami is a Senior Petroleum Engineering Consultant with the Drilling Technology Team of Saudi Aramco's Exploration and Petroleum Engineering Center – Advanced Research Center (EXPEC ARC). He has 24 years of experience with Saudi Aramco and previously worked in different positions, including as a Lab Scientist and Drilling Engineer, conducting research related to drilling engineering.

Abdullah has received several awards during his career, including Saudi Aramco's Research and Development Center (R&DC) Innovation Award and its Successful Field Application Award for his research work. He also received Saudi Aramco's EXPEC ARC Effective Publications Award. A member of the Society of Petroleum of Engineers (SPE), Abdullah was awarded the 2009 SPE Outstanding Technical Editor Award for his work on the SPE *Drilling and Completion Journal*. He also received the 2014 SPE Regional (Middle East, North Africa and South Asia) Drilling Engineering Award, and both the 2015 and 2016 CEO Saudi Aramco Excellence Award. In 2016, Abdullah received Oil & Gas Middle East Award "highly commended" recognition in the category of internal control valve (ICV) Strategy of the Year for his efforts in developing drilling products utilizing a local resources strategy. In 2017, he was awarded the Saudi Arabian Board of Engineering Award.

Abdullah is a coauthor of the textbook *Underbalanced Drilling: Limits and Extremes*; he has 127 granted U.S. patents and 152 filed patents; and has more than 100 publications to his credit, all in the area of drilling and completions.

Abdullah received his B.S. degree in Chemistry from Florida Institute of Technology, Melbourne, FL; his M.S. degree in Petroleum Engineering from King Fahd University of Petroleum and Minerals (KFUPM), Dhahran, Saudi Arabia; and his Ph.D. degree in Petroleum Engineering from Texas A&M University, College Station, TX. Abdullah is currently a Chemistry Ph.D. candidate at KFUPM majoring in Organic Chemistry and Polymer Synthesis.

Dr. Vikrant B. Wagle

Ph.D. in Surfactant
and Colloidal Science,
Mumbai University Institute
of Chemical Technology

Dr. Vikrant B. Wagle is a Science Specialist with the Drilling Technology Team of Saudi Aramco's Exploration and Petroleum Engineering Center – Advanced Research Center (EXPEC ARC). His experience revolves around the design of novel, environmentally friendly drilling fluid additives and the development of high-pressure, high temperature tolerant drilling fluid systems.

Vikrant has 50 technical publications and 120 granted U.S. patents, and he has filed several other U.S. patent applications, all in the area of drilling fluids, cementing, and loss circulation.

He received his M.S. degree in Chemistry from the University of Mumbai, Mumbai, India, and his Ph.D. degree in Surfactant and Colloidal Science from the Mumbai University Institute of Chemical Technology, Mumbai, India.

Novel Approach of Autonomous Drilling Using Rotary Steerable System in Middle Eastern Oil and Gas Wells

Victor C.C. De Oliveira, Abdullah M. Dossary, Ahmed Osman, Mohammed A. Elsadig and Ayman Al-Ghazzawi

Abstract /

The history of trajectory control can be traced back to the days of drilling with rotary assemblies, when experienced directional drillers used the knowledge about the response of bottom-hole assemblies (BHA) in a specific area or field via drilling parameters and assembly configuration changes. This required intensive field and human experience and still resulted in considerable deviations from required trajectories.

Technologies evolved with the introduction of motor and rotary steerable systems (RSS), which can have more predicted directional responses; however, considerable human intervention was still required to control the trajectories. As the RSS tools matured, hold sections of the well trajectories were automated with closed loop trajectory control with minimum human intervention. Although, the curved sections were still being drilled in manual modes with directional driller interventions.

The study focused on evaluating and validating the potential of using the AutoCurve drilling mode to automatically drill the curved sections (directional drilling wells) without human intervention and to complete the missing puzzle of the autonomous well construction. The system is based on a minimum curvature method, which updates the target inclination and azimuth in a close loop system, similar to the one used to hold inclination and azimuth. The expected run rate of penetration and planned dogleg severity (DLS) are needed while programming the tool for the RSS calculation update. Once the AutoCurve mode is engaged in the RSS, it will keep updating the target inclination and azimuth along the well to deliver the programmed DLS as per the inputted rate of penetration.

A strict and detailed comparison of the measurements has been completed through three directional drilling curve sections (three wells). Combining the data of the three wells, a total of 5,632 ft were drilled in the three different hole sections. The results were promising and showed an average reduction of 70% of human intervention. In addition, for the well positioning, the new AutoCurve automation technology delivered the wells within the required profile target tolerances with minimum tortuosity.

The novel autonomous curve drilling technology helped minimize human error, enhance the accuracy of well positioning, and improve hole quality for drilling and workover operations. The system proved that this autonomous drilling technology is capable of better well trajectory delivery with minimum intervention, faster well delivery, and a reduction of operation costs.

Introduction

The intelligence of the rotary steerable systems (RSS) has been improving since its introduction. Around 1990, when the RSS was introduced, communication with the RSS tools was only one-way, by sending downlink commands through flow variations and monitoring the response afterwards. For any needed correction, human intervention was required by sending new downlinks. Between 2003 and 2013, the downhole automation journey for the RSS started with the introduction of closed loop features where they can maintain either verticality or target inclination, and azimuth in tangent sections.

The technology evolved to have closed loop responses in these vertical or tangent modes to automatically adjust the trajectory to the target directions to within 0.5° in inclination and 2° in azimuth. The next step for automating the downhole trajectory control for RSS was to close loop the curve section, Fig. 1. This used to take an increased level of focus from the directional drillers to ensure they kept reviewing the directional responses of the RSS with different intervals to update the steering requirements, steering ratio, and toolface commands. That made a good driver to improve the RSS intelligence to update its desired steering requirement capabilities as per the curve section's needs as well.

The AutoCurve downhole automation module was developed to address the need of automating the curve

Fig. 1 *Introducing AutoCurve to automate the curve directional control.*

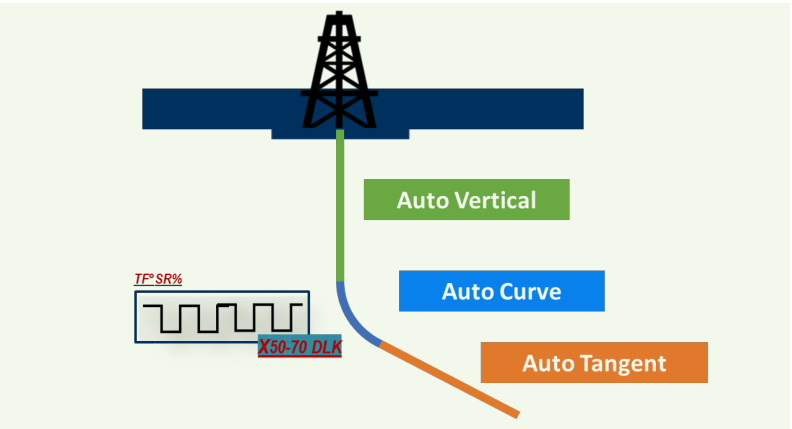

section's directional control. The intelligent algorithm was developed to change the communication process from including surface intervention to only the downhole closed loop system once a directional requirement is made. The system moved away from the toolface and steering ratio downlinking commands to dogleg and toolface commands. This is further elaborated on in Gabriel et al. (2022)[1].

With that, the RSS will no longer be dependent on surface intervention for steering requirements, but rather adapt itself to deliver the required dogleg severity (DLS) communicated. This innovative process change approach solved the need for surface dependency. Upon having this information, the tool will use its latest known inclination and azimuth and its programed rate of penetration to create pseudo changes to direction and inclination to follow, and will then automatically calculate its required steering ratio to follow the required path. This closed loop design is done on a continuous basis within a second compared to the average 20-minute thought process cycle that was used conventionally. Also, this will minimize the command downlink requirements to the tool, which further enables the automation path, Fig. 2.

Field Implementation and Qualification

As this this novel concept was being developed, multiple trials were needed to evaluate its performance and progress. A total of 11 runs were completed in different shallow and deep intervals of the fields to evaluate the technology development. The field-testing criteria started from a 300 ft interval until it eventually managed to drill a complete section for over 2,000 ft with great success.

Table 1 is a list of the performed runs and intervals of the fields. It can be seen that the attempts targeted all well profiles and different hole sections and bottom-hole assemblies (BHAs). The trials were mostly performed from inclinations above 10° to ensure proper kickoff before initiating the AutoCurve mode.

During the trial run evaluations, two criteria were required to demonstrate the success of the technology. First, the downhole automation had to ensure the trajectory follows the planned requirement with minimum tortuosity. And, second, it was needed to demonstrate the reduction of surface downlinking requirements to show the value from the downhole automation.

Three successful runs are presented in detail to demonstrate the operational aspect and the successful implementation of the technology.

Example 1: Slant Profile — Well-A

This trial run targeted a slanted profile to build from a 10° to 26° inclination with 2°/100 ft DLS requirement

Fig. 2 *Comparing the conventional RSS communication in the curve section to the AutoCurve automation.*

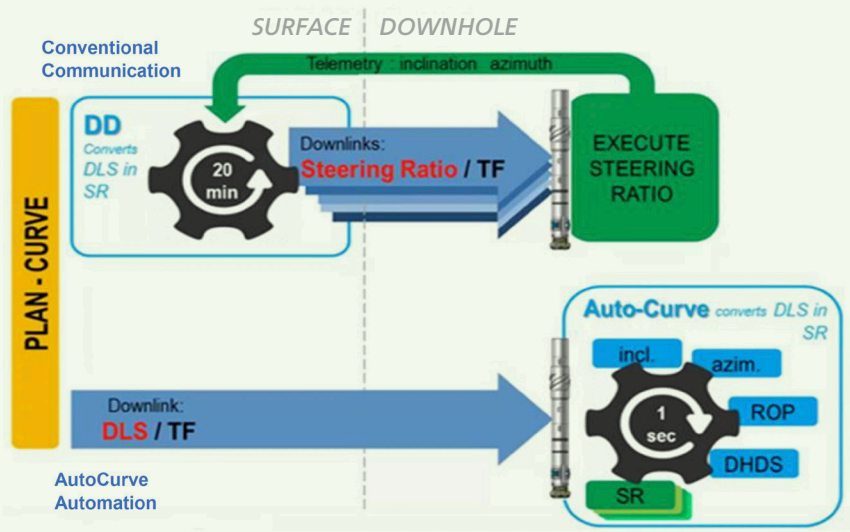

Table 1 *A list of AutoCurve trial runs done in a major Middle Eastern field.*

Rig	Well	Type	Hole	Profile	Footage	Incl. From	Incl. To	Azim. From	Azim. To	Assembly
A	1	Oil	8.5″	Landing	570	28	48	224	227	Motorized RSS
B	2	Oil	8.5″	Landing	615	20	39	137	135	Motorized RSS
C	3	Gas	8.375″	Landing	350	26	37	343	343	Stand-alone RSS
D	4	Gas	8.375″	Landing	559	16	34	133	132	Stand-alone RSS
E	5	Gas	8.375″	J-Type	416	17	25	70	73	Stand-alone RSS
F	6	Gas	16″	S-Shape	2,807	14	0	41	42	Stand-alone RSS
E	7	Gas	5.875″	J-Type	1,455	55	57	335	278	Stand-alone RSS
G	8	Gas	16″	S-Shape	2,929	12	10	150	153	Stand-alone RSS
H	A	Gas	16″	J-Type	2,069	10	26	89	88	Stand-alone RSS
H	B	Gas	8.375″	Landing	1,116	27	82	120	131	Stand-alone RSS
I	C	Gas	8.375″	Landing	2,447	13	80	107	90	Stand-alone RSS

in a 16” hole size, Fig. 3. The BHA used was a stand-alone RSS, Fig. 4. The footage drilled was 2,069 ft in 126.3 pumping hours.

The profile was drilled in one run. The AutoCurve downhole automation demonstrated that it automatically changed the required steering ratio based on the required DLS needed with no surface intervention as demonstrated in Fig. 5.

The run was compared to an offset well with the same profile in the field that showed excellent trajectory control to deliver the directional profile with an approximate 70% reduction in downlink commands, Fig. 6. The trajectory ended with 7 ft above plan and 23 ft right of planned.

Example 2: Horizontal Landing Profile with single DLS — Well-B

This trial run targeted a horizontal profile to build from a 27° to 82° inclination with 4.66°/100 ft DLS requirement in an 8¾” hole size, Fig. 7. The BHA used was a stand-alone RSS, Fig. 8. The footage drilled was 1,116 ft in 59 pumping hours.

The profile was drilled in one run. The AutoCurve downhole automation demonstrated that it automatically changed the required steering ratio based on the required DLS needed with no surface intervention as demonstrated in the below plot, Fig. 9.

The run was compared to two offset wells with the same profile in the field that showed similar to slightly improved tortuosity with an approximate 72% reduction in downlink commands, Figs. 10 and 11. The trajectory ended with 0.5 ft above plan and 3.74 ft right of planned.

Fig. 3 *The directional profile for Well-A.*

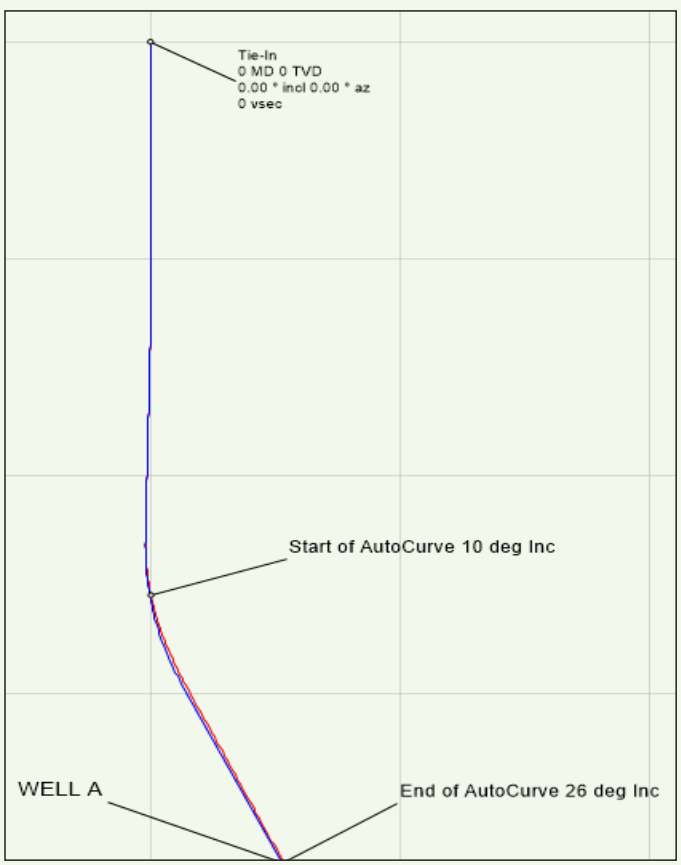

Fig. 4 *The stand-alone RSS BHA for Well-A.*

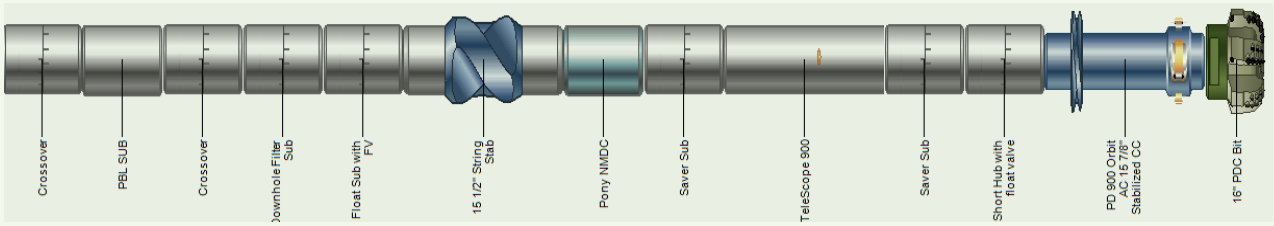

Fig. 5 *The Well-A toolface changes automatically to follow the planned trajectory without surface downlinks.*

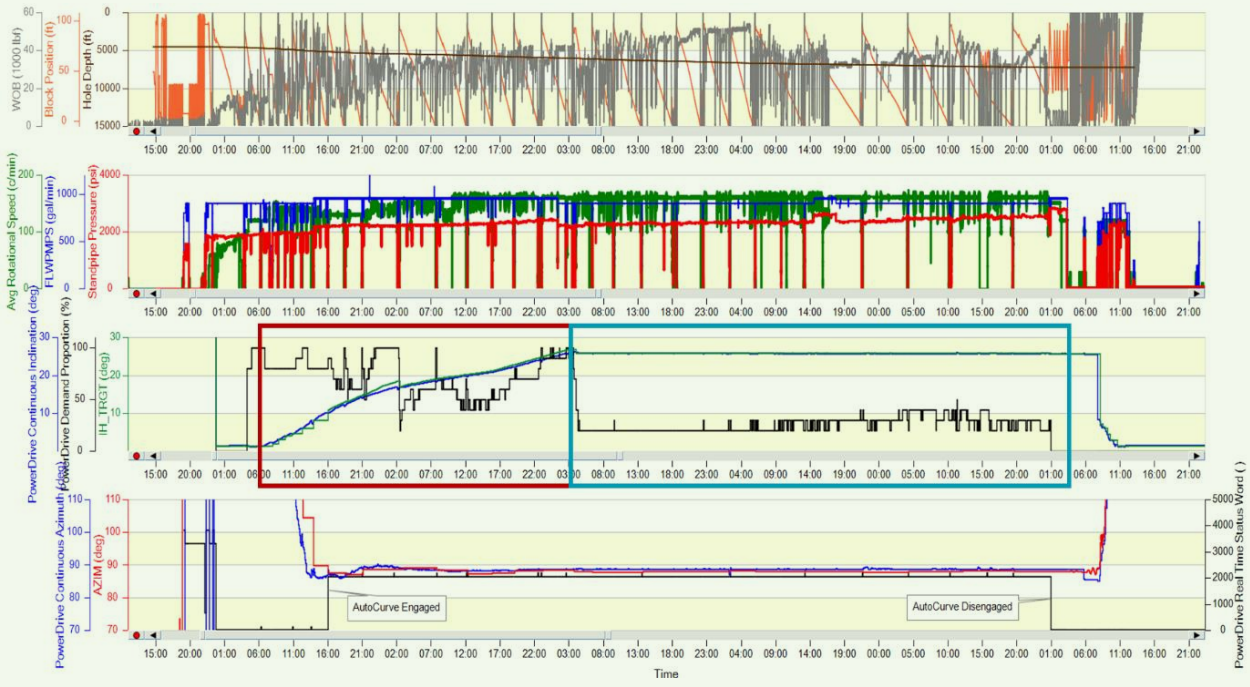

Fig. 6 *The downlinks reduction of Well-A compared to the offset using AutoCurve automation.*

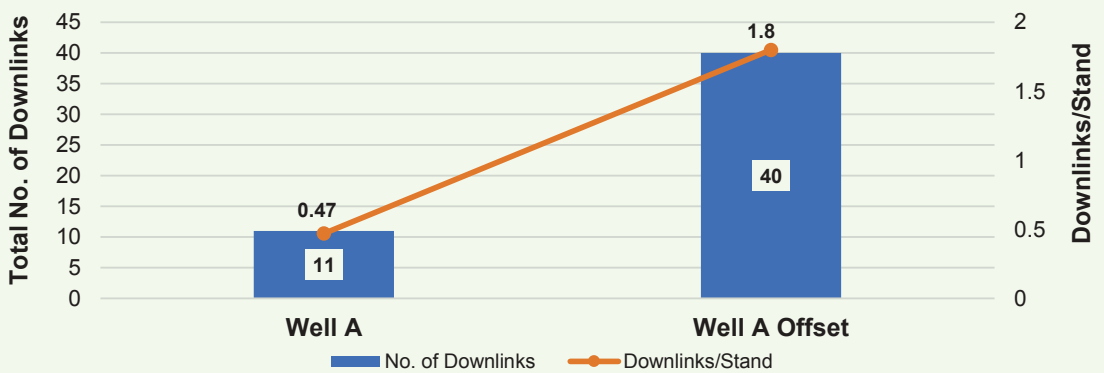

Fig. 7 *The directional profile for Well-B.*

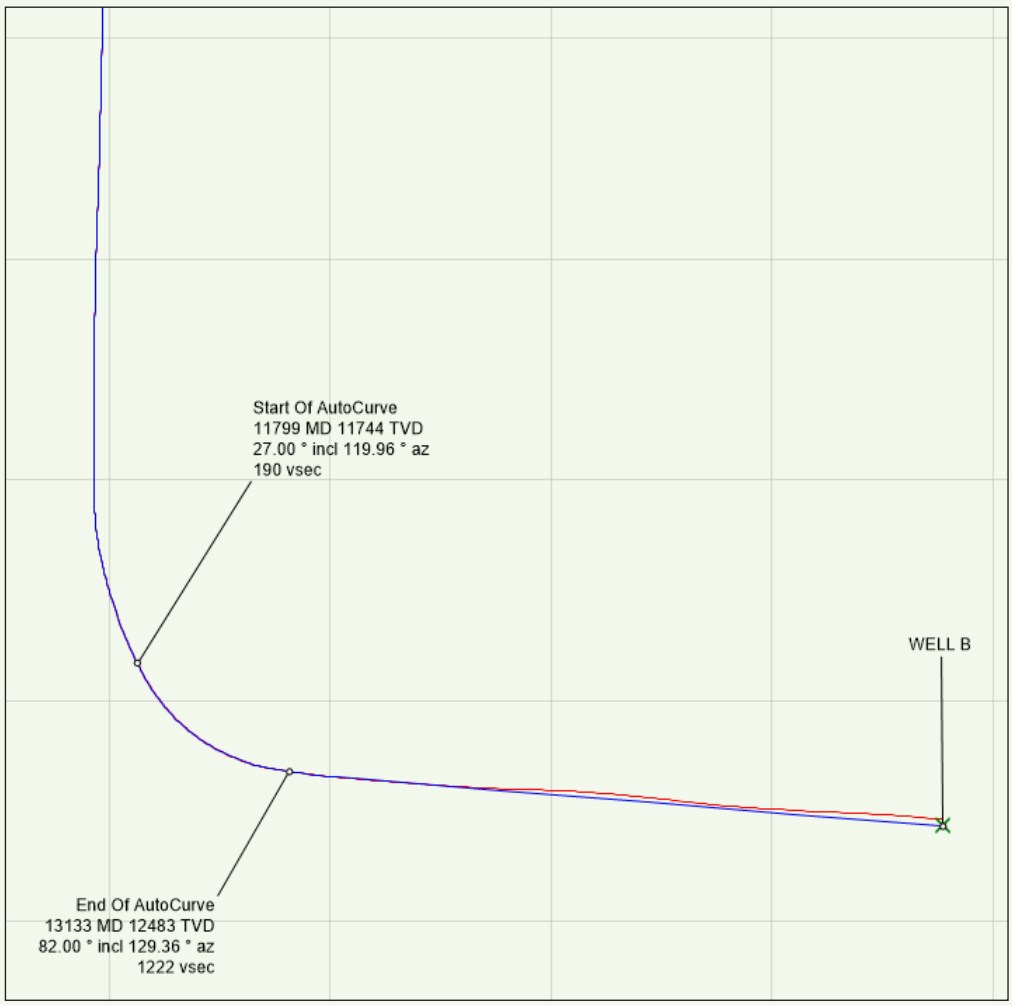

Fig. 8 *The stand-alone RSS BHA for Well-B.*

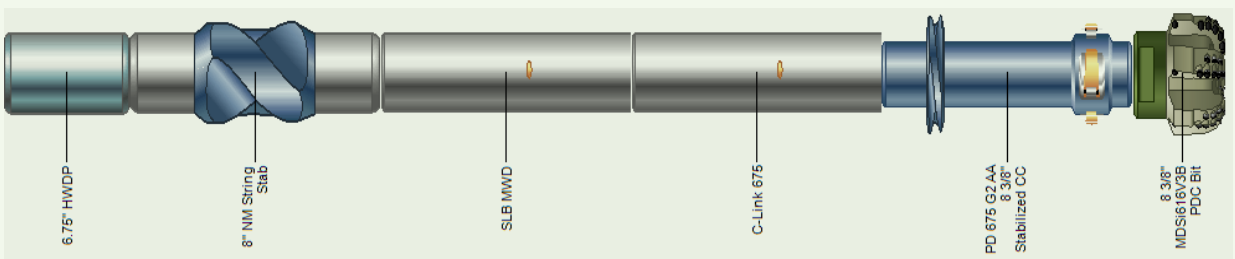

Example 3: Horizontal Landing Profile with double DLS — Well-C

This trial run targeted a horizontal profile to build from a 13° to 80° inclination with 2.25°/100 ft and 4.3°/100 ft DLS requirement in an 8¾" hole size, Fig. 12. The BHA used was a stand-alone RSS, Fig. 13. The footage drilled was 2,447 ft in 136 pumping hours.

The profile was drilled in one run. The AutoCurve downhole automation demonstrated that it automatically changed the required steering ratio based on the required DLS needed with no surface intervention as demonstrated in Figs. 14 and 15.

Fig. 9 *The Well-B toolface changes automatically to follow the planned trajectory without surface downlinks.*

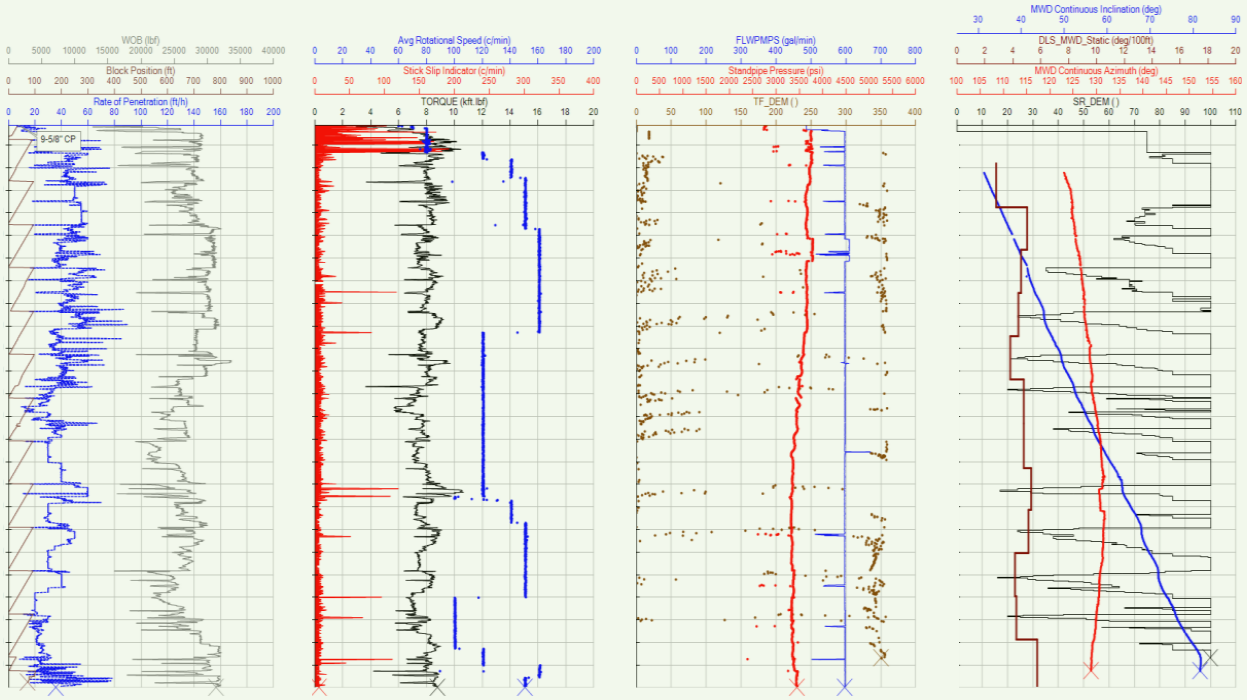

Fig. 10 *The tortuosity of Well-B compared to the offset using AutoCurve automation.*

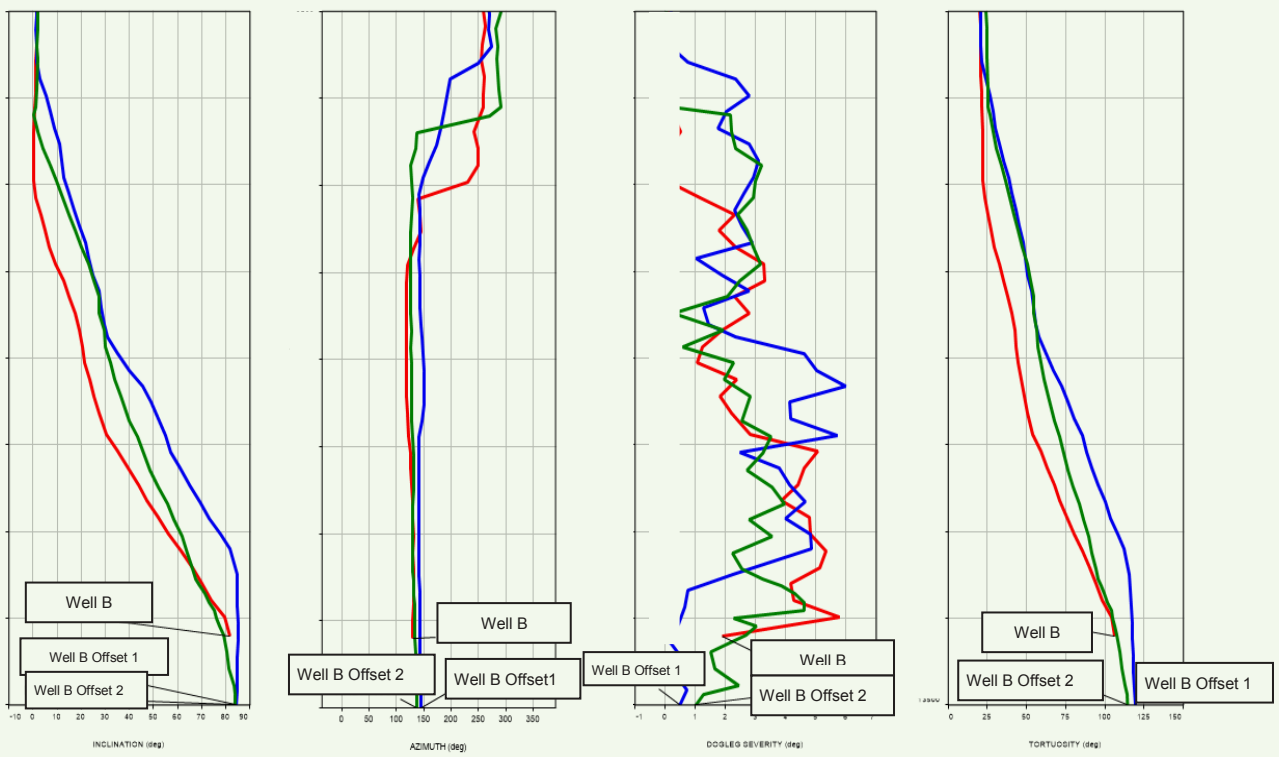

Fig. 11 *The downlinks reduction of Well-B compared to the offset using AutoCurve automation.*

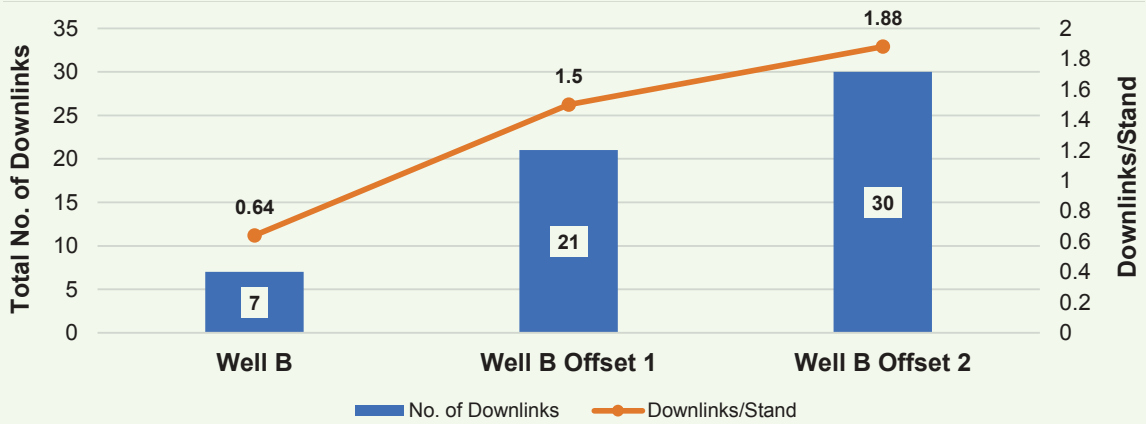

Fig. 12 *The directional profile for Well-C.*

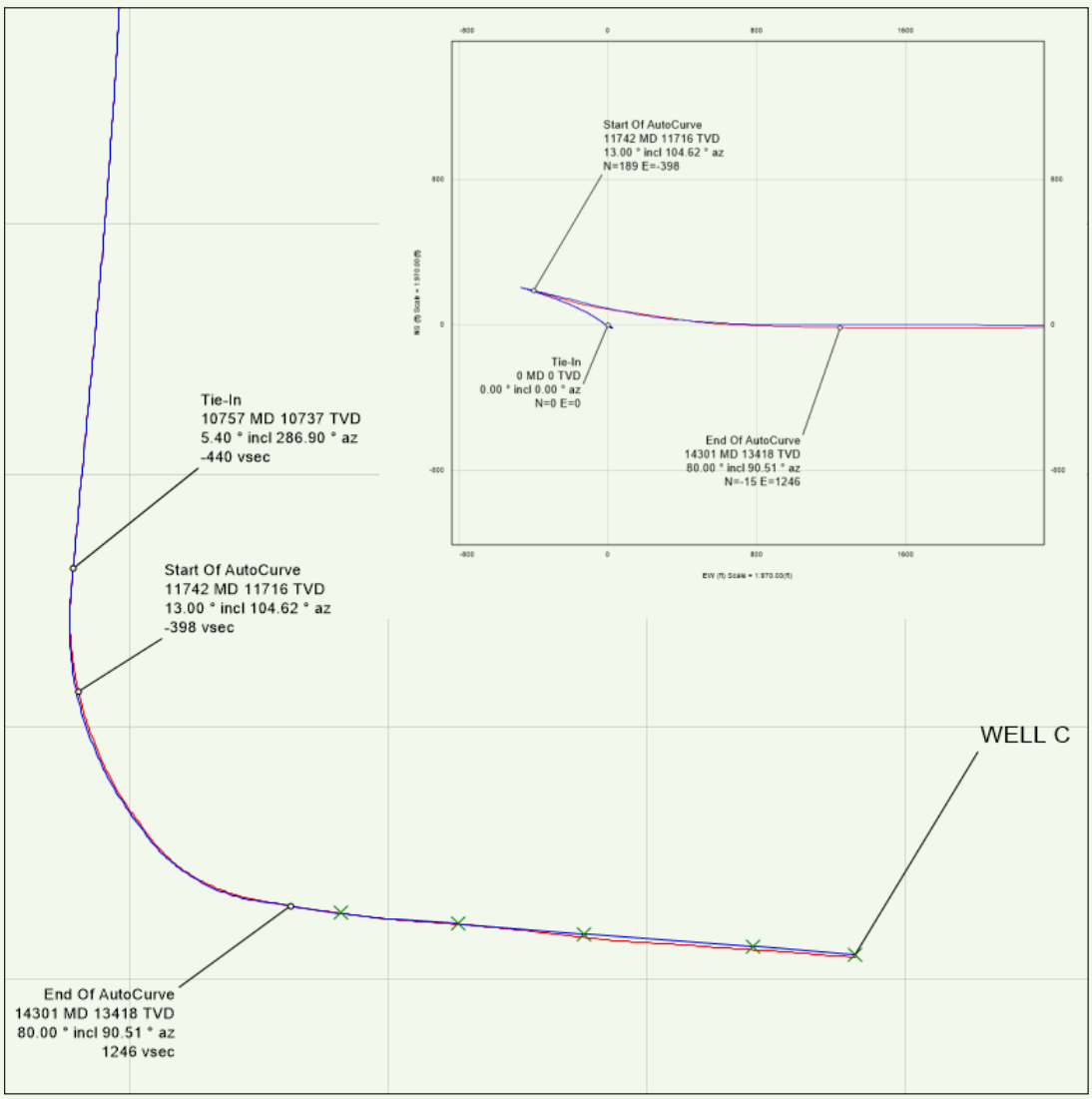

The run was compared to two offset wells with the same profile in the field that showed similar to slightly improved tortuosity, with an approximate 64% reduction in downlink commands, Fig. 16 and 17. The trajectory ended with 0.5 ft above plan and 11 ft right of planned.

Technology Proven Benefits and Applications

The benefit of AutoCurve downhole automation trials have been demonstrated in the shown trials in terms of trajectory and tortuosity control as well as reduction of downlinking requirements by approximately 70%. This value was quantified as well to rig savings of around 8 hours per 3,000 ft section, and 10 tons of CO_2 emissions reduction for the same.

The downhole automation is recognized to be one of the main pillars of the autonomous directional drilling future of the industry. AutoCurve automation development completes the final puzzle piece in the downhole automation requirement for RSS after auto vertical and auto tangent modes, Fig. 18. The continuous development of the technology will have the overall benefit of reducing the footprint on the rig site and enable remote operations on the rigs.

In the current trials, the manpower on the rig was reduced to single personnel in the field and a single office-based remote engineer. The overall benefit will end with higher operational efficiency, better service quality and personnel safety due to minimizing the rig footprint.

Conclusions

It has been demonstrated that the RSS AutoCurve downhole automation has become a reality, and that the benefits of it has become tangible. The field trials have shown that directional control with downhole automation without surface intervention is possible

Fig. 13 *The stand-alone RSS BHA for Well-C.*

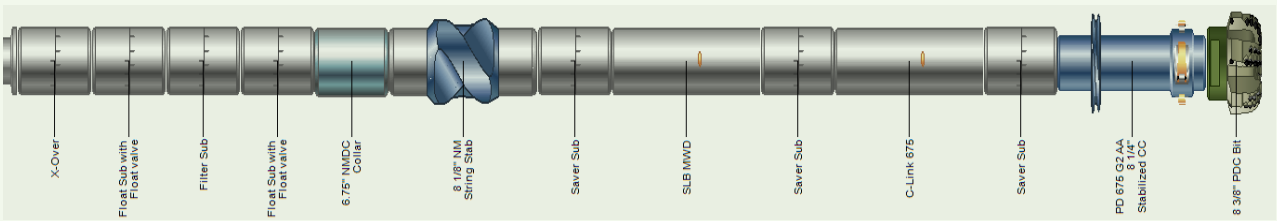

Fig. 14 *The toolface changes automatically in Well-C to follow the planned trajectory without surface downlinks — time based.*

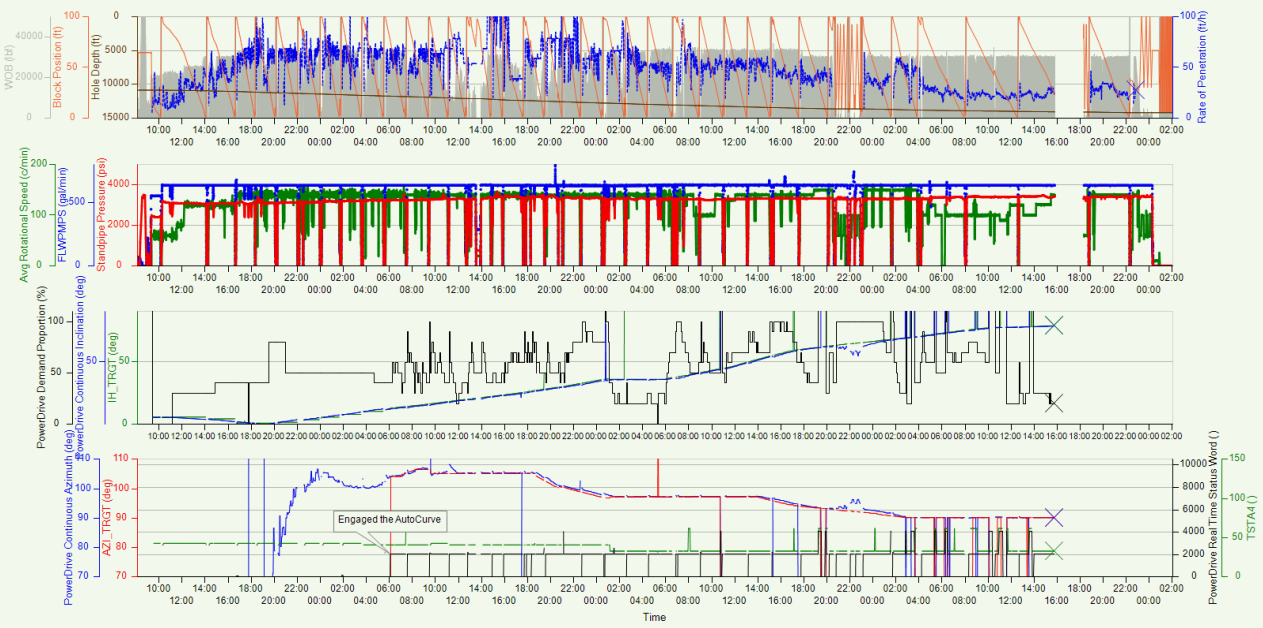

Fig. 15 *The toolface changes automatically in Well-C to follow the planned trajectory without surface downlinks — depth based.*

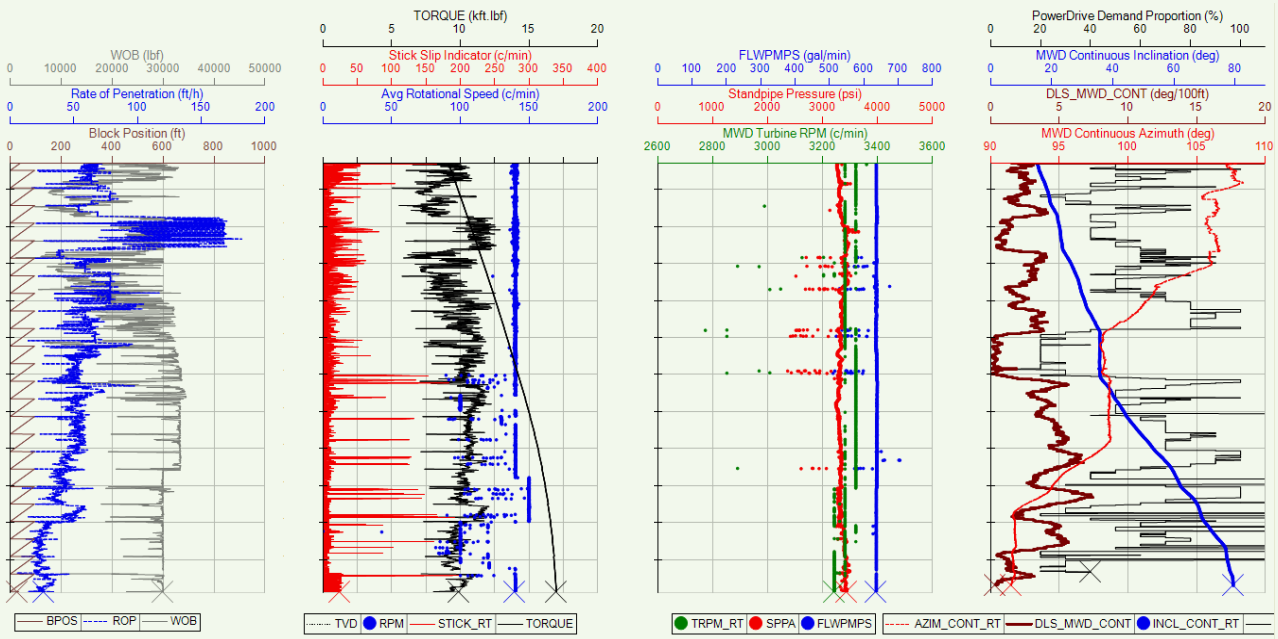

Fig. 16 *The tortuosity of Well-C compared to offset using AutoCurve automation.*

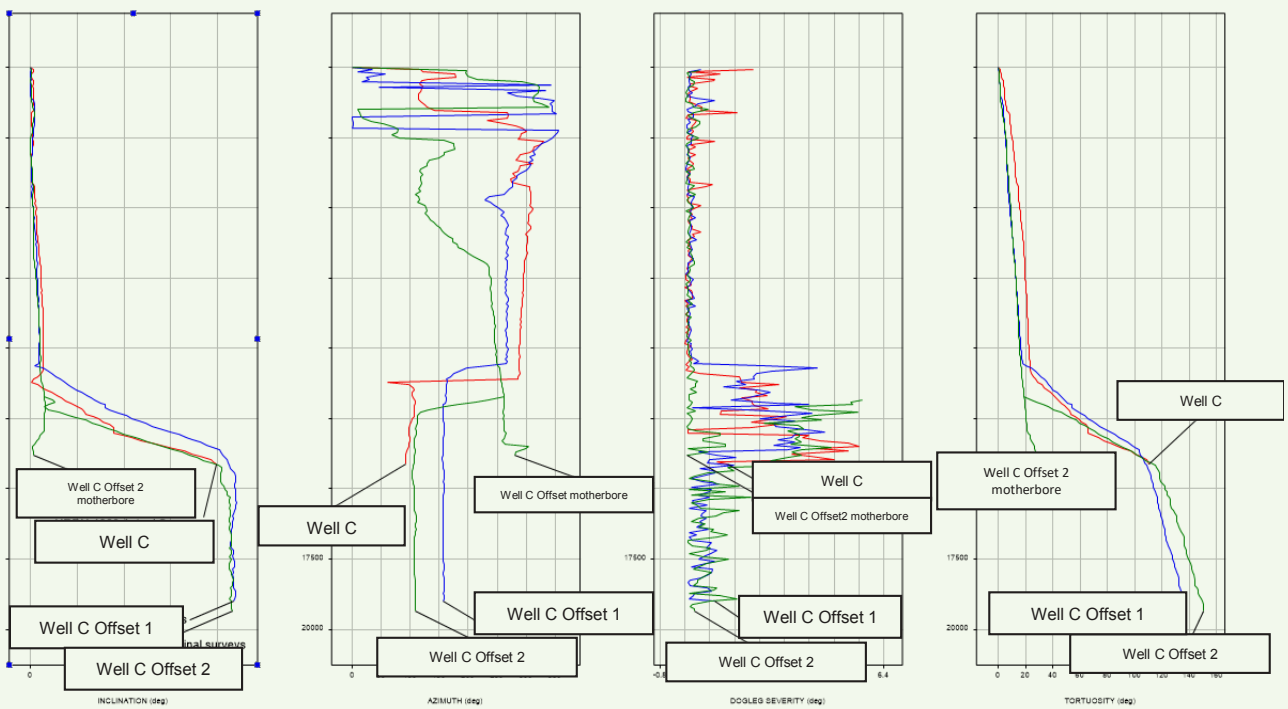

Fig. 17 *The downlinks reduction of Well-C compared to the offset using AutoCurve automation*

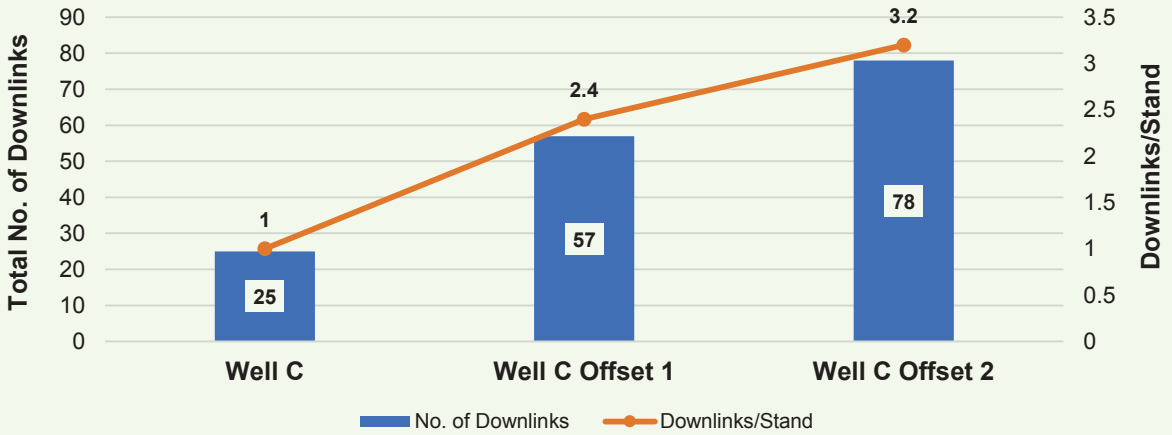

Fig. 18 *The AutoCurve automation position in the autonomous direction drilling future.*

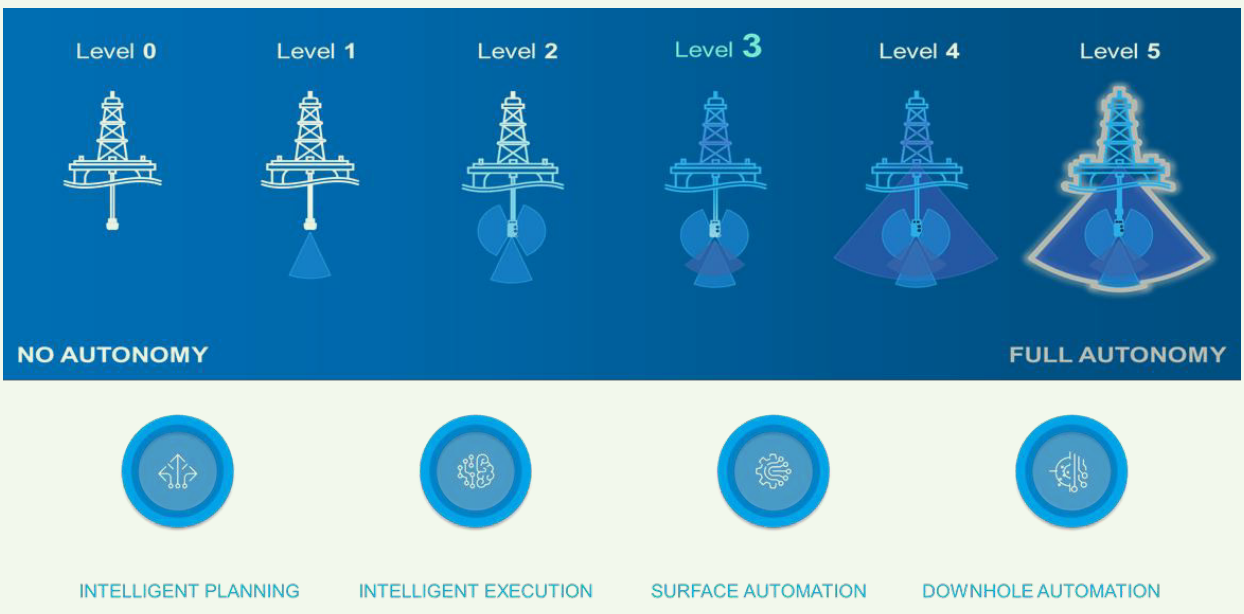

and delivers excellent results. Deviation from the plan in the trial runs were within 25 ft center to center. The rig savings benefits of less intervention from the surface and less personnel on the rig can be quantified to deliver higher operational efficiency.

Downlinking time was reduced by 70% and rig field personnel were reduced by another 50%. With the continuous development and roll out of this technology, these benefits will help the operator to reduce overall well delivery times with minimum personnel on the rig; which eventually increases operational efficiency and minimizes the operational carbon footprint.

Acknowledgments

This article was presented at the Abu Dhabi International Petroleum Exhibition and Conference, Abu Dhabi, UAE, October 31 – November 3, 2022.

Reference

1. Gabriel, S., Brovoko, K., Ignova, M., Mantle, K., et al.: "Auto-Curve: Downhole Trajectory Automation with Cost Reduction to the Operator by Reducing the Time-to-Target," IPTC article 22639, presented at the SPE International Petroleum Technology Conference, Riyadh, Kingdom of Saudi Arabia, February 21-23, 2022.

About the Authors

Victor C.C. De Oliveira

M.S. in Science and Petroleum Engineering, State University of Campinas

Victor C.C. De Oliveira is a Drilling Engineer working in the Drilling Technical Services Evaluation Unit of Saudi Aramco's Drilling Technical Department, where he is a directional drilling subject matter expert. Victor has extensive experience in deep water and high-pressure, high temperature operations across the globe. With over 19 years in the oil and gas industry, he has experience in team building, strategic thinking, services delivery, technical support, and technology development.

Victor has 22 granted patents to his credit.

Victor received his B.S. degree in Civil Engineering from Potiguar University, Natal, Brazil, and an M.S. degree in Science and Petroleum Engineering from State University of Campinas, São Paulo, Brazil.

Abdullah M. Dossary

B.S. in Petroleum Engineering, King Fahd University of Petroleum and Minerals

Abdullah M. Dossary is a Drilling Engineer working in the Drilling Technical Services Evaluation Unit of Saudi Aramco's Drilling Technical Department. He has 11 years of experience in the oil and gas industry focused in drilling engineering and directional drilling.

Abdullah is the first Saudi Directional Drilling Specialist within the company, providing technical support to Drilling & Workover, including a focus on new technologies, development of new standards and best practices, qualifying new companies, performance analysis and providing technical courses for young and inexperienced Drilling Engineers.

He received his B.S. degree in Petroleum Engineering from King Fahd University of Petroleum and Minerals (KFUPM), Dhahran, Saudi Arabia.

Ahmed Osman

B.S. in Mechanical Engineering, American University

Ahmed Osman is currently the Drilling Engineering Manager for Schlumberger's Saudi Arabia and Bahrain region. He has been working for Schlumberger for almost 20 years, covering multiple drilling engineering roles in different regions.

Ahmed started his career working as a MWD/LWD Engineer in Venezuela, Egypt, Algeria, and Jordan. He then became a Directional Drilling Engineer in Egypt and Sudan, using different drilling systems in various drilling applications. Ahmed then went on to work and manage several different drilling engineering projects in Egypt, Sudan, Vietnam, Thailand, and Myanmar for different big operators, such as BP, Shell, Eni, and Petronas.

He is the recipient of several internal awards. Ahmed also has several published papers on advanced drilling systems and technologies in different applications.

He received his B.S. degree in Mechanical Engineering from the American University in Cairo, Cairo, Egypt.

Mohammad A. Elsadig

B.S. in Electrical Engineering, Shahjalal University of Science and Technology

Mohammed A. Elsadig works at Schlumberger, where his current role is in drilling performance and digital drilling deployment in Saudi Arabia for well construction, focusing on drill plans and drill operations deployment, autonomous solutions, and data visualization.

He has proven track record in new technology introduction, drilling performance improvement projects and advance business intelligent solutions. Mohammed is skilled in creative, design-based thinking approaches in solving highly complex problems.

He received his B.S. degree in Electrical Engineering from Shahjalal University of Science and Technology, Sylhet, Bangladesh.

Ayman Al-Ghazzawi

B.S. in Chemical Engineering, King Fahd University of Petroleum and Minerals

Ayman Al-Ghazzawi is the Product and Service Delivery Manager for Schlumberger's drilling activity within Saudi Arabia and Bahrain. Having more than 16 years of experience with Schlumberger, he has held a variety of positions in different locations: Measurements and Logging while Drilling Field Engineer in Malaysia; Directional Drilling Field Engineer and Real-Time Operations Support Center Engineer in Qatar; in-house Drilling Engineer for Al-Khafji Joint Operations, and Wellbore Surveying Specialist in Saudi Arabia.

For the past 3 years, Ayman has worked as the Lead Drilling Engineer with Saudi Aramco, primarily in exploration projects for gas and unconventional gas in the Northern Area. He is also one of the specialists in wellbore surveying and anti-collision within the Middle East geographic location.

Ayman received his B.S. degree with honors in Chemical Engineering from King Fahd University of Petroleum and Minerals (KFUPM), Dhahran, Saudi Arabia. He is currently working on his M.S. degree in Sustainable and Renewable Energy.

Ayman is a member of the Society of Petroleum Engineers (SPE).

Effect of High Power Laser on Mechanical Properties of Steel

Dr. Wisam J. Assiri, Dr. Damian P. San-Roman-Alerigi and Dr. Sameeh I. Batarseh

Abstract /

Metal laser processing has been commonly employed in the manufacturing industry to cut steel and clean rust due to its speed, precision, limited heat affected zone, and low-cost. These features are possible because laser beams can be manipulated with extreme precision in frequency and energy distribution. Yet, lasers have seldom been employed in Upstream applications beyond cutting. Recently, we deployed the first high power laser (HPL) scale removal tool for surface operations. The field exercise demonstrated that the HPL beam could thoroughly remove scale without damaging the integrity of the pipes, thereby enabling their reuse. This article explains the HPL method and its outcome.

Upstream HPL processes use the laser beam as a highly localized heat source, which can be directed precisely toward a target to produce a localized thermal change without damaging the surrounding area. Our research developed techniques to dissociate, spall, melt, or vaporize different materials, including rocks, scales, and metals. The HPL tool combines these methods with an optomechanical system that drives dissociation of scale without damaging the tube. Mechanical tests were performed before and after the field tests to assess the mechanical integrity of the metallic substrates. The characterization focused on unconstrained acoustic velocimetry and micrographs.

Video feeds and thermal imaging during field operation showed the process kept the temperature of the steel pipe below 200 °C. The micrographs and ultrasound velocimetry showed no significant change in the structure of the metal substrate. Infrared spectrometry indicated that the scale was removed entirely. Consequently, the descaled pipe sample was reinstalled and put back into service.

This work shares the field results of the first HPL descaling process in Upstream. The technology could significantly affect production operations by enabling field engineers to descale and reuse flow lines, thereby saving cost and reducing waste.

Introduction

Known as a laser, the device produces a narrow beam of amplified light by stimulating emission of radiation. The evolution in the laser manufacturing industry has increased its efficiency, and has reduced the cost per energy unit and dissipation, which led to more energy efficiency, and therefore, an environmentally friendly operation.

Lasers have been widely used in many different applications, including medicine, various technologies and industries, and especially the manufacturing industry for its unique properties. This includes being precise and controllable — shortening the time of processing, less maintenance, high preciseness and accurate processing. A laser can deliver a massive amount of energy at a small, predetermined target, such as a human eye in the medical field, and steel cutting in the manufacturing field.

Use of lasers in the oil and gas industry has been recently introduced, and many articles have discussed its potential for many applications starting from simple cleanout to drilling, passing through completion and complicated workover operations.

One of the newly deployed technologies is descaling. The laser has proven to be effective in removing scales in the flow lines, especially when conventional methods such as acidizing and scraping are not an option due to heavy scaling to the point of fully plugging the flow line. The current practice is to replace the line, which is considered more expensive, due to the work required and the down time needed. A laser can be more efficient to remove scale without damaging the flow line and restore normal operations[1].

Another application that will be tested soon is laser perforation, where it has the ability to create perforations with a designed dimension. The diameter and length are determined by the design and duration of the perforation. It may not be as instant as shape charges, but it will create more cleaner perforation tunnels of less compaction and skin than those created conventionally.

More workover applications, such as the casing-casing annulus remedy and section milling, can use a laser to

reach the second and third casing. Lasers can be used to create a slot to ease the injection cement/sealant to cure the communication channels.

Oil producers usually produce a water cut, which may have a high salinity. Scale is a byproduct of salt precipitation in the flow lines due to the change of temperature and pressure. Different types of scales occur depending on the content of the hydrocarbon flow. A water cut with high salinity usually deposits certain types of inorganic scale, such as calcium carbonate ($CaCO_3$) and calcium sulfate ($CaSO_4$), which are common in carbonate formations and reservoirs with seawater flooding. Another type of inorganic scale is related to sanding in a poorly cemented sandstone formation and weakened formation due to over stimulation. Other organic scale may also be deposited by dropping heavy hydrocarbons such as paraffins and asphaltenes. All of these types of scale will create a plug, fully or partially, to the flow lines and thereby reduces the productivity of the well.

There are three main classes of scales: (1) sulfate-based, which is hard to remove by acidizing; (2) carbonate-based, which can be removed by acids; and (3) oxides, which acid solubility varies. Generally, scale can be one or a multiple combination of these categories, which may vary the acid sensitivity. Table 1[2] shows the different types of scale classifications and chemical compositions.

In the current applications, the laser has been targeting inorganic scale. The $CaCO_3$ dissociates with heat to form calcium oxide (CaO), Eqn. 1:

$$CaCO_3 + Heat \rightarrow CaO + CO_2 \quad (1)$$

The heat source in this process is the laser and the temperature should reach to a range between 1,000 °C to 3,500 °C to dissociate[3]. The CaO dissolves easily in water and can then be removed by water flush. The lab experiments show that CaO forms to powder which even makes it easy to remove.

$CaSO_4$ comes in different forms depending on the presence of water in their chemical composition. The compound ($CaSO_4 \cdot 2\,H_2O$) is also known is gypsum, which can be dried out by heating up to 205 °C, and will remove the water and leave you with $CaSO_4$, also called anhydrite[4,5]. When the anhydrite is heated up to 1,200 °C[6], it will dissociate following Eqn. 2 or Eqn. 3:

$$CaSO_4 + Heat \rightarrow CaO + SO_2 + O_2 \quad (2)$$

or

$$CaSO_4 + Heat \rightarrow CaO + SO_3 \quad (3)$$

These high temperatures are reached fairly quickly and localized by the high power laser (HPL). The sweep with a laser beam on the scale dissociates the material. In addition to that, thermal shocking will introduce cracks into the scale accumulation and when blowing nitrogen onto the scale, it will cool the scale faster and create more fractures and speed the descaling process.

Scale usually deposits around zones of high change in pressure and temperature such as zones between the wellhead and choke valves and around bends and pipes with elevation changes. Turbulence can be another reason, especially in areas of pipe size changes from a larger to a smaller diameter.

Descaling in flow lines is an extensive operation that requires precision and diagnostics. When the flow is reduced and a pressure drop is noticed across a line, it is evident that there is a plug in the line. Sections of the line are isolated and measure the pressure drop across that section to pinpoint the zone of restriction. Other diagnosis such as looking at water cut and geochemistry analyses is required to detect incompatibility and if the precipitation conditions are met. Solutions such as sending a scraper down the line may help to remove some soft accumulation such as organic scale and may be able to crush inorganic accumulations as

Table 1 *The various types of scale classifications and chemical compositions[2].*

Classification	Name	Chemical Formula
Carbonates	Calcium carbonate	$CaCO_3$
	Ferrous carbonate	$FeCO_3$
Sulfates	Gypsum	$CaSO_4 \cdot 2H_2O$
	Hemihydrate	$CaSO_4 \cdot H_2O$
	Anhydrite	$CaSO_4$
	Barium sulfate	$BaSO_4$
	Strontium sulfate	$SrSO_4$
	Ferrous sulfide	FeS
Oxides	Ferrous hydroxide	$Fe(OH)_2$
	Ferrous hydroxide	$Fe(OH)_3$

well. The good thing about this operation production will not be impacted as the flow will continue.

The next solution when inorganic scale is present is to pump acids. Acidizing is able to dissolve most of the inorganic scale such as $CaCO_3$, but it may create corrosion issues and degrade the flow line. Acidizing is not advised if the line is fully plugged, as circulation may not be achieved. Consequently, with a laser, organic and inorganic scales can be removed and heavy scaling will not create an issue as the laser will spall the accumulation. In addition, damage to the flow line will not happen. One downside is the line shall be isolated. After each descaling process, a series of nondestructive testing (NDT) is performed to ensure the thickness of the line is within an acceptable range.

As previously mentioned, the laser is known for cutting steel in the manufacturing industry. Although, there a limit to its use, and techniques to use to prevent any damage. The laser beam can be designed to be less intense when focused toward the walls of the pipe to ensure that the temperature stays within the operable range. It is known that steel can handle up to 750 °C without showing any damage to the substructure of the pipe[7]. After each descaling process, an NDT was performed across the pipes to ensure that the pipe has not been damaged by the laser.

Laser descaling is helpful to the environment as the process will reduce the frequency of replacing flow lines and enable the reuse of plugged pipes. In addition, it prevents the corrosion damage introduced by acidizing.

Methodology

The laser descaling system is used for descaling a flow line joint. The system consists of a head, connection lines, and waste tube. The head consists of a laser prism that is rotating, nitrogen jets, and a set of sensors, which include a camera to see the progress. The connection lines carry the laser fiber, cooling lines, and nitrogen feed. The waste tube is connected to a sucker system (vacuum) to remove the debris. The tool is pushed forward to remove the scale further down the line. Figure 1 shows the system setup along with the scaled up pipe.

The tool and the pipe should be aligned horizontally and the optics adjusted to the conditions of the joint. The speed is manually controlled depending on the density of scale. The system can go up to 30 ft/min, and the optimum speed can vary. For a 20 ft joint, it takes around 11 minutes to fully descale.

The beauty of the system is that it is portable and can be relocated in a facility or near the flow line location. Figure 2 is a schematic of the full system where it shows the vacuum truck, the nitrogen generator, and the power generator.

The sensors in the system also detect misalignment or overheating of the pipe to ensure successful operation. Post-operation the pipe will undergo an NDT inspection to ensure the integrity of the pipe.

Results

Further testing in the lab to analyze the integrity of the pipe was performed. The steel sample of the pipe was analyzed using photomicrographs, which visually inspects the structure of the pipe.

Visual inspection during the descaling process shows the laser was able to remove all the scale in the pipe without any visible damage to the walls. Figure 3 shows the status of the pipe throughout the descaling process.

The experiments in both the lab and field focused on scale samples deposited on metal pipes. The ideal removal method should be capable of removing the scale without affecting the substrate. This part of the study characterized metal samples before and after HPL descaling through photomicrographs and unconstrained velocity measurements. Figures 4a and 4b are photomicrographs of the steel pipe sample, both at 50 μm. It can be seen that the condition of the microstructure of the pipe did not change due to

Fig. 1 *A photo of the laser descaling system.*

Fig. 2 *A schematic of the full laser descaling system layout.*

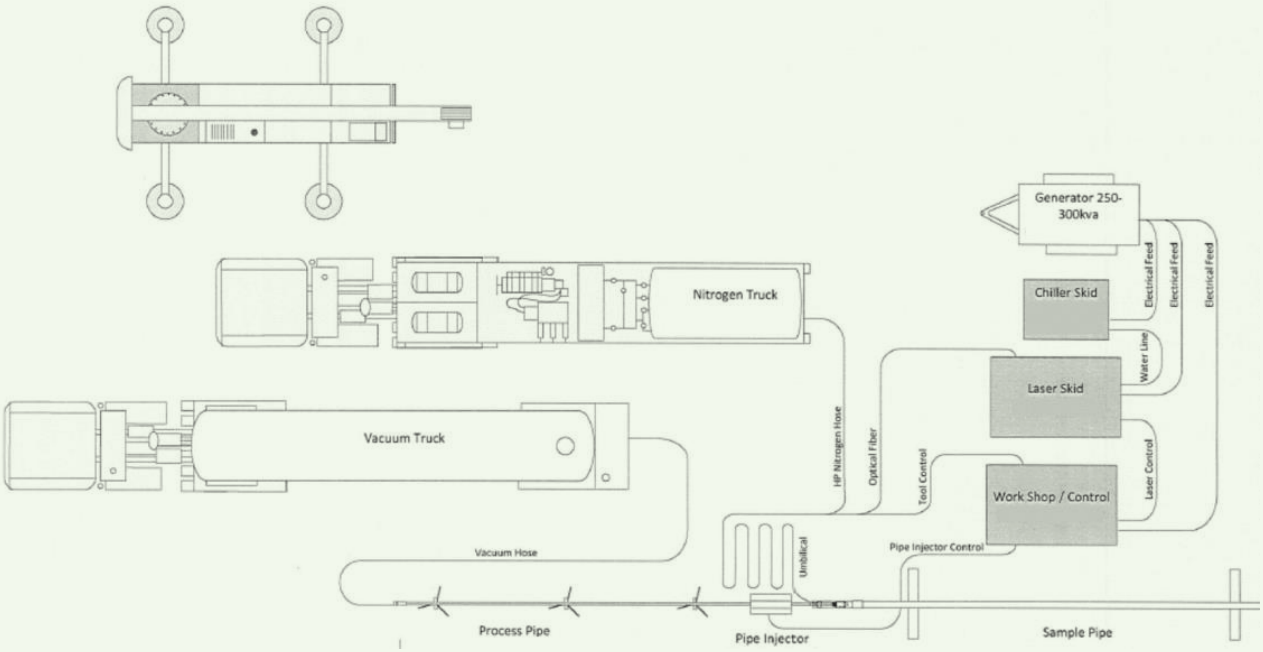

Fig. 3 *A visual inspection of the pipe, (a) before, (b) during, and (c) after descaling.*

the laser descaling process.

During the descaling process, an infrared spectrometry camera measured the temperature across the pipe. The temperature during the test did not exceed 200 °C, which is way below the threshold of 750 °C.

The mechanical properties of the sample after descaling were also measured, Table 2. The values were compared to the literature values of steel of the same grade. The values are within 5% of the standard values, which means the pipe has passed the inspection and can be reused.

Conclusions

The results of HPL descaling can be summarized as follows:

- The laser descaling is proven to be good alternative to conventional methods of acidizing and scraping.
- The process is fast enough to remove scale without damaging the flow line.
- The laser beam can be adjusted to remove the scale completely off the walls without over heating the pipe.
- The laser descaling system is easily portable.
- The integrity of the flow lines was not compromised.
- The lab analysis shows that the pipe is in good

Fig. 4 *Photomicrographs of the steel pipe sample; (a) before, at 50 µm, and (b) after, at 50 µm.*

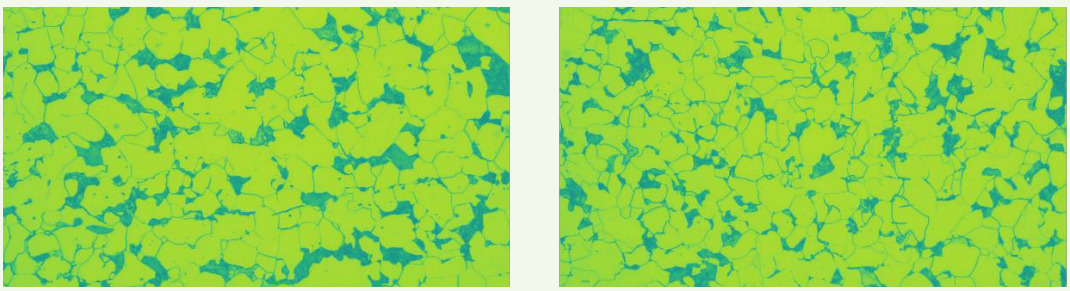

Table 2 *The mechanical properties of the steel sample after laser descaling.*

Property	Standard	After (+/- 5%)
E (GPa)	200	199.3
Poisson ratio	0.3	0.3
P wave (m/s)	5,800 – 6,100	6,102.3
S wave (m/s)	3,100 – 3,300	3,093.0

condition and passes the NDT inspection.

- There is room for upgrading the system and automating the process.

Acknowledgments

This article was presented at the Abu Dhabi International Petroleum Exhibition and Conference, Abu Dhabi, UAE, October 31 – November 3, 2022.

References

1. San-Roman-Alerigi, D.P., Mutairi, S., Batarseh, S. and Assiri, W.: "Principles and Advantages of High Power Lasers for Descaling Surface Equipment," SPE paper 209977, presented at the SPE Annual Technical Conference and Exhibition, Houston, Texas, October 3-5, 2022.
2. BinMerdhah, A.B., Yassin, A.A.M. and Muherei, M.A.: "Laboratory and Prediction of Barium Sulfate Scaling at High Barium Formation Water," *Journal of Petroleum Science and Engineering*," Vol. 70, Issues 1-2, January 2010, pp. 79-88.
3. Karunadasa, K.S.P., Manoratne, C.H., Pitawala, H.M.T.G.A. and Rajapakse, R.M.G.: "Thermal Decomposition of Calcium Carbonate (Calcite Polymorph) as Examined by in Situ High Temperature X-ray Powder Diffraction," *Journal of Physics and Chemistry of Solids*, Vol. 134, November 2019, pp. 21-28.
4. Bollen, W.M.: "Thermal Decomposition of Calcium Sulfate," Ph.D. thesis, Iowa State University, 1954, 236 p.
5. Alissa, F.M., Aljuryyed, N.W., Balharth, S.A. and Leoni, M.: "Calcium Sulfate Scale Dissolution Efficiency by Various Chemicals Additives," SPE paper 208819, presented at the SPE International Conference and Exhibition on Formation Damage Control, Lafayette, Louisiana, February 23-24, 2022.
6. Newman, E.S.: "Behavior of Calcium Sulfate at High Temperatures," *Journal of Research of the National Bureau of Standards*, Vol. 27, August 1941, pp. 191-196.
7. Li, N., Huang, S., Zhang, G., Qin, R., et al.: "Progress in Additive Manufacturing on New Materials: A Review," *Journal of Materials Science & Technology*, Vol. 35, Issue 2, February 2019, pp. 242-269.

About the Authors

Dr. Wisam J. Assiri

Ph.D. in Petroleum Engineering, Colorado School of Mines

Dr. Wisam J. Assiri is a Petroleum Engineer working with Production Technology Team of Saudi Aramco's Exploration and Petroleum Engineering Center – Advanced Research Center (EXPEC ARC). Currently, he is working with the Unconventional Resources Focus Area leading the field deployment of the high-power laser technology.

Wisam was involved in different research projects related to formation damage in the areas of condensate banking and emulsified acids characterization.

In 2006, he received his B.S. degree in Chemical Engineering from King Fahd University of Petroleum and Minerals (KFUPM), Dhahran, Saudi Arabia. In 2012, Wisam received his M.S. degree in Petroleum Engineering from the Colorado School of Mines, Golden, CO. In 2017 he received his Ph.D. degree in Petroleum Engineering, also from the Colorado School of Mines.

Dr. Damian P. San-Roman-Alerigi

Ph.D. in Electrical Engineering, King Abdullah University of Science and Technology

Dr. Damian P. San-Roman-Alerigi is a Petroleum Scientist working with the Production Technology Team of Saudi Aramco's Exploration and Petroleum Engineering Center – Advanced Research Center (EXPEC ARC). His focus is on developing the next generation of subsurface photonic and electromagnetic tools.

Damian's previous research focused on the interaction of waves with complex media and its application to subsurface technologies. His work encompasses different areas of science and engineering, from oil and gas to applied mathematics. He has published papers in various international journals and conferences around the world.

Damian received his B.S. degree in Physics from the National Autonomous University of Mexico, Mexico City, Mexico. In 2008, he enrolled in King Abdullah University of Science and Technology (KAUST) as a founding class student where he completed his M.S. degree in 2010, and his Ph.D. degree in 2014, both in Electrical Engineering.

Dr. Sameeh I. Batarseh

Ph.D. in Petroleum Engineering, Colorado School of Mines

Dr. Sameeh I. Batarseh is a Petroleum Engineering Consultant working with the Production Technology Team of Saudi Aramco's Exploration and Petroleum Engineering Center – Advanced Research Center (EXPEC ARC). Currently, he is the Focus Area Champion of the Unconventional Resources leading the High-Power Laser Program. Sameeh's area of interest is to develop an in situ laser application in drilling, perforation and fracturing, among many other applications with a focus on unconventional reservoirs.

He is an active member of the Society of Petroleum Engineers (SPE), serving the society since 1992 while holding different positions, including sitting on the SPE Executive Advisory Committee, ATCE Program Committees (Chairperson), subcommittees (chair and member). Sameeh was also on the board and Vice Chair for the Western Region USA San Joaquin Valley chapter. His service is recognized worldwide as he received the SPE President Section Award of Excellence, Regional Service Award, and is a SPE Distinguished Lecturer, Distinguished Member and Editorial Review Committee Technical Editor. He has organized over 54 SPE technical workshops.

Sameeh has authored or coauthored more than 92 articles with high-impact publications, and has an H-Index of 36. He holds 85 patents (41 granted patents and 44 patents in progress).

Sameeh received his Ph.D. degree in Petroleum Engineering from the Colorado School of Mines, Golden, CO.

Have an article you would like to publish? Here are our guidelines.

These guidelines are designed to simplify and help standardize submissions. They need not be followed rigorously. If you have any questions, please call us.

Length

Average of 2,500-4,000 words, plus illustrations/photos and captions. Maximum length should be 5,000 words. Articles in excess will be shortened.

What to send

Send text in Microsoft Word format via email. Illustrations/photos should be clear and sharp. Editable files are requested for graphs, i.e., editable in Excel.

Procedure

Notification of acceptance is usually within three weeks after the submission deadline. The article will be edited for style and clarity and returned to the author for review. All articles are subject to the company's normal review. No paper can be published without a signature at the manager level or above.

Format

No single article need include all of the following parts. The type of article and subject covered will determine which parts to include.

Working Title
Lorem Ipsum here.

Abstract
Usually 150-300 words to summarize the main points.

Introduction
Different from the abstract in that it sets the stage for the content of the article, rather than telling the reader what it is about.

Main body
May incorporate subtitles, artwork, photos, etc.

Conclusion/Summary
Assessment of results or restatement of points in introduction.

Endnotes/References/Bibliography
Use only when essential. Use author/date citation method in the main body. Numbered footnotes or endnotes will be converted. Include complete publication information. Standard is *The Associated Press Stylebook*, 52nd ed. and *Wesbter's New World College Dictionary*, 5th ed.

Acknowledgments
Use to thank those who helped make the article possible.

Illustration/Tables/Photos and explanatory text

If the files are large, these can be submitted separately, due to email size limits. Initial submission may include copies of originals; however, publication will require the originals. When possible, submit original images. Color is preferable.

File Format

Illustration files with .EPS extensions work best. Other acceptable extensions are .TIFF/.JPEG/.PICT.

Permission(s) to reprint, if appropriate

Previously published articles are acceptable but can be published only with written permission from the copyright holder.

Author(s)/Contibutor(s)

Please include a brief biographical statement.

Submission/Acceptance Procedures

Papers are submitted on a competitive basis and are evaluated by an editorial review board comprised of various department managers and subject matter experts. Following initial selection, authors whose papers have been accepted for publication will be notified by email.

Papers submitted for a particular issue but not accepted for that issue may be carried forward as submissions for subsequent issues, unless the author specifically requests in writing that there be no further consideration.

Submit articles to:

Editor
The Saudi Aramco Journal of Technology
C-10B, Room AN-1080
North Admin Building #175
Dhahran 31311, Saudi Arabia
Tel: +966-013-876-0498
Email: *william.bradshaw.1@aramco.com.sa*

Submission deadlines

Issue	Paper submission deadline	Release date
Fall 2023	May 24, 2023	September 30, 2023
Winter 2023	August 3, 2023	December 31, 2023
Spring 2024	November 5, 2023	March 31, 2024

There is more.

Application of Machine Learning for Real-Time Prediction of Sonic Well Logs Using Surface Drilling Parameters and Gamma Ray

Rima T. Alfaraj, Dr. Murtadha J. AlTammar and Osman Hamid

Abstract / The objective of this study is to utilize drilling parameters and gamma ray (GR) well logs to predict compressional and shear sonic logs while drilling using machine learning techniques. Surface drilling parameters and various wellbore logs of 10 horizontal gas wells were used in this study to train the machine learning model. The drilling parameters include the rate of penetration (ROP), weight on bit (WOB), drillpipe rotation (rpm), torque (TOR), standpipe pressure (SPP), and mud flow rate (gpm).

Rheological Studies and Numerical Investigation of Barite Sag Potential of Drilling Fluids with Thermochemical Additive Using Computational Fluid Dynamics (CFD)

Dr. Olalekan Alade, Dr. Mohamed Mahmoud and Ayman R. Al-Nakhli

Abstract / A novel method of improving the rheological performance of drilling fluids, water-based mud (WBM) against barite particle settling, otherwise known as barite sag, has been developed. This method involves adding a certain quantity of thermochemical fluid to the fluid to increase the temperature and increase viscosity. We have substantiated this claim experimentally by conducting rheological tests and theoretically using computational fluid dynamics (CFD) simulation. WBM, with encapsulated thermochemical fluid (TCF), was prepared. Rheological tests were conducted under low and high temperature ranges.

Theoretical and Experimental Comparison Study of Weak Point Shape Effect on Open Hole Fracturing Pressure

Dr. Murtadha J. AlTammar, Dr. Khalid M. Al-Ruwaili, Dr. Gallyam Aidagulov, Hussain K. Al-Dakheel, Dr. Devon C. Gwaba and Dr. Mustapha Abbad

Abstract / Placing weak point(s) within the well's stimulated section can reduce fracture initiation pressure (FIP), and thereby stimulate the intervals, which otherwise could not be broken down within the pressure limits of completion and pumping equipment. In this work, two essential weak point shapes applicable to the open hole environment were considered: 360° (or circular) notches, and perforation holes. The former included blunt (U) and sharp (V) notches, while the latter were represented by single and triple in-plane perforation holes. Triple holes were 120° phased, and similar to notches, penetrated the rock within a single plane perpendicular to the wellbore. With a focus on an open hole wellbore parallel to the minimal far-field stress, these weak points were compared by their ability to initiate transverse fracture and reduce fracturing pressure.

To read these articles and others, go to www.saudiaramco.com/jot

أرامكو السعودية
saudi aramco

Aramco
Journal
of Technology

Liked this issue? Sign up. It's free.

To begin receiving the *Aramco Journal of Technology* please complete this form, scan and send by email to ***william.bradshaw.1@aramco.com.***

Got questions?

Just give us a call at +966-013-876-0498 and we'll be happy to help!

Scan the QR code to go straight to your email and attach the form!

Subscription Form

Name

Title

Organization

Address

City

State/Province

Postal code

Country

Email address

Phone number

Number of copies